Dissertation zur Erlangung des Doktorgrades
der Fakultät für Chemie und Pharmazie
der Ludwig-Maximilians-Universität München

Endothelial hyperpermeability: characterization of novel drug targets and appropriate analytical methods

Michael Christopher Hornburger
aus München, Deutschland
2013

Erklärung

Diese Dissertation wurde im Sinne von § 7 der Promotionsordnung vom 28. November 2011 von Frau Prof. Dr. Angelika M. Vollmar betreut.

Eidesstattliche Versicherung

Diese Dissertation wurde eigenständig und ohne unerlaubte Hilfe erarbeitet.

München, den 27. September 2013

Michael Christopher Hornburger

Dissertation eingereicht am:	27. September 2013
1. Gutachter:	Prof. Dr. Angelika M. Vollmar
2. Gutachter:	Prof. Dr. Robert Fürst
Mündliche Prüfung am:	25. Oktober 2013

für Anja und meine Eltern

CONTENTS

1 INTRODUCTION

1.1 Background and aim of the work

A broad range of diseases with an inflammatory component, such as acute lung injury (ALI), acute respiratory distress syndrome (ARDS), sepsis, ischemia-reperfusion injury, diabetes mellitus or burn edema, shares a pathologically elevated endothelial permeability as common clinical picture.[1] Still today, drugs that specifically interfere with barrier-regulating signaling pathways in the endothelium are widely lacking. Therefore, the identification of novel pharmacological drug targets is of utmost importance. The characterization of possible targets requires quantitative and sensitive techniques to monitor barrier properties of endothelial cell monolayers *in vitro* mimicking physiological and pathophysiological conditions.

The content of my thesis addresses two important aspects of endothelial permeability research: **(1)** The characterization of Inhibitor of apoptosis proteins (IAPs) as new targets in endothelial barrier dysfunction and **(2)** a comparative study of analytical methods to assess barrier function of cultured endothelial cells.

(1) Characterization of IAPs as regulators of endothelial hyperpermeability

IAPs are well-established suppressors of the programmed cell death. As overexpression of IAPs frequently occurs in cancer and correlates with tumor progression, poor prognosis and resistance mechanisms, they became attractive targets for the development of anti-cancer therapeutics.[2] Besides their key role in apoptosis, IAPs have emerged as important regulators of inflammatory processes.[3] Recently, we could provide evidence that IAPs are promising anti-inflammatory drug targets, since IAP inhibition significantly reduced the knee joint swelling in a mouse model of antigen-induced arthritis.[4] Additionally, we introduced IAPs as important regulators of endothelial activation, in particular of the interaction of leukocytes and endothelial cells.[4] Based on the finding that IAP inhibition reduced leukocyte diapedesis, we hypothesized that IAPs might not only regulate the expression of adhesion molecules (ICAM-1), but also govern the endothelial barrier function.

The aims of the first study were:

I. to characterize IAP antagonism as novel approach to prevent endothelial barrier dysfunction and
II. to elucidate the role of IAPs in the underlying permeability-regulating cell signaling events.

(2) A comparative study of macromolecular permeability measurement and impedance sensing

For the validation of potential drug targets, the barrier function of cultured endothelial cells can be analyzed with distinct *in vitro* methods.[1] Thus, we set up a comparative study, in which the properties of the classic measurement of macromolecular permeability and the modern real-time cell-impedance sensing were characterized after the application of different established endothelial barrier-modulating agents.

The aims of the second study were:

I. to evaluate impedance sensing as approach for the analysis endothelial barrier function and
II. to decipher the advantages and limitations of impedance sensing and macromolecular permeability measurement.

1.2 The vascular endothelium

The endothelium represents the largest “organ” in the human body, with a surface area up to 7000 m^2, although it is only one cell layer thick.[5] It regulates important physiological functions, such as tissue homeostasis, hemostasis, the vascular tone, angiogenesis or the immune response.[6, 7] Endothelial cells show a characteristic polarized structure; they carry a polysaccharide seam (termed *glycocalyx)* on the luminal side and, on the opposite side, they are anchored to the basement membrane (termed *basal lamina*), which consists of extracellular matrix (ECM) proteins. A monolayer of closely connected endothelial cells outlines the inner surface of all blood vessels. Due to the strategically unique position between the blood and the underlying tissue, the endothelium functions as semi-permeable barrier to plasma fluid, nutrients, leukocytes and molecules. The supply with nutrients as well as the elimination of metabolic byproducts is essential for tissue viability and organ function.

Dysregulation of the endothelial barrier function is a hallmark for inflammatory processes. As consequence, excessive flux of plasma proteins and fluid across the endothelium leads to their accumulation in the extravascular space. The subsequent tissue swelling (termed edema) is detrimental to a vital tissue, because oxygen and nutrient supply is impaired.[8]

1.2.1 The endothelium as anti-inflammatory drug target

The vascular endothelium represents an interesting drug target system for anti-inflammatory strategies due to its dynamic barrier properties, which regulate the extravasation of both, macromolecules and leukocytes. Conventional anti-inflammatory therapeutics, such as glucocorticoids and non-steroidal anti-inflammatory drugs, are not always effective and may provoke serious side-effects.[9, 10] Although inflammatory processes, as for example the regulation of endothelial barrier function, were subject of extensive research efforts for years, the precise mechanisms of the inflammatory response remain elusive.[1, 11] Therefore, the search for new target-oriented approaches that counteract endothelial barrier dysfunction is an ongoing need.[12]

1.2.2 Regulation of endothelial permeability

The prevailing model for the transport of plasma proteins and solutes across the endothelium describes two different pathways: the transcellular route (mediated by vesicles) and the paracellular pathway (through cell-cell contacts).[13] Under physiological conditions, macromolecules, *e.g.* plasma proteins, are transported across the endothelial barrier in caveolin-1-rich vesicles (termed caveolae).[14] In contrast, smaller molecules (diameter < 3 nm) permeate through interendothelial junctions (IEJs), structures that mediate cell-cell contacts.[15] Inflammatory processes, such as the release of inflammatory mediators or the extravasation of leukocytes, affect mainly the paracellular transport. Typical pro-inflammatory mediators, like *e.g*. histamine, thrombin or TNFα, which are secreted by mast cells, platelets, macrophages or endothelial cells themselves, disrupt the organization of IEJs and thus evoke endothelial barrier dysfunction.[16, 17]

The endothelial barrier is determined by a fine balance of adhesive forces, represented by IEJs, and contractile forces, generated by intracellular actin-myosin interaction (**Figure 1**).[16] IEJs are comprised of mainly adherens junctions (AJs) and, to a lesser extent, of tight junctions. This makes the integrity of AJs, which consist primarily of the *homophilic* transmembrane protein vascular endothelial (VE)-cadherin, crucial for the endothelial barrier function. Disassembly of AJs is induced upon tyrosine phosphorylation of VE-cadherin (*e.g.* at Y^{731}), thus initiating its internalization or degradation.[18] Furthermore, the intracellular domain of VE-cadherin is connected to the actin cytoskeleton *via* catenins (α, β, γ and p120).[19] Hence, the remodeling of the actin cytoskeleton directly influences junctional integrity. While a cortical actin rim at the cell periphery promotes AJs stability, the reorganization into cytosolic, cell-spanning stress fibers disrupts AJs.[16] The contractile machinery of endothelial cells is driven by a mechanochemical interaction of actin and myosin. Activation occurs after phosphorylation of the myosin light chain2 (MLC2) (T^{18}/S^{19}) and builds up a *centripetal* force that retracts endothelial cells from each other, leading to the formation of intercellular gaps. All major signaling cascades in the regulation of endothelial permeability either promote (*i.e.* barrier-disruptive signaling) or inhibit (*i.e.* barrier-protective signaling) the three key mechanisms of endothelial hyperpermeability: the activation of the contractile machinery, the actin remodeling and the disruption of IEJs.

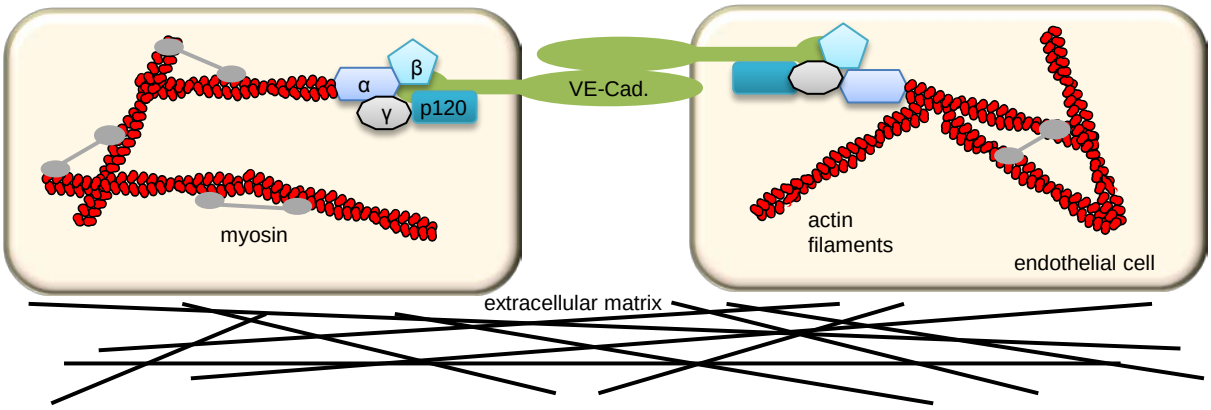

Figure 1 Regulation of the endothelial barrier. *Homophilic* VE-cadherin, the most prominent protein of IEJs, connects two adjacant endothelial cells, which are embeded in the extracellular matrix. Regulatory proteins (α-, β-, γ-, p120-catenin) link the intracellular part of VE-cadherin to cytoskeletal actin filaments. Cytoskeletal contraction is promoted through activation of myosin.

1.2.3 Barrier-disruptive signaling events

Typical mediators of the acute inflammatory response, such as thrombin and histamine, induce endothelial hyperpermeability via an activation of G-protein coupled receptors. Histamine activates the histamine (H)-1 receptor, which causes only a transient increase of permeability (5 min), whereas the serine protease thrombin induces a prolonged hyperpermeability (1 h) after cleavage and activation of its receptor, the protease-activated receptor (PAR)-1.[20] Alternatively to the serine protease thrombin, the thrombin receptor activating peptide (TRAP), mimicking the extracellular cleaved N-terminus of PAR, can be used for receptor activation.[21, 22] Both the activation of H-1 and PAR-1 lead to Ca^{2+} mobilization, protein kinase C (PKC) activation and mitogen-activated protein kinase (MAPK) signaling, whereas the small GTPase RhoA is exclusively activated by PAR-1 (**Figure 2**).[23]

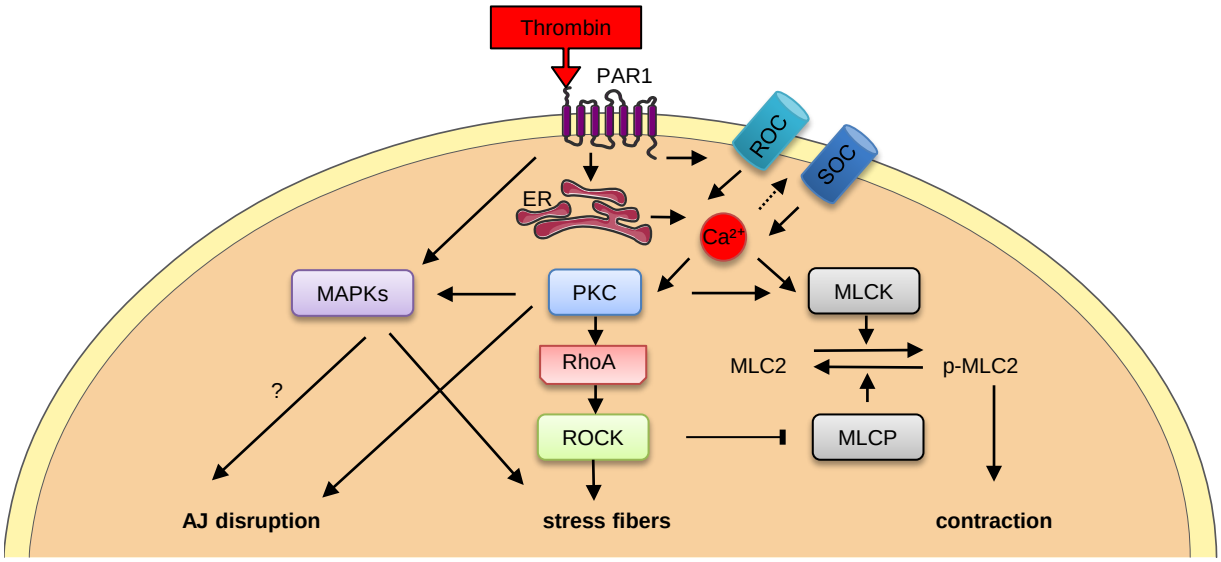

Figure 2 Thrombin-induced signaling transduction for endothelial hyperpermeability. Thrombin-induced PAR-1 cleavage activates MAPKs and elevates cytosolic Ca^{2+}. The subsequent activation of various signaling pathways induces stress fiber formation, an activation of the contractile machinery and the disassembly of AJs. For details see the following text passages.

1.2.3.1 Cytosolic calcium

Calcium is a ubiquitous second messenger with a central role in the regulation of endothelial permeability. Upon PAR-1 activation, phospholipase Cβ (PLCβ) catalyzes the production of inositol triphosphate (IP_3) and diacylglycerol (DAG) from phosphatidylinositol 4,5-bisphosphate (PIP_2).[15] IP_3 evokes an immediate release of Ca^{2+} from its endoplasmic stores, whereas DAG triggers the receptor-operated Ca^{2+} channel (ROC) influx through transient receptor potential channels (TRPC 3/6) from the extracellular compartment.[24] This first wave of Ca^{2+}, activates store-operated Ca^{2+} channels (SOCs) (TRPC 1/4), which further augment intracellular Ca^{2+} ($[Ca^{2+}]_i$) levels.[25]

Free cytosolic Ca^{2+} binds to calmodulin, which leads to an activation of the myosin light chain kinase (MLCK).[26] The main biological function of MLCK is the phosphorylation of MLC2 at S^{19} and subsequently at T^{18}.[27]

1.2.3.2 Protein kinase C

PKCs are a large family of serine/threonine kinases that are differentially regulated by Ca^{2+}, DAG or phospholipids. Despite the minor effects on the *basal* barrier properties of the endothelium, PKCs, especially the classical isoforms (PKC α, β), are described as important regulators of induced endothelial hyperpermeability.[28, 29] For example, it is known that PKC activates MLCK, and furthermore, promotes AJ disassembly.[30, 31] Additionally, PKC can induce RhoA activation through phosphorylation of immediate upstream regulators of RhoA.[13]

1.2.3.3 Mitogen-activated protein kinases

While extracellular signal-related kinase (ERK) predominantly controls cell proliferation, p38 and c-*jun* N-terminal kinase (JNK) are involved in the cellular stress response. The activation of MAPKs is regulated by an upstream phosphorylation cascade, where multiple kinases, as for example PKCs, are involved. Although the molecular mechanisms are not completely understood, it is evident that ERK and p38 contribute to the thrombin-induced endothelial hyperpermeability.[32, 33] Furthermore, it is known that p38 and its downstream target HSP27 are critical regulators of stress fiber formation and TNFα-induced hyperpermeability.[34] Moreover, a role for ERK as activator for MLCK has been hypothesized.[27] JNK was reported to be crucially involved in microvascular leakage and neutrophil accumulation *in vivo*.[35] Thus, also the best studied MAPKs (ERK, JNK and p38) are implicated in the permeability regulation.[35, 36]

1.2.3.4 RhoA GTPase

The family of small GTPases acts as molecular switches, cycling between an inactive GDP- and an active GTP-loaded state.[37] The activation of these GTPases is controlled by three different classes of proteins (**Figure 3**): (1) Guanine exchange factors (GEFs) that catalyze the substitution of GDP by GTP, (2) GTPase-activating proteins (GAPs) that hydrolyze GTP into GDP and phosphate and (3) guanine nucleotide dissociation inhibitors (GDIs) that stabilizes and sequesters inactive RhoA in the cytosol.[37] RhoGTPases modulate the organization and dynamics of the actin cytoskeleton and, thus they regulate endothelial barrier properties.[38, 39]

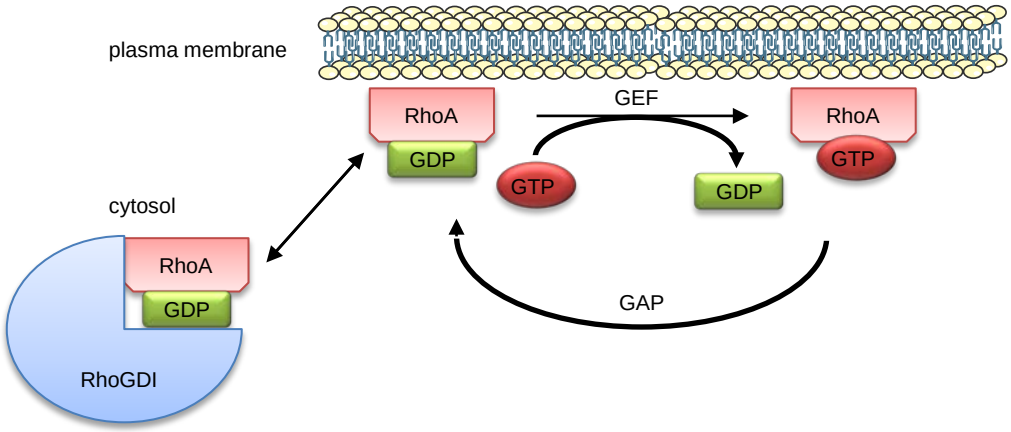

Figure 3 Regulation of RhoGTPase activity. Small GTPases like RhoA are stabilized in the inactive (GDP-bound) conformation by cytosolic RhoGDIs. Upon release from GDI binding, RhoA translocates to the plasma membrane, where it is converted to the activated (GTP-bound) form. The activation is promoted by GEFs. Inactivation occurs when GTP gets hydrolzed by GAPs.

Activation of RhoA increases endothelial permeability, whereas a certain *basal* RhoA activity is necessary for the physiological barrier function.[39] Upon thrombin treatment, PKCα either activates the specific p115-RhoGEF or inhibits RhoGDI-1, both leading to RhoA activation.[13] The subsequently induced cellular contraction, stress fiber formation and endothelial permeability are mediated through the activation of the RhoA downstream target RhoA kinase (ROCK).[40] ROCK inhibits the myosin light chain phosphatase (MLCP) by phosphorylation of the inhibitory myosin phosphatase targeting (MYPT) subunit 1.[23] Hence, MLCP inhibition extends and enhances the phosphorylation of MLC2 and, thus, acto-myosin-based contraction.

1.2.4 Barrier-protective signaling events

A broad variety of substances induces endothelial hyperpermeability, but only few are known that possess protective characteristics.[12] For example, phospholipids released from platelets tighten the endothelial barrier.[41] The typical assembly of an actin ring at the cell periphery, encompassing the plasma membrane, enhances the endothelial barrier. This cortical actin rim stabilizes the cell morphology and strengthens IEJs.[42]

1.2.4.1 cAMP

The second messenger cAMP is the most important signaling molecule that generally enhances endothelial barrier function (**Figure 4**).[12] Activation of the adenylyl cyclase (*e.g.* by forskolin) generates cAMP, which is subsequently degraded by phosphodiesterases (PDE). Increasing cAMP levels activate protein kinase A (PKA), which mediates the dephosphorylation of MLC2, leading to the dissociation of actin from myosin.[43, 44] More recently, a second mechanism independent of PKA was introduced: cAMP triggers the exchange protein directly affected by cAMP (EPAC)1 signaling cascade. EPAC1 is a GEF for the Ras-like GTPase Rap1, which induces the formation of cortical actin and the stabilization of AJs.[45] Interestingly, a recent study demonstrated that the RhoGTPase Rac1 is a hub for both the PKA- and the EPAC1-mediated barrier protective effects of cAMP.[46]

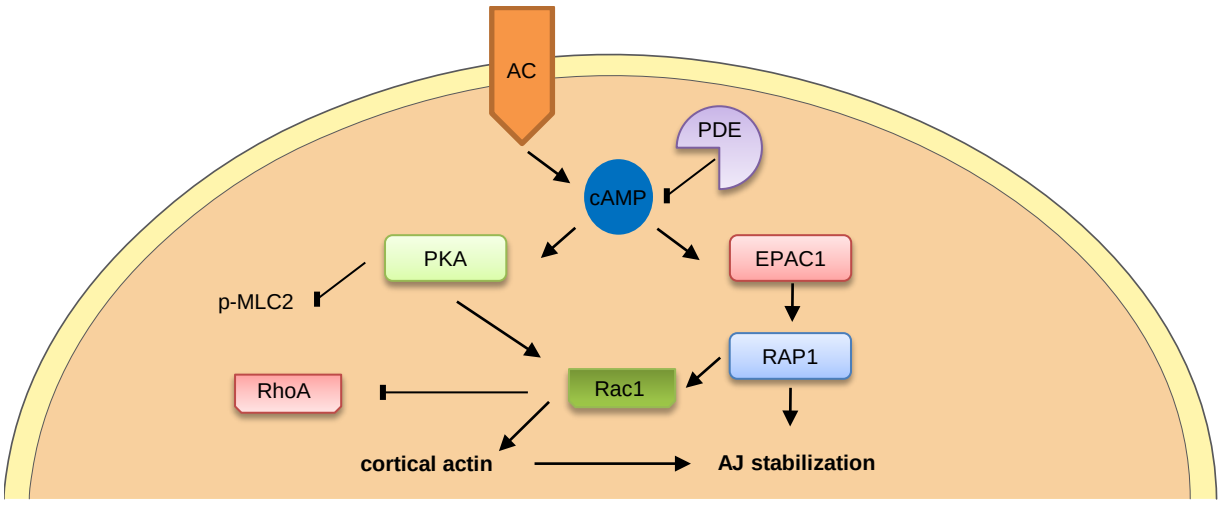

Figure 4 Signaling pathways of cAMP-dependent barrier stabilization. Upon its activation, the adenylyl cyclase (AC) initiates cAMP synthesis, whereas phosphodiesterases (PDE) degrade cAMP. cAMP induce both PKA- and EPAC1-dependent signaling pathways, which converge in Rac1 activation. Rac1 promotes endothelial barrier protection through the formation of cortical actin. For details see the text passage **1.2.4.1** and **1.2.4.2.**

1.2.4.2 Rac1 GTPase

Even though the activation pattern of Rac1 and RhoA is identical (see **1.2.3.4 RhoA GTPase**), both small GTPases fulfill antagonistic functions in terms of permeability regulation. Rac1 stabilizes the endothelial barrier under resting conditions and protects against inflammatory incitement. Rac1 induces a translocation of cortactin to the cell periphery, thus promoting a cortical actin assembly.[39] Furthermore, the Rac1 downstream target p21-activated kinase (PAK) activates LIM kinase (LIMK) 1. LIMK1 phosphorylates and inactivates the actin *severing* molecule cofilin, which further stabilizes cortical actin.[47] Finally, also a crosstalk between Rac1 and RhoA is suggested, as Rac1 activation was found to limit RhoA activity.[39]

1.2.5 Measurement of endothelial permeability

A variety of methods exist to determine endothelial permeability *in vivo* and *in vitro*. Quantitative measurements with classic *in vivo* approaches like the Miles assay,[48] where a colored dye is injected into the blood circulation, or the intravital microscopic measurement of the transvascular flux of labeled-macromolecules[49] are labor intensive and challenging to perform.[1] Complex molecular and pharmacological approaches are more easily addressable in cultured endothelial cells that allow a better control of experimental conditions. Cultured endothelial monolayers display many physiological properties of the endothelial barrier, including the expression of IEJs, a physiological electrical resistance, a selective size-dependent passage of macromolecules, endothelial polarity and the response to vasoactive agents.[20] Two techniques have been considered as gold standard throughout the last decades: the measurement of macromolecular permeability and the determination of the transendothelial resistance. More recently, C. Keese and the Nobel laureate I. Giaever introduced impedance sensing as alternative approach.[50]

1.2.5.1 Macromolecular permeability measurement

The transvascular solute flux is simulated with a Transwell® two-compartment *in vitro* model (compare chapter **2.4**). Malik and colleagues initially introduced the size-selective transport through endothelial pore equivalents (*i.e.* IEJs) to study endothelial barrier function.[51] In the absence of convective fluid flow, the permeation across an endothelial cell layer depends entirely on diffusive forces.[1] A labeled macromolecule is added to the upper compartment at a defined concentration, and its appearance in the lower

compartment is determined at fixed time points and used for quantification. Endothelial cells respond to permeability-inducing agonists, such as thrombin, with an increasing passage of macromolecules.[52]

1.2.5.2 Transendothelial electrical resistance

Lipophilic cell membranes function as electrical insulators that maintain the physiological membrane potential. Charge carriers (*i.e.* ions) in aqueous solution cross the endothelium through IEJs, which function as biological resistors. The resistance across an endothelial cell layer is referred to as transendothelial electrical resistance (TEER) and serves as measure for the ionic permeability of intercellular clefts. Changes of the TEER are determined according to Ohm's law by application of a constant direct current. For example, the treatment of endothelial cells with inflammatory mediators, like *e.g.* histamine or thrombin, causes a rapid drop of TEER values, which accounts for the induced endothelial hyperpermeability.[20]

1.2.5.3 Impedance measurement

Electric cell impedance sensing is a label-free method to study morphologic alterations of cultured cells on gold electrodes under real-time conditions. Impedance, also known as resistance in alternating currents, is a complex physical quantity consisting of an imaginary capacitive (membrane properties) and a real resistive (IEJ integrity) contribution (compare chapter **2.6**).[53] Thus, impedance sensing monitors changes of cellular morphology in terms of altered cell-electrode contacts.[54] The non-invasive impedance measurement offers a variety of applications, such as the investigation of cell growth, attachment and spreading, cell motility, *in situ* electroporation, cytotoxicity of compounds, cell differentiation, wound healing and migration or receptor stimulation, which all can be monitored in real-time with a temporal resolution ranging from seconds up to weeks.[55-62] Soon after its introduction, impedance measurement was utilized for the assessment of the endothelial barrier function.[63] The measured impedance is used as indicator for ionic permeability, comparable to TEER readings. However, this model is oversimplified as it does not account morphological changes that appear independently of IEJs. A profound validation of impedance measurement as alternative technique to monitor endothelial permeability is still missing to date.

1.3 Inhibitor of apoptosis proteins

As already indicated by their name, inhibitor of apoptosis proteins (IAPs) represent crucial regulators of cell death. Today, however, this is only one amongst many different cellular functions known for IAPs. They are also involved in cell proliferation, differentiation, cell morphogenesis, cell invasion, metastasis, immunity and inflammatory signaling.[64, 65]

1.3.1 IAP family

20 years ago, a gene that inhibits apoptosis in virus-infected *Spodoptera frugiperda* (engl. fall armyworm) cells was discovered and named *iap*.[66] The IAP family members are highly conserved in different organisms like yeast, nematodes, flies or higher vertebrates.[67] These proteins are characterized by the presence of a variable number of baculovirus IAP repeat (BIR) domains and their anti-apoptotic capacity. Up to date, there are 8 human homologues described: NAIP, survivin, livin, ILP-2, apollon, X-chromosomal linked IAP (XIAP), cellular IAP1 (cIAP1) and cellular IAP2 (cIAP2). The last three mentioned are the best-characterized mammalian representatives, on which we consequently focused on.[65]

1.3.2 Structure and function of IAPs

IAPs were first believed to be functionally restricted to the inhibition of apoptosis due to the discovery that the BIR domains bind and inhibit the proteolytic activity of caspases.[68] This view was extend and refined with the structural characterization of the distinct IAP domains.

XIAP, cIAP1 and cIAP2, each contain three N-terminal BIR domains, an ubiquitin-associated (UBA) domain as well as a really interesting new gene (RING) domain at the C-terminus. Both cIAPs additionally bear a caspase recruitment domain (CARD).

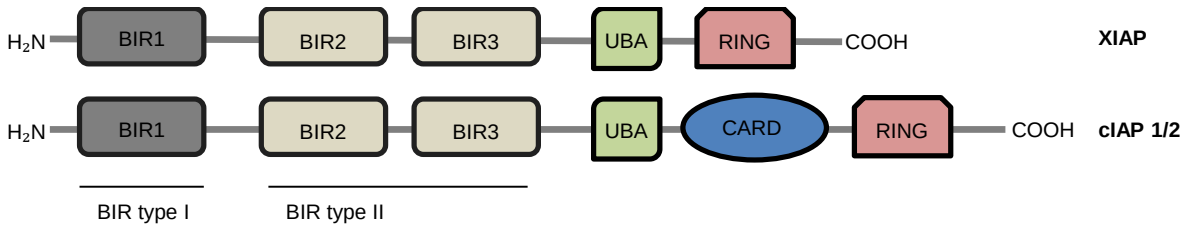

Figure 5 **Structural elements of IAPs.** BIR: baculoviral IAP repeat, UBA: ubiquitin-associated, CARD: caspase recruitment domain, RING: really interesting new gene. A describtion of the functional features of distinct domains is found in the subsequent text passage.

BIR domains can be divided into type I (BIR1) and II (BIR2, 3) depending on the appearance of a deep peptide-binding groove within their sequence. This hydrophobic cleft is only found in type II BIR domains and is responsible for the binding of special N-terminal peptide sequences called IAP-binding motifs (IBMs).[3] These IBMs are present in second mitochondria-derived activator of caspases (Smac), which is the endogenous IAP antagonist, and in caspases-3, -7 and -9.[69] Although XIAP, cIAP1 and cIAP2 were shown to bind these caspases, XIAP is the only inhibitor of caspases activity.[70] Of note, cIAPs regulate cell death not directly via caspases, but through inhibition of the ripoptosome. The ripoptosome is a recently discovered death-inducing complex, that assembles spontaneously upon cIAP depletion.[71] Type I BIR is not involved in the binding of caspases, but interacts with signaling adapter molecules, such as tumor necrosis factor (TNF)-associated factor (TRAF) 1 and 2, that are associated with TNF receptor signaling.[72] Summing up, BIR domains are versatile protein-protein interaction domains with diverse binding partners in apoptotic and signaling processes, despite their structural similarity.[69]

The RING domain possesses ubiquitin protein ligase (E3) activity. Ubiquitin (Ub) residues are transferred to target proteins in conjunction with an Ub activating enzyme (E1) and an Ub conjugating enzyme (E2).[73] Target selectivity is determined only by the substrate recognition through the respective E3 ligase. For example, IAPs, as E3 ligases, promote the ubiquitination of various substrates, like *e.g.* Rac1, caspases, Smac or IAPs themselves.[74-76] Different linkages of the mono- or poly-Ub residues determine the fate of the targeted protein. Recent findings indicate that K6-, K11-, K27-, K29-, K33- and K48-linked modifications promote proteasomal degradation.[77] In contrast, K63-linked and M1-linked Ub chains have a scaffolding function in the activation of kinases in NFκB signaling.[78]

The UBA domain binds to poly-Ub residues, thus affecting NFκB signaling.[79] Furthermore, CARD was recently determined as auto-inhibitory domain to suppress the E3 ligase activity of cIAP1.[80]

1.3.3 IAP antagonists

IAPs are expressed at elevated levels in various solid tumors including esophageal, hepatocellular, cervix, liver, lung and pancreatic cancer as well as in diverse hematological malignancies.[2, 81] Their crucial contribution for tumor cell survival and resistance development made IAPs attractive targets in cancer research. The approach to neutralize IAPs, led to the development of small molecule antagonists that mimick the endogenous IAP inhibitor Smac.[81]

Upon proapoptotic stimuli, Smac is liberated from its mitochondrial stores in order to bind cytosolic IAPs, which in turn leads to unimpeded caspase activation.[82] The first four N-terminal amino acids of Smac (AVPI), known as most prominent IBM, are essential for the binding to the BIR3 domain.[83]

Indeed, peptides derived from AVPI were proven to mimic the activity of the Smac protein and were consequently used to antagonize IAPs.[84] It was subsequently demonstrated that IAP antagonists induce apoptosis through degradation of cIAP1, NFκB activation and autocrine TNFα production.[76, 85] A recent study revealed that IAP antagonists induce a conformational change of cIAP1 prompting RING dimerization, thus mediating a rapid auto-ubiquitination and subsequent degradation of cIAP1.[86] In contrast, XIAP is not degraded upon treatment with Smac mimetics.[76]

As the therapeutic application of peptides is limited by their proteolytic stability, restricted cell permeation and poor pharmacokinetics, synthetic peptidomimetics with improved pharmacological properties were designed. Oost *et al*. used the IBM AVPFY, which binds to XIAP with 4-fold higher affinity than AVPI,[87] to generate four peptide libraries. Based on structure-activity relationship (SAR) studies, they identified a series of proteolytically stable, capped tripeptides.[88] One of these peptidomimetics, compound 11 (A 4.10099.1, in the following referred to as ABT), exhibited a high binding affinity to the XIAP BIR3 domain (K_d = 16 nM). ABT, depicted in **Fig. 6**, was used as IAP antagonist in this work.

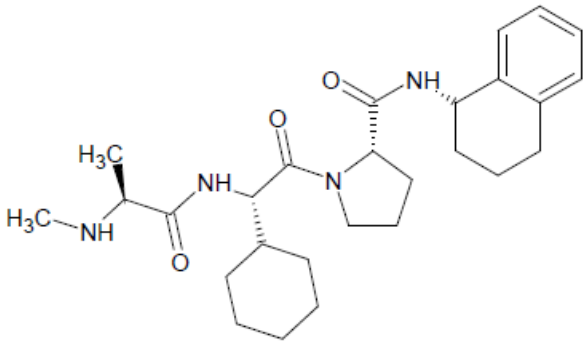

Figure 6 Structure of the IAP antagonist ABT. A 4.10099.1 (ABT) was synthesized and characterized in the publication Oost *et al.*(2004) as compound 11.

In general, IAP antagonists have demonstrated good anti-tumor properties in several *in vivo xenograft* models, showing no remarkable toxicity profile.[89] Notably, IAP antagonists do not induce a sensitization to apoptosis in normal primary cells, nor do they affect highly proliferative tissues in mice.[2, 90] Currently, there are at least five clinical trials in phase I evaluating the potential of small molecule IAP antagonists as cancer therapeutics.[2] Since IAPs are involved in various physiological processes, as the immune- or the inflammatory response, the targeting of IAPs might open up therapeutic strategies in other diseases than cancer.[91]

2 MATERIALS AND METHODS

2.1 Materials

2.1.1 ABT

The IAP antagonist A-4.10099.1, here referred as ABT, was previously characterized in Oost *et al.*.[88] It was kindly provided by Abbott Bioresearch Corp. (Worcester, MA, USA). The compound was dissolved in DMSO for complete solubilization at a concentration of 50 mM and stored at -80 °C for further use.

2.1.2 Smac085

The dimeric compound Smac085 (unpublished structure) was kindly provided by Prof. Pierfausto Seneci (Department of Organic and Industrial Chemistry, University of Milano, Italy). The substance was dissolved in DMSO for complete solubilization at a concentration of 10 mM and stored at -80 °C for further utilization.

2.1.3 Biochemicals, inhibitors, cell culture reagents and technical equipment

Table 1 Biochemicals

Reagent	Producer
Accustain® formaldehyde	Sigma-Aldrich, Taufkirchen, Germany
Amaxa™ Nucleofector HUVEC kit	Lonza, Cologne, Germany
BC Assay reagent	Interchim, Montulocon, France
Blebbistatin	Sigma-Aldrich, Taufkirchen, Germany
Non-fat dry milk powder (Blotto)	Carl Roth, Karlsruhe, Germany
Bovine Serum Albumin (BSA)	Sigma-Aldrich, Taufkirchen, Germany
Bradford reagent Roti®-Quant	Carl Roth, Karlsruhe, Germany
p-Coumaric acid	Sigma-Aldrich, Taufkirchen, Germany
DMSO	AppliChem, Darmstadt, Germany
ECL Plus WB Detection reagent	GE Healthcare, Munich, Germany
FITC-Dextran 40 kDa	Sigma-Aldrich, Taufkirchen, Germany
FluorSave™ Reagent mounting medium	Merck, Darmstadt, Germany
Forskolin	Enzo Life Sciences GmbH, Lörrach, Germany

Reagent	Producer
FURA-2 AM ester	Biotrend, Cologne, Germany
Glutathione-sepharose	Sigma-Aldrich, Taufkirchen, Germany
Histamine	Sigma-Aldrich, Taufkirchen, Germany
Luminol	Sigma-Aldrich, Taufkirchen, Germany
Page Ruler™ Prestained Protein Ladder	Fermentas, St. Leon-Rot, Germany
Protein A-agarose	Sigma-Aldrich, Taufkirchen, Germany
Protein G-agarose	Calbiochem, Darmstadt, Germany
Protein A/G-sepharose	Roche, Mannheim, Germany
Targefect HUVEC kit	Targeting Systems, El Cajon, CA, USA
Thrombin	Sigma-Aldrich, Taufkirchen, Germany
Thrombin receptor activating peptide (TRAP)	Mo-Bi-Tec, Göttingen, Germany
Triton X-100	Merck, Darmstadt, Germany
Tumor necrosis factor-α (TNFα)	PeproTech GmbH, Hamburg, Germany
Tween®20	BDH/Prolabo®, Ismaning, Germany
Y-27632 (hydrochloride)	Cayman Chemical, Ann Arbor, MI, USA

All other common biochemical substances were purchased from Sigma-Aldrich, AppliChem, Carl Roth or Merck.

Table 2 Inhibitors

Inhibitor	Producer
Aprotinin	Sigma-Aldrich, Taufkirchen, Germany
ß-glycerophosphate	Calbiochem, Darmstadt, Germany
Complete® mini EDTA free	Roche diagnostics, Penzberg, Germany
Leupeptin	Sigma-Aldrich, Taufkirchen, Germany
NaF	Merck, Darmstadt, Germany
Na_3VO_4	ICN Biomedicals, Aurora, OH, USA
Phenylmethylsulfonyl fluoride (PMSF)	Sigma-Aldrich, Taufkirchen, Germany

Table 3 Cell culture reagents

Reagent	Producer
Amphotericin B 250 µg/ml	AppliChem, Darmstadt, Germany
Collagen A/G	Biochrom AG, Berlin, Germany
Collagenase A	Roche, Mannheim, Germany
DMEM/High Glucose	PAA Laboratories, Pasching, Austria
Endothelial Cell Growth Medium (ECGM) with Supplement Mix #C-39215	PromoCell, Heidelberg, Germany
FCS gold	PAA Laboratories, Pasching, Austria
M199 Medium	PAA Laboratories, Pasching, Austria
Penicillin/Streptomycin 100x	PAA Laboratories, Pasching, Austria

Table 4 Technical equipment

Name	Device	Manufacturer
Axiovert 200	Inverted microscope	Zeiss, Jena, Germany
Cell culture flasks, plates, dishes	Disposable cell culture material	TPP, Trasadingen, Switzerland
Curix 60	Tabletop film developer	Agfa, Cologne, Germany
Ibidi µ-slides	Microscopy slides	Ibidi GmbH, Munich, Germany
LSM 510 META	Confocal laser scanning microscope	Zeiss, Jena, Germany
Mikro 22R	Table centrifuge	Hettich, Tuttlingen, Germany
Nanodrop® ND-1000	Spectrophotometer	Peqlab, Wilmington, DE, USA
Nucleofactor™ 2	Transfection device	Lonza, GmbH, Cologne, Germany
Odyssey 2.1	Infrared Imaging System	Li-COR Biosciences, Lincoln, NE, USA
Protein electrophoresis and blotting equipment	Unit, power supplies	Bio-rad, Munich, Germany
SpectraFluor™	Microplate multifunction reader	Tecan, Männedorf, Switzerland
Sunrise™	Microplate absorbance reader	Tecan, Männedorf, Switzerland
Custom-built TEER reader	Transendothelial resistance reader	Prof. Dr. W. Nagel, Munich, Germany
Transwell® plate (0.4 µm, Ø 12 mm, PET)	Two-compartment permeability assay	Corning, New York, USA

Name	Device	Manufacturer
Vi-Cell™ XR	Cell counter	Beckman Coulter, Fullerton, CA, USA
xCELLigence™ DP	Real-Time Cell Analyzer	Roche Diagnostics, Mannheim, Germany

2.2 Cell culture

2.2.1 Cell culture solutions and reagents

The following solutions were used for the isolation and cultivation of endothelial cells.

Table 5 Cell culture buffers

PBS (pH 7.4)	
NaCl	132.2 mM
Na_2HPO_4	10.4 mM
KH_2PO_4	3.2 mM
H_2O	

PBS$^+$ Ca^{2+}/Mg^{2+} (pH 7.4)	
NaCl	137 mM
KCl	2.7 mM
Na_2HPO_4	8.1 mM
KH_2PO_4	1.5 mM
$CaCl_2$	0.7 mM
$MgCl_2$	0.5 mM
H_2O	

HEPES (pH 7.4)	
NaCl	125 mM
KCl	3 mM
NaH_2PO_4	1.25 mM
$CaCl_2$	2.5 mM
$MgCl_2$	1.5 mM
Glucose	10 mM
HEPES	10 mM
H_2O	

Table 6 Cell culture solutions

Endothelial Cell Growth Medium	
ECGM	500 ml
Supplement Mix #C-39215	23.5 ml
FCS gold	50 ml
Amphothericin B (250 µg/ml)	5 ml
Penicillin (10,000 U/ml)/ Streptomycin (10 mg/ml)	5 ml

Stopping medium	
M 199 Medium	500 ml
FCS gold	50 ml

DMEM/High Glucose	
DMEM	500 ml
glucose	4.5 g/ml

Collagen G	
Collagen G	0.001 %
PBS	

Freezing medium	
FCS gold	50 %
DMSO	8 %
ECGM	

Trypsin/EDTA (T/E)	
Trypsin	0.05 %
EDTA	0.20 %
PBS	

Annotation: FCS gold (fetal calves serum) was partially thawed for 30 min at room temperature, and subsequently fully thawed at 37 °C. For heat inactivation it was kept at 56 °C for 30 min. Aliquots of FCS were stored at -20 °C.

2.2.2 Endothelial cells

Endothelial cells (ECs) were cultured in an incubator (Heraeus, Hanau, Germany) at 37 °C with 5 % CO_2. Routine tests for mycoplasma contamination were performed with the PCR detection kit Venor®GeM (Minerva Biolabs, Berlin, Germany). All utilized cell culture flasks, dishes and multiwell-plates were coated before use with Collagen G at least 20 min.

2.2.2.1 HMEC-1 (Human dermal microvascular endothelial cells)

The cell line CDC/EU.HMEC-1 was kindly provided by the Centers for Disease Control and Prevention (Atlanta, GA, USA). The immortalized HMEC-1 cell line was developed by transfecting human dermal microvascular endothelial cells with a plasmid coding for the

transforming SV40 large T-antigen. HMECs maintain endothelial morphology, phenotype, and functional characteristics.[92, 93] HMECs were exclusively used for macromolecular permeability assays and impedance measurement.

2.2.2.2 HUVECs (Human umbilical vein endothelial cells)

Human umbilical cords were kindly provided by Klinikum München Pasing, Frauenklinik München West/Krüsmannklinik, Rotkreuzklinikum München and Wolfart Klinik Gräfelfing. Immediately after childbirth, umbilical cords were stored in PBS^+ Ca^{2+}/Mg^{2+} containing penicillin (100 U/ml)/streptomycin (100 µg/ml) at 4 °C. HUVECs were freshly isolated every week. The umbilical veins were washed with PBS^+ Ca^{2+}/Mg^{2+}, filled with 0.1 g/l collagenase A, and incubated for 45 min at 37 °C. To extract endothelial cells, the veins were flushed with stopping medium and the cell suspension was centrifuged (1,000 rpm, 5 min). Then, HUVECs were resuspended and carefully vortexed in growth medium and plated in a 25 cm^2 flask (passage #0). After reaching confluency, cells were trypsinized and plated in a 75 cm^2 flask (passage #1). Cells were used until passage #3 for experiments.

2.2.3 Passaging

Confluent cells were either sub-cultured 1:3 in 75 cm^2 culture flasks or plated for experiments in multiwell-plates, dishes or ibidi µ-slides. For passaging, growth medium was removed; cells were washed twice with PBS and were afterwards incubated with trypsin/EDTA (T/E) for 1-2 min at 37 °C. The detached cells were collected in stopping medium, which terminated the enzymatic reaction. After centrifugation (1,000 rpm, 5 min, room temperature), the pellet was resuspended in growth medium and cells were plated.

2.2.4 Freezing and thawing

Before freezing, confluent HMECs cultured in a 75 cm^2 flask were trypsinized, centrifuged (1,000 rpm, 5 min, room temperature) and resuspended in 3 ml ice-cold freezing medium. 1.5 ml aliquots were frozen in cryovials. After an initial storage at -80 °C for 24 h, aliquots were transferred into liquid nitrogen tanks for long-term storage.

For thawing of cells, a cryovial was heated to 37 °C and the content was immediately mixed with growth medium at 37 °C. Before seeding in a 75 cm^2 culture flask, the DMSO-containing freezing medium was removed by centrifugation and resuspension in growth medium.

2.3 Western blot analysis

2.3.1 Preparation of total cell lysates

HUVECs were grown until reaching confluency in 60 mm dishes and then treated as indicated. Cells were washed once with PBS and afterwards lysed in a modified RIPA lysis buffer. Next, cells were stored at -80 °C until further usage. After thawing on ice, cells were carefully scraped off, transferred to Eppendorf tubes (Peske, Aindling-Arnhofen, Germany) and centrifuged (14,000 rpm, 10 min, 4 °C). The protein concentration of the supernatant was determined by performing a Bradford assay or Pierce assay (only before immunoprecipitation and pull-down experiments). The remaining samples were mixed with either mercaptoethanol sample buffer (3x) or DTT sample buffer (5x) and finally heated at 95 °C for 5 min. Until Western blot analysis, samples were stored at -20 °C.

Table 7 Cell lysis buffer

Modified RIPA buffer	
Tris/HCl (pH 7.4)	50 mM
NaCl	150 mM
Nonidet NP 40	1 %
Deoxycholic acid	0.25 %
SDS	0.1 %
Na_3VO_4	0.3 mM
NaF	1.0 mM
β-Glycerophosphate	3.0 mM
Pyrophosphate	10 mM
H_2O	
Complete® EDTAfree	4.0 mM
PMSF	1.0 mM
H_2O_2	600 µM

Table 8 Sample buffers

5x DTT sample buffer	
Tris/HCl (pH 6.8)	3.125 M
Glycerol	10 ml
SDS	5 %
DTT	2 %
Pyronin Y	0.025 %
H_2O	

3x Mercaptoethanol sample buffer	
Tris/HCl	187.5 mM
Glycerol	30 %
SDS	6 %
Bromphenol blue	0.025 %
H_2O	
ß-mercaptoethanol	12.5 %

2.3.2 Protein quantification

In order to obtain equal amounts of protein in all samples, a quantification of the total protein content was performed before Western blot analysis. The Bradford assay was exerted as standard procedure, whereas the Pierce assay was performed prior to immunoprecipitation and pull-down experiments. After determining the samples' differences in protein content, the concentration was adjusted to the lowest concentration either with (1x) mercaptoethanol - or with (1x) DTT sample buffer.

2.3.2.1 Bradford assay

The Bradford assay was performed as previously described.[94] It is based on binding of Coomassie Brilliant Blue G250 to amino acids, which can then be detected photometrically. 10 µl protein sample were incubated with 190 µl Bradford solution (Roti®-Quant Bradford Reagent, Carl Roth, Karlsruhe, Germany, 1:5 dilution in water) for 5 min upon shaking. Afterwards, the absorbance was measured at 592 nm (Tecan Sunrise™ reader, TECAN, Männedorf, Switzerland). A stock solution of bovine serum albumin (BSA) (2 mg/ml) was stepwise diluted and then used as protein standard. The actual protein concentration of each sample was determined by linear regression.

2.3.2.2 Pierce assay (Bicinchonic acid assay)

The bicinchoninic acid (BCA) assay was described previously.[95] It is based on a colorimetric detection of a protein-dependent copper reduction under alkaline conditions. 10 µl protein sample were incubated with 200 µl BCA reagent (Interchim, Montulocon, France) at 37 °C for 30 min. The absorbance of the colored Cu^{1+}- complex was measured

at 550 nm (Tecan Sunrise™ reader, TECAN, Männedorf, Switzerland). The creation of protein standards was described in the section Bradford assay.

2.3.3 SDS-PAGE electrophoresis

Proteins were separated by discontinuous SDS-polyacrylamide gel electrophoresis (SDS-PAGE) as described by Laemmli.[96] Equal amounts of protein were loaded on polyacrylamide gels, which were composed of a separating and a stacking gel. Depending on their mass, proteins were separated using the Mini-PROTEAN 3 electrophoresis module (Bio-Rad, Munich, Germany). In order to achieve an optimal separation, the concentration of acrylamide (Rotiphorese™ Gel 30, Carl Roth, Karlsruhe, Germany) in the separating gel was adapted to the molecular weight of the protein of interest (**Table 9**). Electrophoresis was run at 100 V for 21 min for protein stacking, and at 200 V for about 45 min for protein separation. The molecular weight of protein bands was indicated by a pre-stained protein ladder (PageRuler™, Fermentas, St. Leon-Rot, Germany).

Table 9 Acrylamide gels

Protein	Acrylamide concentration
VE-cadherin, p-VE-cad., MYPT, p-MYPT	7.5 %
ß-actin, cIAP1/2, XIAP, ERK, p-ERK, p38, p-p38, JNK, p-JNK, p-PKC substrates	10 %
MLC2, p-MLC2, pp-MLC2, RhoA, Rac1	15 %

Separating gel 7.5, 10, 15 %	
Rotiphorese™ Gel 30	25/33.3/50 %
Tris (pH 8.8)	375 mM
SDS	0.1 %
TEMED	0.1 %
APS	0.05 %
H_2O	

Stacking gel	
Rotiphorese™ Gel 30	17 %
Tris (pH 6.8)	125 mM
SDS	0.1 %
TEMED	0.2 %
APS	0.1 %
H_2O	

Table 10 Electrophoresis buffer

Electrophoresis buffer	
Tris	4.9 mM
Glycine	38 mM
SDS	0.1 %
H_2O	

2.3.4 Tank electroblotting

After mass-dependent separation by SDS-PAGE, proteins were electroblotted onto a nitrocellulose membrane (Hybond-ECL™, Amersham Bioscience, Freiburg, Germany).[97] Inside a tank filled with 1x tank buffer, the nitrocellulose membrane was placed over the separating gel and then clamed together in between pads and blotting paper in a sandwich-like structure. The membrane was equilibrated before it's use with 1x tank buffer for 20 min. Proteins attached to SDS migrate towards the anode. Sandwiches were mounted in the Mini Trans-Blot® system (Bio-Rad, Munich, Germany), ice-cold 1x tank buffer was filled in the chamber and a cooling pack was inserted to avoid excessive warming. The protein transfer was performed at 4 °C, 100 V for 90 min.

Table 11 Tank blotting buffer

5x Tank buffer	
Tris base	240 mM
Glycine	195 mM
H_2O	

1x Tank buffer	
5x tank buffer	20 %
Methanol	20 %
H_2O	

2.3.5 Immunological detection of proteins

At first, unspecific protein-binding sites were blocked. For this purpose, the membrane was incubated for 2 h at room temperature in either non-fat dry milk powder (Blotto) 5 % or BSA 5 %. Afterwards, the immunological detection of the protein of interest was achieved through incubation with the respective primary antibody solution at 4 °C overnight (**Table 13**). After four washing steps (5 min each) with PBS containing 0.1 % Tween® 20 (PBS-T), the membrane was exposed to the secondary antibody solution, followed by four additional washing steps with PBS-T (5min each) and one repeat with

PBS only (5 min). All incubation steps were performed under gentle agitation. The protein-antibody complexes were detected with two different methods, depending on the labeling of the secondary antibodies (**Table 14**): enhanced chemiluminescence or infrared imaging.

2.3.5.1 Enhanced chemiluminescence (ECL) detection

Membranes were incubated for 2 h with a horseradish peroxidase (HRP)-conjugated secondary antibody. HRP is a catalyst for the cleavage of luminol together with H_2O_2 under the emission of light. The membranes were either incubated with homemade ECL solution for 3 min or with commercially available ECL solution for 1 min (ECL Plus Western Blotting Detection Reagent RPN 2132, GE Healthcare, Munich, Germany). The appearing luminescence was detected by exposure of the membrane to a X-ray film (Super RX, Fuji, Düsseldorf, Germany). After a certain exposition time, the film was developed with the Curix 60 Developing system (Agfa-Gevaert AG, Cologne, Germany).

Table 12 ECL solution

Homemade ECL	
Tris base (pH 8.5)	100 mM
Luminol	2.5 mM
p-Coumaric acid	1 mM
H_2O_2	17 µM
H_2O	

2.3.5.2 Infrared imaging

Moreover, secondary antibodies coupled to Alexa Fluor® 680 (emission at 700 nm) and IRDye™ 800 (emission at 800 nm) were used. Under exclusion of light, membranes were incubated for 1 h and subsequently washed as described above. Protein bands were detected with the Odyssey imaging system (Li-COR Biosciences, Lincoln, NE, USA).

Table 13 Primary antibodies

Antigen	Source	Dilution	In	Provider
β-actin	mouse monoclon.	1:1,000	Blotto 5 %	Millipore
cIAP1	goat polyclon.	1:1,000	Blotto 2 %	Epitomics
cIAP2	rabbit monoclon.	1:500	BSA 5 %	R&D systems
c-Myc	mouse monoclon.	1:1,000	Blotto 5 %	Santa Cruz
p-ERK$^{T202/Y204}$	mouse monoclon.	1:1,000	BSA 5 %	Cell Signaling
ERK	rabbit polyclon.	1:1,000	BSA 5 %	Cell Signaling
FLAG	mouse monoclon.	1:100	Blotto 5 %	Sigma Aldrich
p-JNK$^{T183/Y185}$	mouse monoclon.	1:500	BSA 5 %	Cell Signaling
JNK	rabbit polyclon.	1:500	BSA 5 %	Cell Signaling
pp-MLC2$^{T18/S19}$	rabbit polyclon.	1:1,000	BSA 5 %	Cell Signaling
p-MLC2^{S19}	mouse monoclon.	1:1,000	Blotto 5 %	Cell Signaling
MLC2	rabbit polyclon.	1:500	Blotto 5 %	Santa Cruz
p-MYPT1^{T696}	rabbit polyclon.	1:1,000	Blotto 5 %	Santa Cruz
MYPT1	rabbit polyclon.	1:1,000	Blotto 5 %	Santa Cruz
p-p38$^{T180/Y182}$	rabbit polyclon.	1:1,000	BSA 5 %	Cell Signaling
p38	rabbit polyclon.	1:1,000	BSA 5 %	Cell Signaling
p-PKC substrates	rabbit polyclon.	1:1,000	BSA 5 %	Cell Signaling
Rac1	mouse monoclon.	1:1,000	BSA 3 %	Thermo Fisher
RhoA	rabbit monoclon.	1:750	BSA 3 %	Thermo Fisher
p-VE-cadherin^{Y731}	rabbit polyclon.	1:1,000	BSA 3 %	Biosource
VE-cadherin	mouse monoclon.	1:1,000	Blotto 5 %	Santa Cruz
XIAP	mouse monoclon.	1:1,000	Blotto 5 %	BD Biosciences

Table 14 Secondary antibodies

Antibody	Dilution	In	Provider
Alexa Fluor® 680 goat anti-mouse	1:20,000	Blotto 1 %	Molecular Probes
IRDye™ 800CW goat anti-rabbit	1:20,000	Blotto 1 %	LI-COR Bioscie.
Donkey anti-goat: HRP	1:1,000	Blotto 1 %	Santa Cruz
Goat anti-mouse IgG1:HRP	1:1,000	Blotto 1 %	Biozol
Goat anti-mouse IgG2b:HRP	1:1,000	Blotto 1 %	Southern Biotech.
Goat anti-rabbit: HRP	1:1,000	Blotto 1 %	Dianova
Goat anti-rabbit: HRP	1:1,000	Blotto 5 %	Thermo Fisher

2.4 Macromolecular permeability measurement

Filter membranes of Transwell® plate inserts (pore size 0.4 µm, 12 mm diameter, polyester membrane, Corning, New York, USA) were coated with collagen G. The lower chambers were filled with 1.5 ml ECGM. 500 µl HMECs in suspension with ECGM (0.125×10^6 cells/well) were seeded onto the upper compartment and grown to confluence for 24-48 h. Cells were treated as indicated following two different schemes: 1) Generally, the different inhibitors were pre-incubated for 30 min, before FITC-dextran (40 kDa, 1 mg/ml; Sigma-Aldrich, Taufkirchen, Germany) was added to the upper compartment at t = 0 min. Subsequently, thrombin receptor activating peptide (TRAP) (Mo-Bi-Tec, Göttingen, Germany) or media control was added. 2) Alternatively, cells were loaded initially with FITC-dextran (t = 0 min). Thereupon, the compound of interest was added. In both cases, samples were taken from the lower compartment at indicated time points (**Fig. 7**). The fluorescence intensity (excitation 485 nm; emission 535 nm) of the samples was measured with a microplate reader (SpectraFluor Plus, Tecan, Männedorf, Switzerland). The mean fluorescence of untreated cells at the final time point was set as 1. Data are expressed as relative changes compared to control levels.

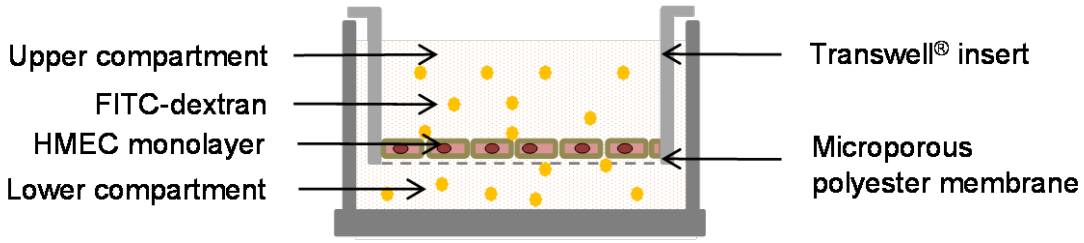

Figure 7. Drawing of a single Transwell® plate insert to determine macromolecular permeability. After treatment, the upper compartment was loaded with FITC-dextran (40 kDa). At different points in time, the flux of the tracer across an HMEC monolayer and a microporous membrane was determined by picking of samples from the lower compartment.

2.5 Transendothelial electrical resistance (TEER)

Intercellular junctions limit the net ion flux across endothelial cell layers, and thus function as biological resistors. TEER measurement was performed with an Ussing-like chamber, engineered and custom-built by Prof. Dr. W. Nagel (Department of Physiology, LMU Munich, Germany).[98, 99] HUVECs (0.24 x 10^6 cells/well) were seeded onto collagen A-coated Millicell® polycarbonate filter (PCF) inserts (pore size 0.4 µm, 12 mm diameter, Merck Millipore, Darmstadt, Germany) and grown to confluence for 24 h. The device was pre-heated to 37 °C for 90 min. Cell inserts were carefully placed into the chamber, which was subsequently filled with HEPES + 10 % FCS buffer. Bidirectional square current pulses of 50 µA (200 ms duration) were applied every third second. A custom-built voltage/current clamp unit in connection with a computer-supported evaluation program was utilized to calculate TEER according to Ohm's law. HUVECs were treated with ABT 30 min in prior to TRAP exposure. The device's and medium's own resistance was determined after addition of Triton X-100 (Merck, Darmstadt, Germany), which was then subtracted to obtain the cell-specific resistance. The resistance immediately before TRAP addition was used as control and therefore set as 100 %.

2.6 Impedance measurement

Real-time measurement of impedance was performed with the xCELLigence™ Real-Time Cell Analyzer (RTCA) DP (Roche Diagnostics, Mannheim, Germany) consisting of a RTCA DP Analyzer, a personal computer-based RTCA control unit and disposable E-Plates 16. The manufacturer's instruction was the basis of all performed experiments. Solid gold E-plate 16 electrodes were coated with collagen G for 30 min, then drained and refilled with 100 µl ECGM for impedance background measurement. HMECs were seeded at a density of 40,000 cells/well on the electrodes. After sedimentation of cells at room temperature for 30 min, E-Plates were placed into the RTCA DP Analyzer for recording impedance, which is expressed as Cell Index (CI) values. CI is a dimensionless parameter based on relative impedance changes. Of note, xCELLigence™ utilizes three different AC frequencies (10, 25, and 50 kHz) to measure CI levels. Initial CI values are determined by electric conductance of the medium only, but then CI values rise upon increasing cell-electrode contacts. These are caused at an early stage by cell sedimentation and spreading and later on by cell proliferation. Experiments were performed at constant CI levels, indicating confluence of the cell monolayer. After treating cells as indicated, alterations of CI values occurred from changes of the cell morphology, altered cell-cell, or cell-substratum contacts (**Fig. 8**). CI levels were recorded every 15 min to monitor cell growth, but was accelerated up to every 10 s directly before treatment for a time range of about 4 h.

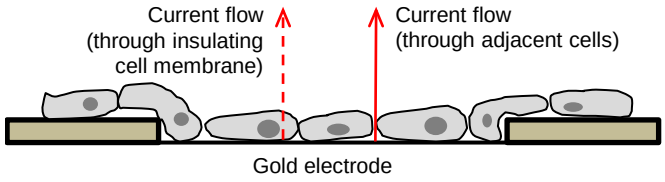

Figure 8. Principle of impedance measurement. The applied alternating current (AC) passes in dependence of the AC frequency either through intercellular clefts (at lower frequencies) or through the cell body (at higher frequencies).

2.7 Transfection of cells

HUVECs were transiently transfected with the indicated siRNAs, thus initiating RNA interference (*RNAi*), or with plasmids encoding for wild type or mutant proteins, hence inducing protein overexpression. The work of the Nobel Laureates Fire and Mello introduced *RNAi* as efficient method to induce gene silencing.[100] Electroporation with the Amaxa™ HUVEC Nucleofector kit and device (Lonza, Cologne, Germany) was used exclusively to introduce siRNA, whereas the non-lipid cationic Targefect-HUVEC kit (Targeting Systems, El Cajon, CA, USA) was used for the delivery of both siRNA and plasmids. Cells were used for Western blot, immunocytological staining, and precipitation experiments 24 h or 48 h *post* transfection.

2.7.1 Transfection with siRNA

For gene silencing, smartpool siRNAs of XIAP (ON-TARGETplus SMARTpool, Human BIRC4; Thermo Scientific, Dreieich, Germany) and cIAP1 (ON-TARGETplus SMARTpool, Human BIRC2; Thermo Scientific), each consisting of four different siRNA sequences, were used. Non-targeting siRNA (ON-TARGETplus siCONTROL; Thermo Scientific) was used as control. The siRNAs were suspended in 1x siRNA buffer (Thermo Scientific) and stored as aliquots at -80 °C. The siRNA concentration was verified with NanoDrop® (Peqlab, Wilmington, DE, USA).

For Amaxa™-based transfections, 2 x 10^6 HUVECs were suspended in 100 µl HUVEC Nucleofector solution, 10 µl of the corresponding siRNA (20 µM) was added and then transfected (program A-034). After addition of pre-warmed cell culture medium (900 µl), cells were cultured under standard conditions for further use.

For RNA silencing with the Targefect-HUVEC kit (Targeting systems), approximately 2 x 10^6 HUVECs were seeded into 25 cm^2 cell culture flasks. After 24 h, cell growth medium was replaced by 2.5 ml DMEM/High Glucose and the transfection complex was added drop wise. This complex consists of DMEM/High Glucose (600 µl), the respective siRNA (29 µl, 20 µM), Targefect F2 (14 µl) and Virofect (30 µl), all mixed by only flicking. Subsequently, the complex was activated at 37 °C for 20 min. After 90 min on cells, the transfection complex was replaced by growth medium. After another 24 h in a 25 cm^2 flask, cells were re-seeded in their final container and were ready for examination.

2.7.2 Transfection of plasmids

In order to induce overexpression of RhoA in HUVECs the Targefect-HUVEC kit (Targeting Systems) was utilized. Therefore, the following plasmids were purchased from Addgene (Cambridge, MA, USA): pcDNA3-EGFP (plasmid 13031), pcDNA3-EGFP-RhoA wild-type (plasmid 12965). 50 x 10^3 HUVECs were seeded into µ-slides (Ibidi GmbH, Martinsried, Germany) for 24 h. After one washing step with DMEM/High Glucose, cells were incubated with the Targefect transfection complex for 90 min. The transfection complex for one single well consists of DMEM/High Glucose (110 µl), the respective plasmid (10 ng), Targefect F2 (0.7 µl) and Peptide Enhancer (2.1 µl). The complex was mixed by only flicking and heat-activated for 25 min at 37 °C. After the incubation time, the complex was removed and cells were cultured for 24 h under normal conditions and were then used for F-actin staining.

Transfection of HEK 293T cells with pRK5-Myc-RhoA wild-type (Addgene, Cambridge, MA, USA), pRK5-Myc-RhoA Q63L (Addgene), pRK5 N19T (Addgene), pEGZ-Flag-EV (cloned in the Rajalingam lab) and pEGZ-Flag-XIAP (Rajalingam lab) was carried out with GeneJuice® transfection reagent (Novagen®, Merck Millipore, Schwalbach, Germany), at a final concentration of 1 µg/ml. The transfection of HEK 293T cells and the subsequent immunoprecipitation experiments were kindly performed by T. Oberoi from the group of Dr. K. Rajalingam, Institute for Biochemistry II, Goethe-University Medical School, Frankfurt/Main, Germany.

2.8 Immunofluorescence and confocal laser scanning microscopy

HUVECs were cultured until confluence on collagen G-coated 8 well µ-slides (ibidi, Martinsried, Germany). Cells were treated as indicated, washed once with warm PBS+ and fixed with 4 % Accustain® paraformaldehyde (Applichem, Darmstadt, Germany) at room temperature for 10 min. After three washing steps with PBS, HUVECs were permeabilized for 2 min with 0.2 % Triton X-100/PBS and again washed three times. Unspecific antibody binding is prevented by blocking with 0.2 % BSA/PBS for 20 min. The primary antibodies in 0.2 % BSA/PBS were added over night at 4 °C. After three washing steps with PBS, cells were incubated for 45 min at room temperature with the respective AlexaFluor®-labeled secondary antibodies or rhodamine-phalloidin for F-actin staining in 0.2 % BSA/PBS. Finally, cells were washed again three times with PBS, then situated in FluorSave™ Reagent mounting medium (Merck, Darmstadt, Germany) and covered with 8 mm x 8 mm glass coverslips (custom made by Helmut Saur Laborbedarf, Reutlingen, Germany). Samples were stored protected from light at 4 °C.

Images were acquired with a Zeiss LSM 510 META confocal microscope (40x or 63x oil objective, Zeiss, Oberkochen, Germany).

Table 15 Primary antibodies

Antigen	Source	Dilution	In	Provider
pp-MLC2$^{T18/S19}$	rabbit polyclon.	1:400	BSA 0.2 %	Cell Signaling

Table 16 Secondary antibodies

Antibody/dye	Dilution	In	Provider
Alexa Fluor® 488 goat anti-rabbit IgG (H+L)	1:400	BSA 0.2 %	Molecular Probes
rhodamine-phalloidin	1:400	BSA 0.2 %	Molecular Probes

2.9 Affinity precipitation of small GTPases

The affinity precipitation (also called pull-down assay) is a fast tool to monitor the activation state of small GTPases.[101, 102] Only the active, GTP-bound form can interfere with its specific downstream effector (**Fig. 9**). In this approach, the effector's GTPase-binding domain is expressed as recombinant fusion protein with glutathione S-transferase (GST). Glutathione agarose beads bind (or pull down) the GST fusion proteins, where the activated GTPases are attached. After washing and centrifugation steps, the activated GTPases are separated from the total cell lysate and can be analyzed by Western blot.

The activation state of RhoA and Rac1 were analyzed with active pull-down and detection kits (Thermo Scientific, Dreieich, Germany). HUVECs were grown until confluence in 100 mm dishes and then treated as indicated. The experiments were conducted after the manufacturer's instructions. The provided lysis/binding/washing buffer was supplemented with aprotinin (10 µg/ml), leupeptin (10 µg/ml) and PMSF (1 mM). Of note, the entire experiment was performed exclusively at 4 °C. The Pierce assay was performed in order to correctly adjust the protein content. A part of the RhoA and Rac1 affinity precipitations was kindly performed by S. Leonhardt during her Master thesis in the Vollmar lab, Department of Pharmacy, Pharmaceutical Biology, LMU Munich, Germany.

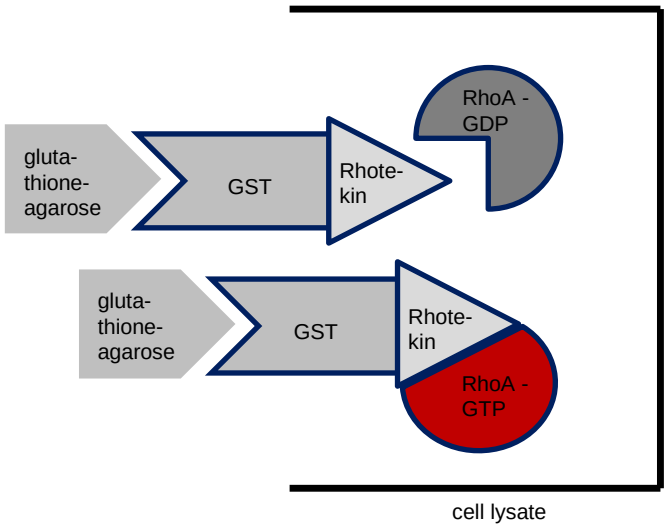

Figure 9. Principle of a RhoA affinity precipitation. Active, GTP-loaded RhoA binds selectively to a Rhotekin-GST fusion protein. Rhotekin is a specific RhoA downstream effector. The complex is pulled down by glutathione-agarose beads and analyzed by Western blotting.

2.10 Immunoprecipitation

Physical protein interaction was determined by immunoprecipitation experiments. HUVECs were grown until confluence in 60 mm cell culture dishes and then treated as indicated. Of note, the lysis/binding/washing buffer of the RhoA pull-down kit (Thermo Fisher, Dreieich, Germany), supplemented with aprotinin (10 µg/ml), leupeptin (10 µg/ml) and PMSF (1 mM) was used. Cells were scrapped off and transferred into Eppendorf caps, vortexed vigorously and incubated on ice for 5 min. Thereafter, the cell lysate was centrifuged (16,000 g, 15 min, 4 °C) and the protein concentration of the supernatant was adjusted using the Pierce method. Subsequently, 5 µl of the respective precipitation antibody was added and samples were kept under gentle agitation at 4 °C overnight. Protein A (Sigma Aldrich, Taufkirchen, Germany)-agarose beads (for rabbit IgG) and protein G (Calbiochem, Darmstadt, Germany)-agarose beads (for mouse IgG) were washed with lysis/binding/washing buffer and 60 µl bead suspension was added to each sample. After 3 h incubation, under constant agitation at 4 °C, the beads were centrifuged (14,000 g, 45 s, 4 °C) and the supernatant was collected as binding control. The bead pellet was washed three times with 500 µl lysis/binding/washing buffer and was again centrifuged (14,000 g, 45 s, 4 °C). Next, samples were filled up with 25 µl (3x)- and 25 µl (1x)-mercaptoethanol sample buffer and heated to 95 °C for 5 min. Samples were stored at -20 °C until Western blot analysis was performed.

For detection of RhoA-XIAP interaction after overexpression, the co-transfected HEK 293T cells were lysed 48 h post transfection with lysis buffer as previously described.[103] Myc-tagged RhoA was then incubated overnight with an anti-Myc antibody (Santa Cruz, Heidelberg, Germany). The antigen-antibody complex was precipitated with sepharose-coupled protein A/G beads (Roche, Mannheim, Germany), and purified by several washing steps with lysis buffer. Proteins were identified with Western blot analysis. The immunoprecipitation of RhoA-XIAP in co-transfected HEK 293T cells was kindly performed by T. Oberoi from the group of Dr. K. Rajalingam.

2.11 GST pulldown assay

GST fusion proteins of RhoA wild-type, RhoA Q63L (constitutively active mutant) and RhoA T19N (dominant negative mutant) were purified according to standard procedures. The fusion proteins were used for precipitation of recombinant XIAP as described previously.[103] Briefly, GST proteins were incubated with glutathione-sepharose beads (Sigma Aldrich, Taufkirchen, Germany) in binding buffer for 1 h at 4 °C on a rotator. Beads were washed three times with binding buffer and pelleted by centrifugation. Unspecific binding was blocked by incubation with 5 % BSA containing binding buffer for 1-2 h. Beads were again washed three times and then incubated with purified XIAP (R&D Systems, Wiesbaden, Germany) at 4 °C on a rotator for 1 h. Finally, the beads were washed with high-stringency binding buffer and boiled at 100 °C for 5 min in 50 µl sample buffer. The interaction between the proteins was detected by Western blotting. The assay was kindly performed by T. Oberoi from the group of Dr. K. Rajalingam.

2.12 Cytosolic calcium imaging

Changes of the cytosolic calcium concentration were detected ratiometrically using the fluorescent dye Fura-2.[104] The excitation maximum of Fura-2 is strictly calcium dependent (unbound state excitation: 380 nm; Ca^{2+}-loaded Fura-2 excitation: 340 nm), whereas the emission wavelength remains unchanged (emission: 510 nm). Thus, the excitation ratio of 340/380 can be directly correlated to the amount of cytosolic calcium. In our measurements, a membrane-permeable derivative called Fura-2-acetoxymethyl ester (Fura-2-AM) was utilized. After ester cleavage through intracellular esterases, Fura-2 accumulates within the cytosol.

HUVECs were grown to confluence in collagen G-coated 8 well µ-slides (ibidi, Martinsried, Germany) and experiments were performed at 37 °C. Cells were loaded for 30 min with 2 µM Fura-2-AM (Biotrend, Cologne, Germany) in HEPES buffer. Concomitantly, HUVECs were incubated with ABT (1 µM) or only vehicle for control experiments. After washing the cells twice, ABT or vehicle was added again. 1 min after starting the measurement, cells were treated with TRAP (50 µM) (Mo-Bi-Tec, Göttingen, Germany) using a mechanical injection. Fluorescence measurements were obtained by a Zeiss Axiovert 200 inverted microscope (40x objective) with a climatic chamber, a Polychrome V monochromator and an IMAGO-QE camera (TILL Photonics, Gräfelfing, Germany). For each sample, a total period of 15 min with images being acquired every 5 s was analyzed with the TILLvisION Software 4.0.1.2 (TILL Photonics). Each data point of the different graphs was calculated

from a randomly chosen rectangle containing at least 20 adjacent cells. Mean values are expressed. The cytosolic calcium imaging was kindly performed by Dr. E. A. Willer, Department of Pharmacy, Pharmaceutical Biology, LMU Munich, Germany.

2.13 Statistical analysis

Each experiment was performed at least three times; the precise number of independent repetitions is denoted in the respective figure legend. In the case of HUVECs, a different preparation (*i.e.* cells from a different donor) was utilized each time. Representative Western blot images and plot diagrams are shown. Bar graph data are standardized to control measurements and expressed as mean ± S.E.M. Statistical analysis was performed using the GraphPad Prism software version 5.04 (GraphPad Software, San Diego, CA, USA). For analyzing three or more groups, a one-way analysis of variance (ANOVA) followed by a Newman-Keuls post-test was carried out. Statistical significance was assumed if $p \leq 0.05$.

3 RESULTS

3.1 Inhibitor of apoptosis proteins regulate endothelial barrier function through control of RhoA

A precursor study from our group demonstrated that inhibition of IAPs reduced leukocyte extravasation,[4] a phenomenon strongly associated with endothelial hyperpermeability.[105-107] Therefore, we hypothesized that IAPs present a group of unknown regulators of endothelial integrity. Consequently, we aimed to identify the potential of IAPs as drug targets in endothelial barrier dysfunction and to elucidate the role of different IAPs (cIAP1/2, XIAP) in the underlying signaling pathways.

3.1.1 IAP antagonists prevent TRAP-induced endothelial barrier dysfunction

To elucidate the involvement of IAPs in the regulation of endothelial permeability, we tested the potential of IAP antagonists to inhibit TRAP-mediated endothelial barrier disruption. Hence, we performed the most prevalent *in vitro* methods in permeability research: the measurement of macromolecular flux across endothelial cells (**Fig. 10**) and transendothelial electrical resistance (**Fig. 11**).[1]

3.1.1.1 IAP antagonists diminish TRAP-caused hyperpermeability of macromolecules

The flux of macromolecules across a HMEC monolayer was determined with two-compartment Transwell® plates (pore size 0.4 µm; Corning). Pretreatment of endothelial cells with two structurally different IAP antagonists (ABT, Smac085) significantly reduced the thrombin receptor-activating peptide (TRAP)-induced passage of the labeled tracer macromolecule, FITC-dextran (40 kDa), through interendothelial junctions (**Fig. 10**). The time course diagrams show that the flux of FITC-dextran was reduced by both IAP antagonists at any observed time point (**Fig. 10A, B**). The respective statistical endpoint analysis (after 30 min) reveals a reduction of TRAP-evoked hyperpermeability by both IAP antagonists (1 µM) of approximately 50 % (**Fig. 10C, D**).

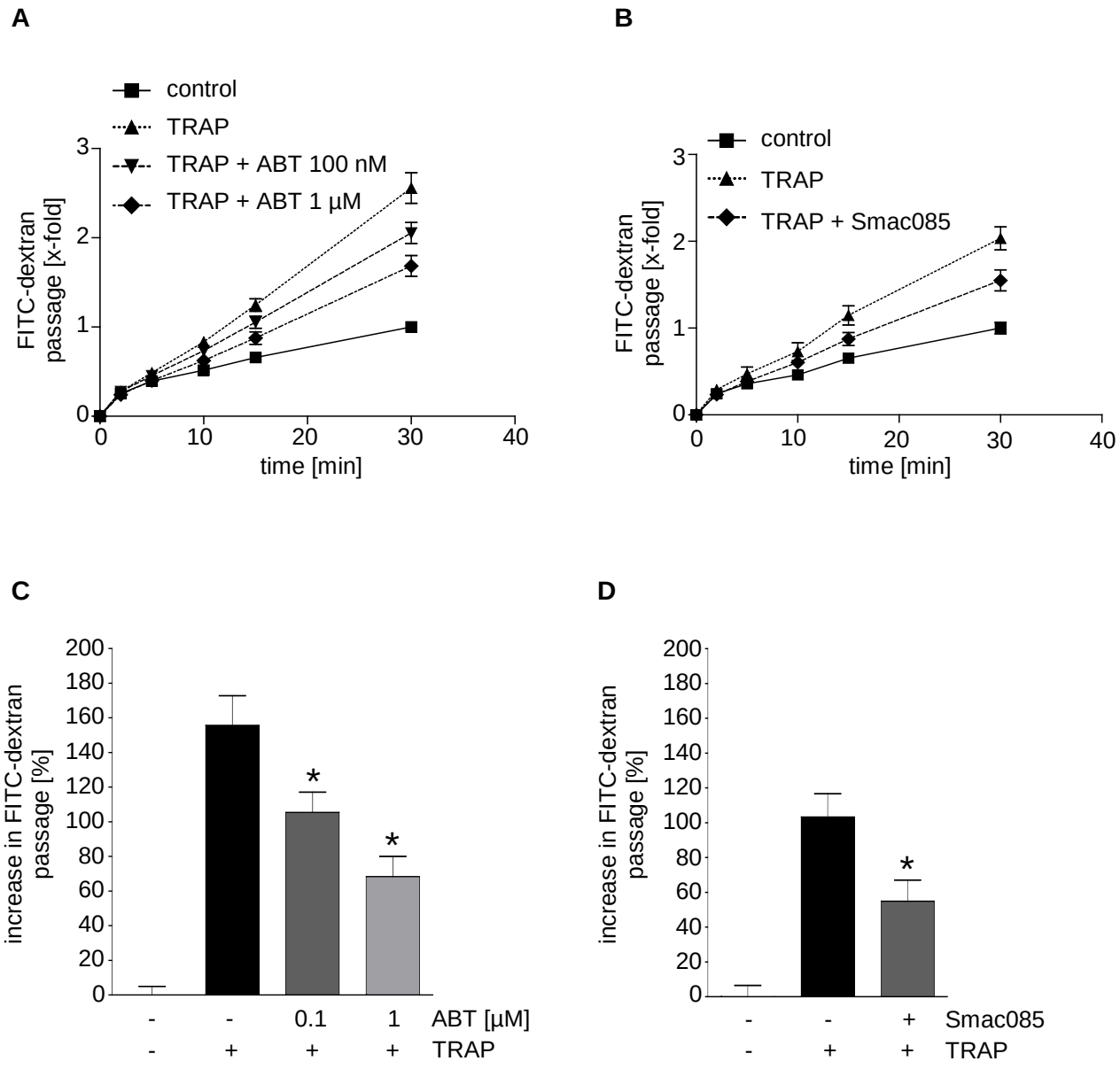

Figure 10. IAP antagonists diminish TRAP-caused hyperpermeability of macromolecules. Macromolecular permeability of FITC-dextran (40 kDa) was measured with a Transwell® two-compartment system. Cells were pretreated for 30 min with ABT (100 nM, 1 µM) (**A, C**) or Smac085 (1 µM) (**B, D**). Immediately before TRAP addition (50 µM), FITC-dextran was added (t = 0 min). Samples were taken from the lower compartment at indicated time points. (**C, D**) The bar diagrams show the statistical endpoint analysis at t = 30 min. Data are expressed as mean ± S.E.M. *P < 0.05 in relation to TRAP, one-way ANOVA followed by Newman-Keuls post-hoc test. (n = 3).

The results showed that IAP antagonists are able to prevent the TRAP-induced increase of macromolecular permeability.

3.1.1.2 ABT decreases the TRAP-induced drop of transendothelial electrical resistance

The transendothelial electrical resistance (TEER) describes the ion permeability of a cell layer and, thus, represents a read-out parameter of the barrier tightness. HUVECs were pretreated with ABT for 30 min prior to TRAP addition. A representative graph indicates that pre-incubation with ABT weakened the TRAP-initiated drop of TEER values at any observed time point (**Fig. 11A**). Statistical evaluation of all performed experiments shows that ABT significantly decreased the maximal TRAP effect, which could be detected 60 s after treatment (**Fig. 11B**). Of note, ABT reduced the maximum response to TRAP by 30 %.

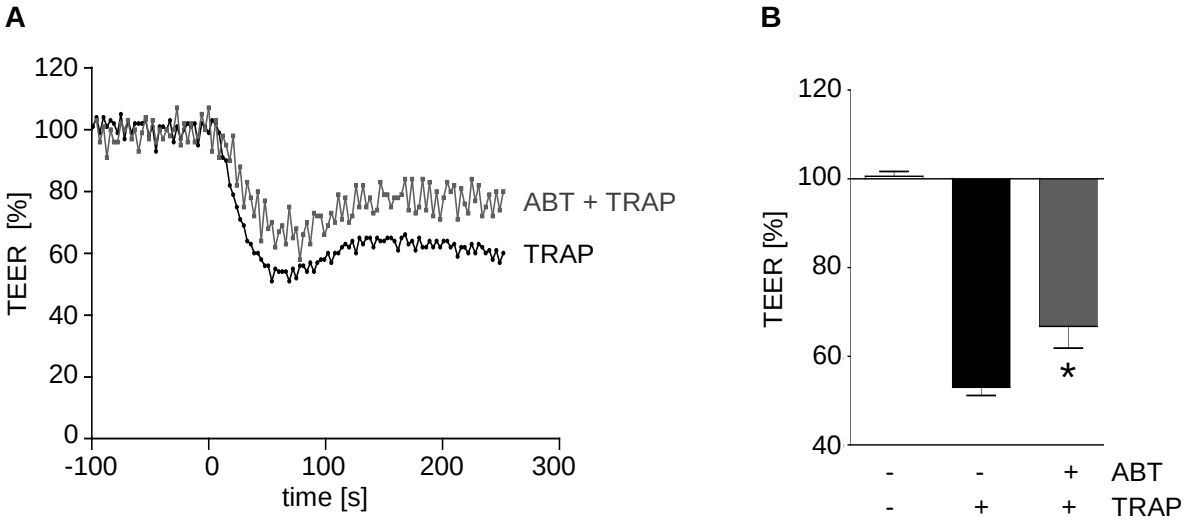

Figure 11. ABT decreases the TRAP-induced drop of transendothelial electrical resistance. TRAP-induced changes of the cell layers electrical resistance were analyzed with (grey graph) and without (black graph) ABT (1 µM) pretreament for 30 min. TRAP (10 µM) was added at t = 0. (**A**) One representative pair of TEER measurements. (**B**) Statistical evaluation of all performed TEER recordings at t = 60 s (time point of the maximum TRAP effect). *P < 0.05 versus TRAP, one-way ANOVA followed by Newman-Keuls post-hoc test. (n = 3).

We concluded that ABT protects against the TRAP-induced decrease of electrical resistance of an endothelial cell layer.

Altogether, IAP antagonists (ABT, Smac085) were proven in two functional permeability assays (measurement of macromolecular permeability and TEER) to prevent TRAP-evoked endothelial hyperpermeability.

3.1.2 IAP inhibition modulates key parameters of endothelial permeability

Endothelial hyperpermeability results from actomyosin-based contraction followed by a disruption of intercellular junctions.[20] The beneficial effect of IAP antagonism on key parameters of interendothelial adhesion (adherens junctions) (**Fig. 12**) and cellular contraction (stress fiber formation, activation of myosin light chain 2) (**Fig. 13, 14**) was subsequently analyzed.

3.1.2.1 ABT stabilizes adherens junctions

It is commonly accepted that adherens junctions (AJs), consisting of *homophilic* extracellular vascular endothelial (VE)-cadherins, are the major regulators of barrier function in the vascular system.[13, 108, 109] Within the first five minutes of treatment, thrombin initiated the phosphorylation of VE-cadherin at Y^{731}, which is a marker for the disruption of AJ.[108, 110] ABT prevented this phosphorylation event after 15 and 30 min, but left the amount of total VE-cadherin unaltered (**Fig. 12**).

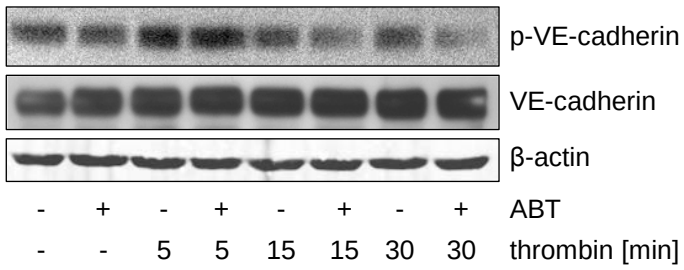

Figure 12. ABT prevents disruption of adherens junctions. HUVECs were treated with ABT (1 µM) 30 min before thrombin (1 U/ml) addition. The levels of phosphorylated (Y^{731}) and total VE-cadherin were analyzed by Westeren blotting. One representative blot out of three independently performed experiments is shown.

Our data indicated that ABT protects against thrombin-evoked disassembly of AJs.

3.1.2.2 Thrombin-induced F-actin stress fiber formation is suppressed by ABT

The second key parameter of endothelial hyperpermeability is the rearrangement of the actin cytoskeleton into fibrilliar structures, known as stress fibers.[111] Immunocytochemistry of the F-actin cytoskeleton revealed a strong stress fiber formation upon thrombin treatment. Interestingly, ABT-treated HUVECs showed no thrombin-induced stress fibers and displayed a phenotype similar to control cells (**Fig. 13**), demonstrating that IAP antagonism abolishes the thrombin-mediated cytoskeletal remodeling.

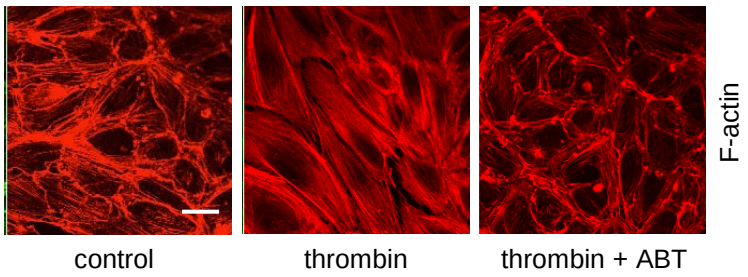

Figure 13 Stress fiber formation is abolished by ABT. HUVECs were either left untreated or pretreated with ABT (1 µM) 30 min prior to thrombin (1 U/ml) (5 min) exposure. F-actin distribution was determined by confocal laser scanning microscopy. The bar indicates 20 µm. One representative image out of three independently performed experiments is shown.

3.1.2.3 ABT inhibits the activation of the contractile machinery

The phosphorylation status of the myosin light chain2 (MLC2) controls the interaction of actin and myosin.[27] Mono- and di-phosphorylation of the MLC2 drive the mechanochemical force generation for cellular contraction.[19] Thrombin rapidly increased the phosphorylation of MLC2 (at T^{18}, S^{19}), as detected after 5 min. IAP inhibition by ABT prevented the di- (5 and 15 min) as well as the mono-phosphorylation (15 min) after thrombin exposure (**Fig. 14A**).

Cellular contraction is compensated by activation of myosin light chain phosphatase (MLCP), which conducts the dephosphorylation of MLC2. The activity of MLCP is regulated by its auto-regulatory subunit myosin phosphatase-targeting subunit 1 (MYPT1).[112] Phosphorylation of MYPT1 at T^{696} results in phosphatase inhibition[113] and is enhanced upon thrombin treatment. However, ABT reduced the phosphorylation of MYPT1 after 5 and 15 min, thus shifting MLCP towards its active conformation (**Fig. 14B**).

A

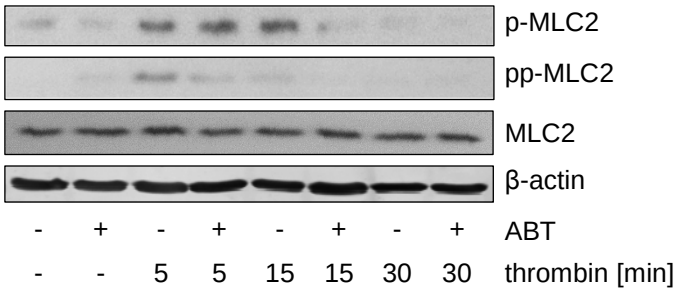

B

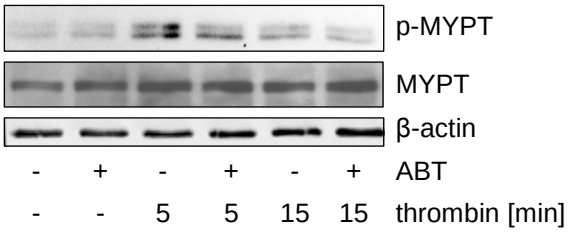

Figure 14. ABT inhibits the activation of the contractile machinery. HUVECs were either left untreated or pretreated with ABT (1 µM) 30 min prior to thrombin (1 U/ml). (**A**) Phosphorylation of myosin light chain (MLC) 2 at T^{18}/S^{19} and (**B**) of the myosin phosphatase-targeting subunit (MYPT)1 at T^{696} was analyzed by Western blotting. One representative blot out of three independently performed experiments is shown.

Here, we showed that ABT suppresses the phosphorylation of MLC2 and MYPT1.

Taken together, ABT positively influenced molecular determinants of endothelial hyperpermeability. The disassembly of AJs, the cytoskeletal rearrangement into stress fibers as well as the activation of the contractile machinery in response to thrombin were rescued by IAP inhibition with ABT.

3.1.3 Neither calcium levels, nor PKC or MAPK signaling is altered by IAP inhibition

Next, we wanted to identify the underlying signaling mechanisms of how IAPs regulate endothelial barrier function. Thrombin is known to induce endothelial hyperpermeabilitiy *via* distinct signaling transduction systems.[114] Therefore, we investigated the influence of ABT on calcium levels (**Fig. 15**) and on important protein kinases (MAPKs, PKC) (**Fig. 16, 17**) known to be crucially involved in thrombin-induced endothelial cell permeability.

3.1.3.1 ABT does not affect cytosolic calcium levels

Thrombin leads to an increase of intracellular calcium ($[Ca^{2+}]_i$) levels through a combination of two distinct mechanisms – the fast depletion of endoplasmatic stores and a more sustained influx of calcium ions across the plasma membrane.[115] To determine the influence of IAP antagonism on $[Ca^{2+}]_i$ levels, we performed ratiometric calcium measurements with Fura-2-AM. ABT did not affect the rapid thrombin-induced depletion of the endoplasmatic reticulum (after 2 min), nor the subsequent sustained plateau phase (after 5 min), which is mediated by opening of store-operated channels (SOCs) (**Fig. 15**).

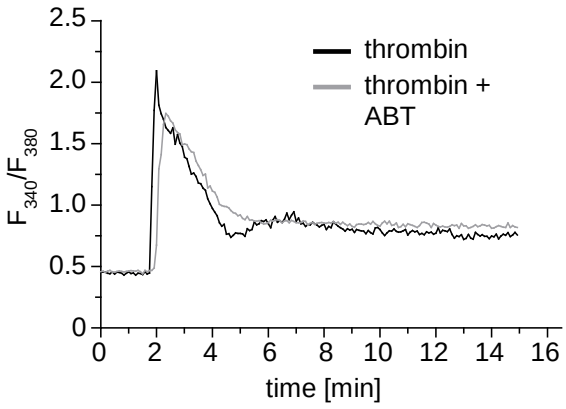

Figure 15. ABT does not affect intracellular calcium levels. Thrombin-induced changes of intracellular calcium ions were measured in HUVECs loaded with FURA-2-AM. Cells were exposed to ABT (1 µM) (grey line) or medium control (black line) for 30 min. Thrombin (1 U/ml) was added at t = 1 min. One representative plot out of three independently performed experiments is shown. This assay was kindly performed by Dr. E. A. Willer, Department of Pharmacy, Pharmaceutical Biology, LMU Munich, Germany.

This data suggested that ABT has no influence on the thrombin-mediated increase of cytosolic calcium.

3.1.3.2 ABT does not influence PKC activation

Since various protein kinase C (PKC) isoforms may contribute to endothelial hyperpermeability,[36] we checked PKC activity by analyzing the phosphorylation status of PKC substrates containing typical S-phosphorylation motives. The observed thrombin-evoked augmentation of phosphorylated PKC substrates, especially after 5 and 15 min, is not affected by pretreatment with ABT (**Fig. 16**). Thus, ABT does not affect the thrombin-induced phosphorylation of PKC downstream targets.

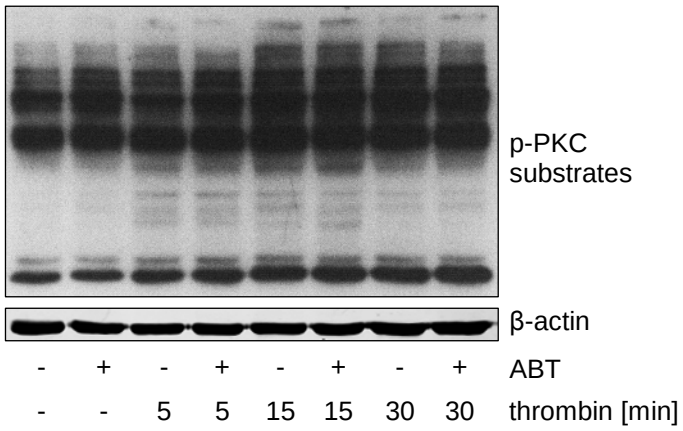

Figure 16. ABT does not affect activation of PKC. The activation of PKC was investigated by analyzing phosphorylation of conventional PKC substrates through Western blotting. HUVECs were challenged with ABT (1 µM) or medium control 30 min prior to thrombin (1 U/ml) addition. One representative blot out of three independently performed experiments is shown.

3.1.3.3 MAPK activity is not altered by IAP inhibition

Also the major mitogen activated protein kinases (MAPKs) – extracellular signal-related kinase (ERK), p38 and c-*jun* N-terminal kinase (JNK) – are important regulators of endothelial permeability.[32, 33, 35] The thrombin-mediated activation of ERK (**Fig. 17A**), JNK (**Fig. 17B**) and p38 (**Fig. 17C**) was analyzed at three different time points. Activation of all three MAPKs was not affected by pre-incubation with ABT.

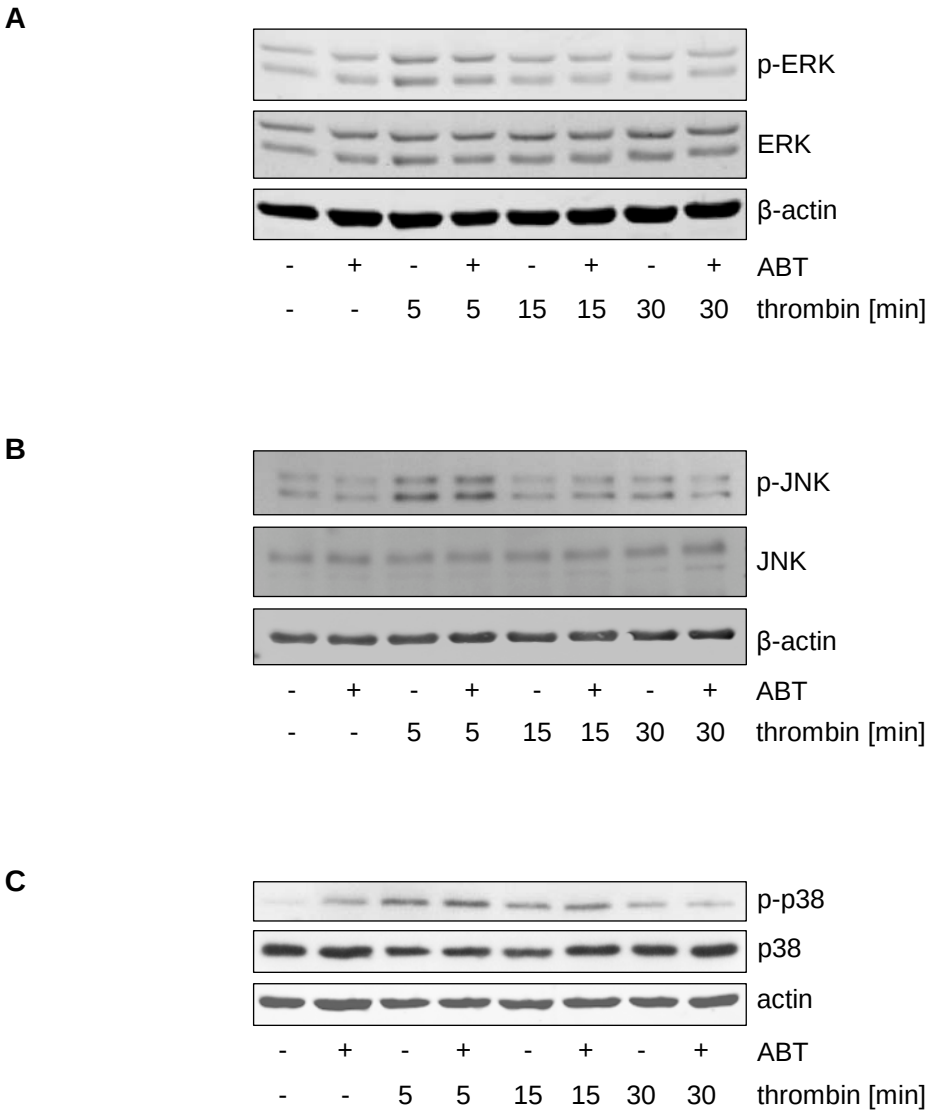

Figure 17. MAPK activity is not altered by ABT. HUVECs were treated with ABT (1 µM) or medium control for 30 min and subsequently with thrombin (1 U/ml). The phosphorylation status of (**A**) ERK (T^{202}/Y^{204}), (**B**) JNK (T^{183}/Y^{185}) and (**C**) p38 (T^{180}/Y^{182}) was analyzed by Western blotting. One representative blot out of three independently performed experiments is shown.

Hence, we could rule out a role of IAPs in thrombin-activated MAPK signaling.

In summary, these data excluded an influence of IAPs in calcium, PKC or MAPK signaling pathways in the thrombin-activated endothelium.

3.1.4 IAP inhibition regulates RhoA activity

Our previous results clearly indicate a novel role for IAPs in the regulation of endothelial barrier function as IAP antagonists protect against TRAP-induced hyperpermeability. The analyzed inflammatory signaling pathways (calcium, PKC or MAPK) downstream of thrombin receptor activation were not altered by IAP inhibition. Interestingly, we observed a strong reduction in stress fiber formation after antagonizing IAPs (**Fig. 13**). Given that small GTPases are master regulators of the actin cytoskeleton rearrangement,[116] we hypothesized that ABT might influence small GTPases signaling. Consequently, we investigated the activation of the small GTPases RhoA and Rac1 (**Fig. 18**), the total protein expression (**Fig. 19**) and stress fiber formation induced by RhoA overexpression (**Fig. 20**) after ABT treatment.

3.1.4.1 ABT reduces RhoA activation, but does not affect Rac1

The effect of IAP inhibition on the barrier disruptive small GTPase RhoA and its physiological counterpart Rac1[47] was investigated by affinity precipitation experiments. ABT abolished the thrombin-triggered RhoA activation, as indicated by precipitated RhoA-GTP levels (**Fig. 18A**). However, activity of the barrier protective small GTPase Rac1 was neither affected by thrombin, nor by ABT (**Fig. 18B**).

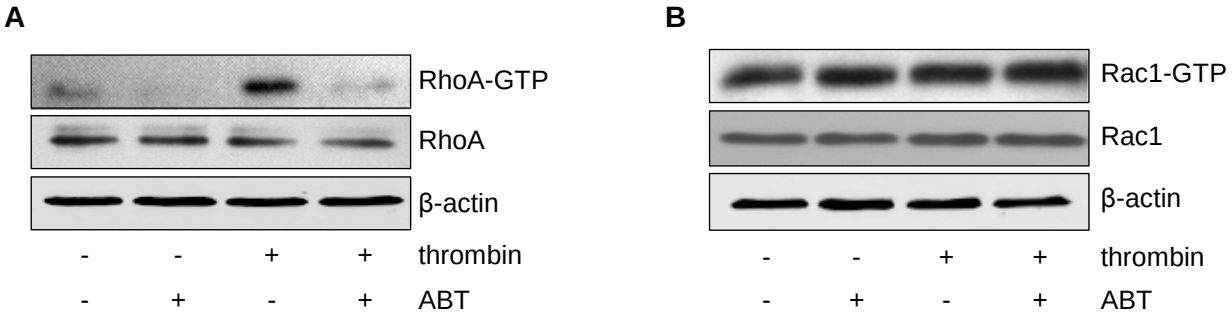

Figure 18. ABT reduces the activation of RhoA, but not of Rac1. HUVECs were treated with ABT (1 µM) or medium control 30 min prior to thrombin (1 U/ml, 10 min). (**A**) RhoA-GTP and (**B**) Rac1-GTP were precipitated and purified with a pull-down assay and analyzed by Western blotting. One representative blot out of at least three independently performed experiments is shown. A part of the performed active RhoA and Rac1 pull-down assays was kindly performed by S. Leonhardt, Department of Pharmacy, Pharmaceutical Biology, LMU Munich, Germany.

3.1.4.2 Total protein levels of RhoA and Rac1 are not altered

We additionally analyzed the expression levels of total (GTP- and GDP-bound) RhoA and Rac1 in whole cell lysates. Neither ABT, nor thrombin altered the amount of total RhoA and Rac1 in HUVECs (**Fig. 19**).

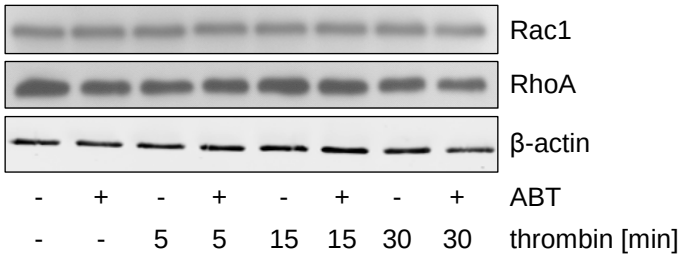

Figure 19. Total protein levels of RhoA and Rac1 are not influenced by ABT and thrombin. HUVECs pretreated with ABT (1 µM) for 30 min are subsequently exposed to thrombin (1 U/ml), and then analyzed by Western blotting. One representative blot out of three independently performed experiments is shown.

3.1.4.3 ABT prevents stress fiber formation induced by RhoA overexpression

Transient overexpression of RhoA wild-type (wt) is a known inducer of stress fibers.[117] Also in HUVECs with increased RhoA levels, ABT potently inhibited the formation of elongated, thick F-actin fibers (**Fig. 20**).

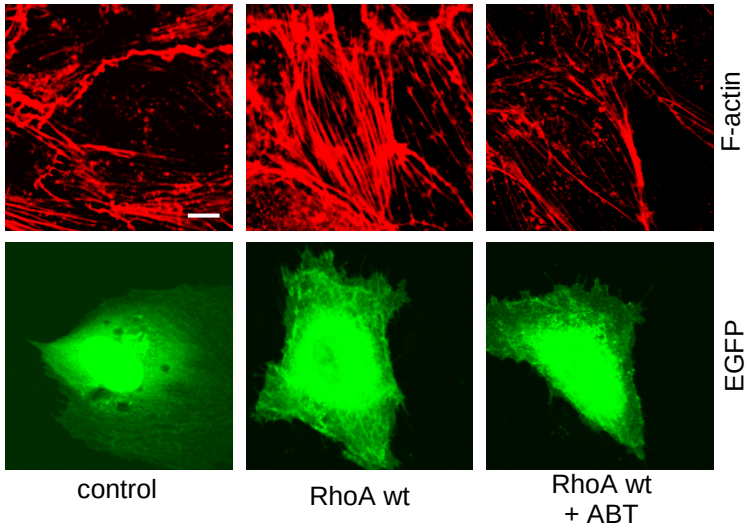

Figure 20. ABT prevents RhoA overexpression-induced stress fiber formation. HUVECs were transfected with pcDNA3-EGFP or pcDNA3-EGFP-RhoA wild-type (wt). ABT (1 µM) or medium control were added for 30 min. F-actin distribution and successful transfection with EGFP-labeled plasmids were analyzed by confocal laser scanning microscopy. The bar indicates 10 µm. Representative images out of four independently performed experiments are shown.

We demonstrated that IAP antagonism interferes with RhoA signaling. ABT prevented the activation of RhoA, but did not influence Rac1, and left the total protein levels of these small GTPases unaltered. Furthermore, we revealed that inhibition of stress fiber formation by ABT was also observed in a RhoA overexpression system.

3.1.5 XIAP is responsible for RhoA activation and cytoskeletal rearrangement

So far, we have described that barrier protective properties of ABT are mediated by limiting RhoA activity. Next, we aimed to elucidate the contribution of different IAP family members on the observed effects. XIAP, cIAP1 and cIAP2 are the most important and best characterized IAP representatives,[65] which we consequently focused on.

3.1.5.1 Characterizing IAP levels after ABT and thrombin treatment

At first, we analyzed the amount of cIAP1/2 and XIAP in HUVECs under *basal* conditions and after thrombin treatment with or without ABT. Surprisingly, cIAP2 was not expressed in untreated or thrombin-conditioned endothelial cells, and therefore excluded from further analysis (**Fig. 21A**). TNFα, a known inducer of cIAP2 expression,[118] was used as positive control to demonstrate, that our setting is able to detect cIAP2. Thrombin activation of HUVECs did not alter the protein levels of cIAP1 and XIAP (**Fig. 21B**). Interestingly, the IAP inhibitor ABT rapidly depleted cIAP1 in HUVECs, whereas XIAP levels remained stable (**Fig. 21C**).

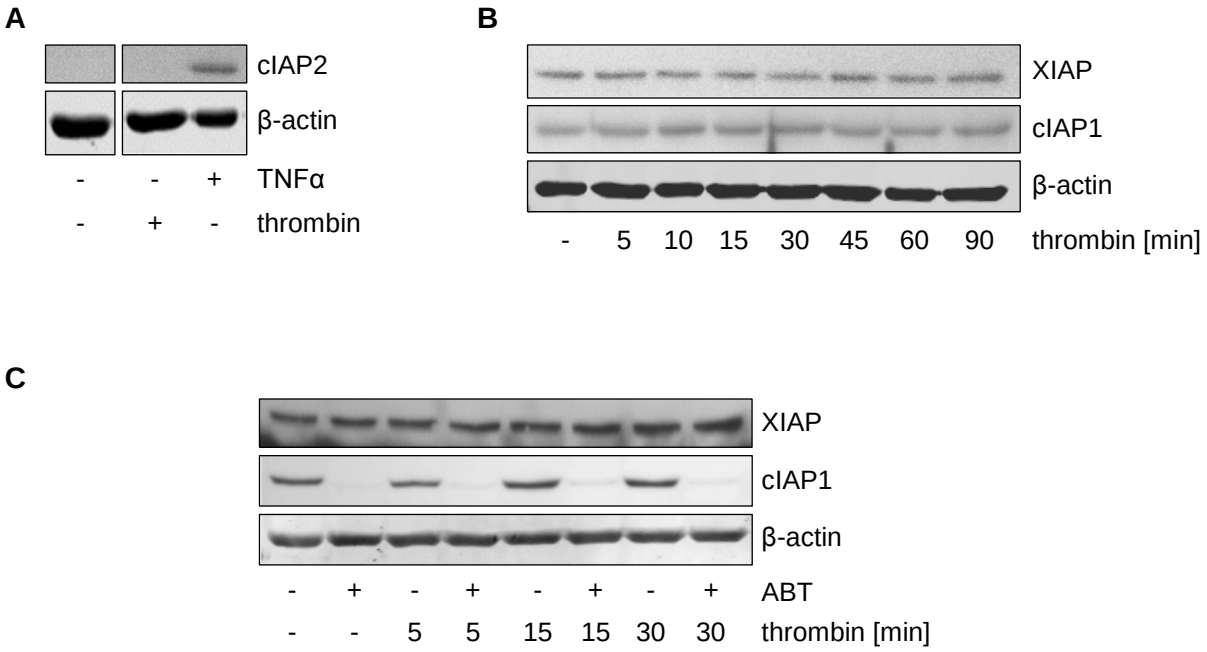

Figure 21. IAP levels after thrombin or ABT treatment. Protein levels of cIAP1/2 and XIAP were determined by Western blot analysis. Thrombin (1 U/ml) was added for 30 min (**A**) or as indicated (**B, C**), TNFα (10 ng/ml) for 24 h (**A**) and ABT (1 µM) 30 min prior to thrombin (**C**). One representative blot out of three independently performed experiments is shown.

3.1.5.2 RhoA activation depends on the presence of XIAP rather than on cIAP1

The role of individual IAPs in RhoA activation was addressed with an *RNAi* approach. Gene silencing of XIAP completely inhibited RhoA activation, whereas loss of cIAP1 caused only a marginal reduction (**Fig. 22**). Successful silencing of IAPs was verified in total cell lysates. Of note, knockdown of one IAP did not trigger the reciprocal upregulation of the other IAP.

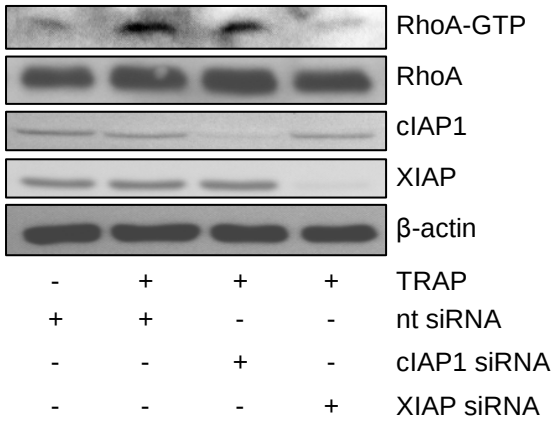

Figure 22. Silencing of XIAP prevents RhoA activation. XIAP or cIAP1 were degraded in HUVECs by *RNAi*. Non-targeting siRNA was used as negative control. TRAP (50 µM) treatment for 10 min induced RhoA activation. RhoA-GTP was precipitated with a pull-down assay and analyzed by Western blotting. One representative blot out of three independently performed experiments is shown.

3.1.5.3 XIAP silencing prevents stress fiber formation and activation of MLC2

Moreover, activation of the contractile machinery (actin, MLC2) was investigated in HUVECs with transiently degraded IAPs. Silencing of XIAP, but not of cIAP1, inhibited the TRAP-evoked stress fiber formation as well as the activation of MLC2 (**Fig. 23A**). Knockdown of XIAP induced cortical actin distribution, a phenotype associated with endothelial barrier stabilization.[119] Successful protein knockdown of cIAP1 and XIAP was controlled by Western blotting (**Fig. 23B**).

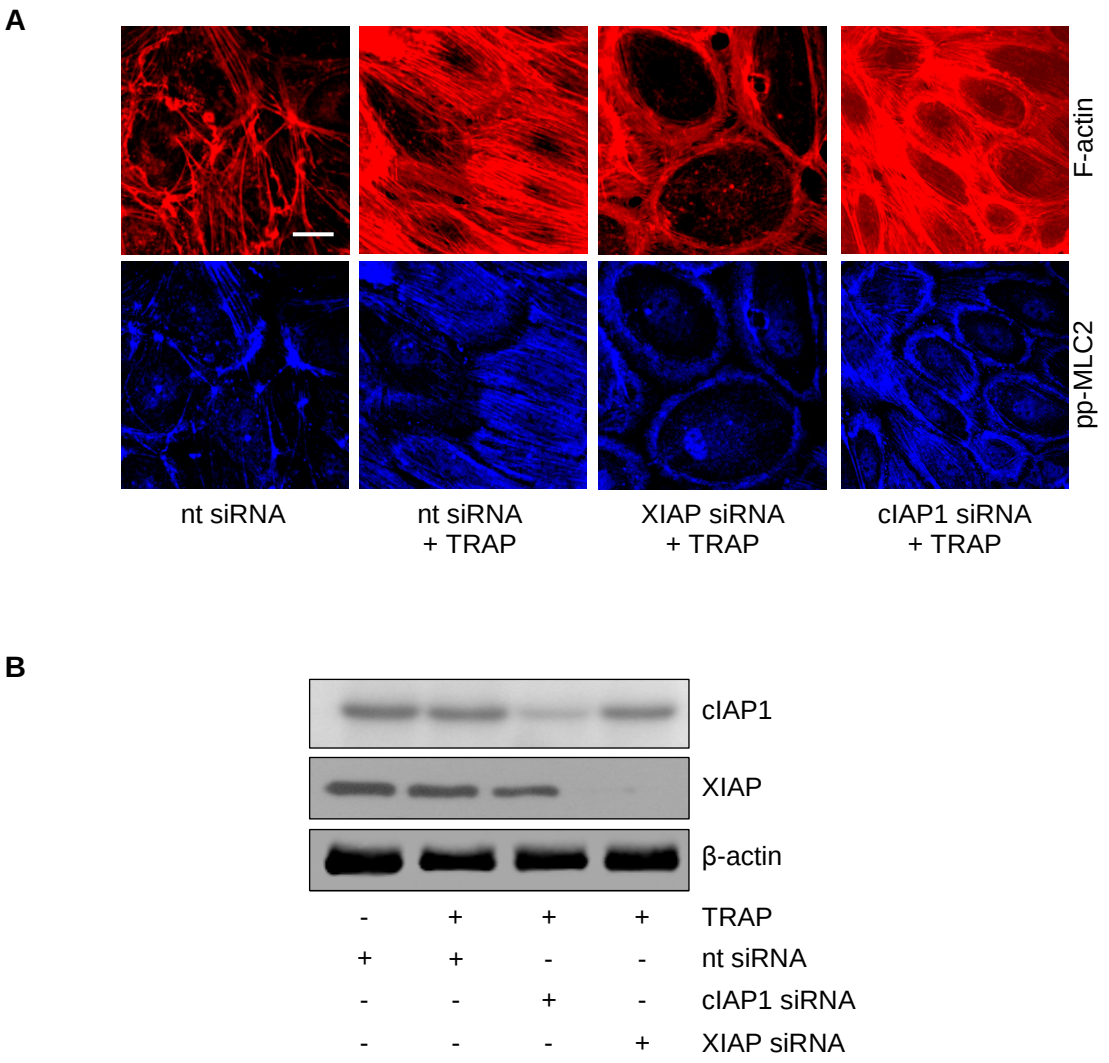

Figure 23. Silencing of XIAP prevents the activation of the contractile machinery. Non-targeting siRNA served as negative control. HUVECs were challenged with TRAP (50 µM) for 10 min. (**A**) Cells with transiently degraded IAPs were stained for F-actin and di-phosphorylated MLC2, and then analyzed by confocal laser scanning microscopy. The bar indicates 20 µm. (**B**) Silencing control of cIAP1 and XIAP through Western blot analysis. One representative image/blot out of four independently performed experiments is shown.

In summary, we demonstrated that XIAP is the major regulator of RhoA activation and subsequent downstream events.

3.1.6 XIAP directly interacts with RhoA

Since XIAP functions as regulator of RhoA activity, we speculated if there might be a direct interaction of IAPs with RhoA. Therefore, we analyzed this supposed interaction both *in vitro* and in a cell-free system.

3.1.6.1 RhoA strongly binds to XIAP

The association of IAPs with RhoA in endothelial cells was confirmed by performing immunoprecipitation experiments. RhoA was found to be firmly attached to XIAP immunoprecipitates (**Fig. 24A**), whereas the interaction of RhoA with cIAP1 was much weaker (**Fig. 24B**). Of note, ABT treatment did not affect the interaction of XIAP and RhoA, but diminished the amount of co-precipitated RhoA bound to cIAP1.

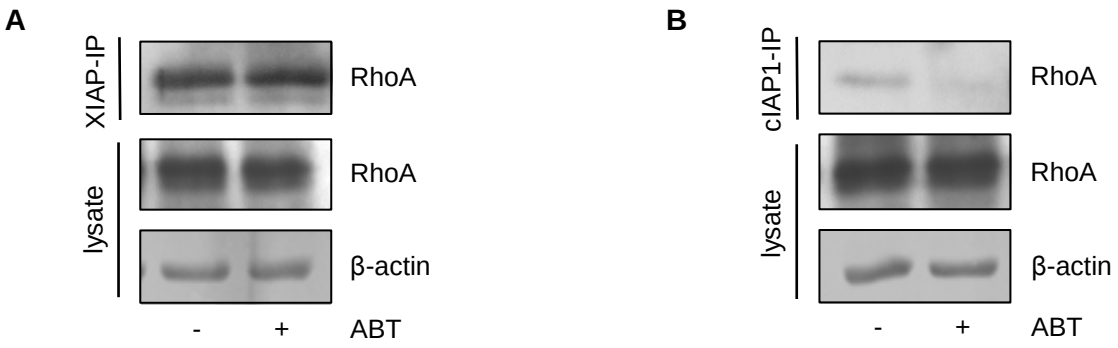

Figure 24. RhoA precipitates with XIAP. HUVECs were treated with ABT (1 µM) or medium control for 30 min. Immunoprecipitation of XIAP (**A**) and cIAP1 (**B**) were performed. The IAP-bound RhoA was detected by Western blot analysis. One representative blot out of three independently performed experiments is shown.

3.1.6.2 XIAP interacts with RhoA independently of the RhoA activation status

Finally, we investigated if the RhoA activation status influences the interaction between XIAP and RhoA. HEK 293T cells were co-transfected with plasmids encoding for XIAP together with either RhoA wild-type (wt) or RhoA Q63L, a constitutively active mutant. Overexpressed XIAP was associated both with RhoA wt and with active RhoA (**Fig.25A**). A direct interaction could be proven in a cell-free system, where recombinant GST fusion proteins of RhoA wt, the constitutively active RhoA Q63L mutant, as well as the dominant inactive RhoA T19N mutant were found to bind to recombinant XIAP (**Fig. 25B**).

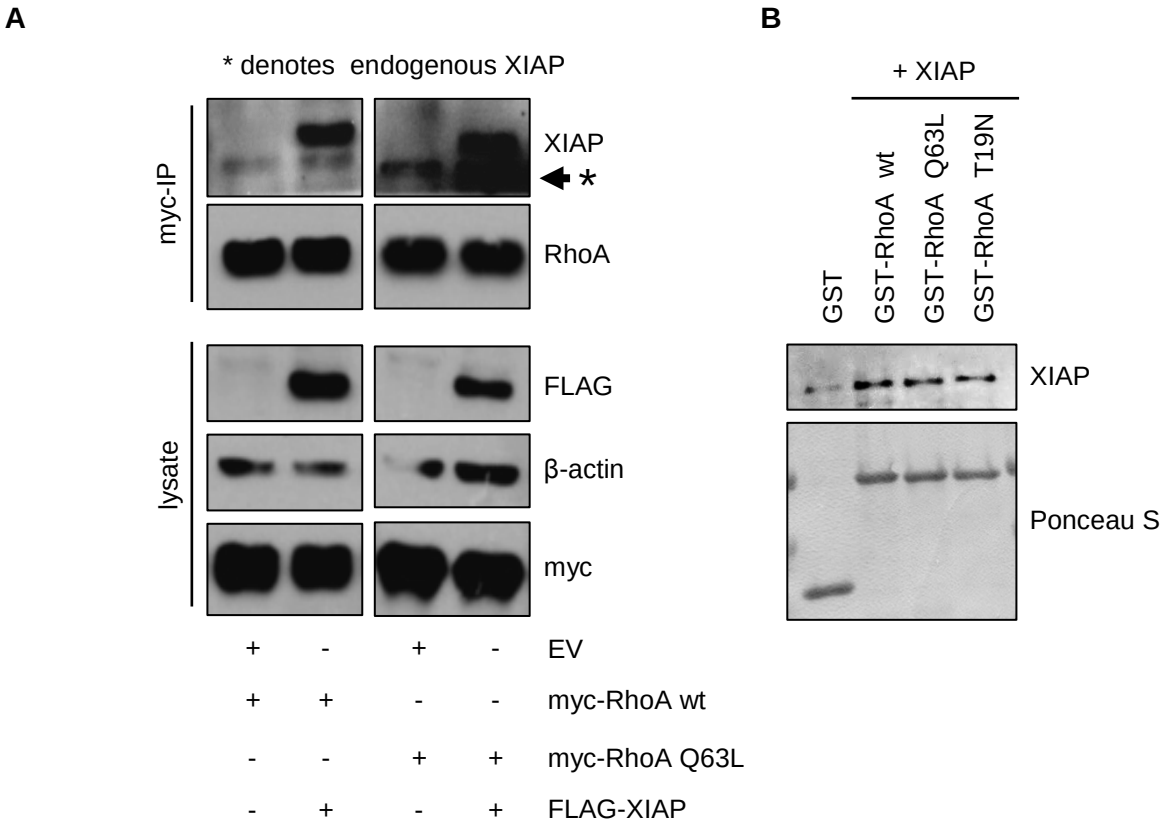

Figure 25. XIAP binds RhoA independently of the RhoA activation status. (**A**) HEK 293T cells were co-transfected with the following plasmids: myc-RhoA wild-type (wt) and myc-RhoA Q63L (constitutively active), with Flag-XIAP or the respective empty vector (EV). The myc-tag was precipitated with a selective anti-myc antibody. Levels of XIAP, RhoA and of the myc- and FLAG-tag were analyzed by Western blotting. (**B**) Recombinant GST-RhoA wt, GST-RhoA Q63L and GST-RhoA T19N (dominant negative) were incubated with recombinant XIAP. A GST pull-down assay was performed. Co-precipitated XIAP was detected by Western blotting. One representative blot out of three independently performed experiments is shown. These experiments were kindly performed by T. Oberoi from the group of Dr. K. Rajalingam, Institute of Biochemistry II, Goethe-University Medical School, Frankfurt/Main, Germany.

We identified an interaction of RhoA and XIAP in endothelial cells. Moreover, co-transfection experiments in HEK 293T cells and GST-pull-down assays of purified recombinant proteins not only confirmed our finding, but also demonstrated that this interaction is independent of RhoA activation.

3.2 A comparative study of *in vitro* assays for the analysis of endothelial permeability

A typical hallmark of inflammatory processes is the increased vascular permeability and the subsequent edema formation.[120] Validated *in vitro* methods are indispensable for the identification of novel drug targets in the regulation of endothelial permeability as well as for the investigation of the underlying signaling pathways.

In our study, we compare the following two methods: 1) the classic measurement of macromolecular permeability (MP) and 2) the modern real-time cell impedance sensing, which employs alternating currents to analyze morphological changes. Endothelial cells were challenged with different well-established modulators of the endothelial barrier function in both approaches for an unbiased judgment.

3.2.1 The barrier protective compound forskolin shows congruent results in both approaches

Since many years, the adenylyl cyclase activator forskolin is known to strengthen the endothelial barrier.[121] This made it an ideal compound for the initial characterization of the utilized permeability assays.

3.2.1.1 Forskolin elevates the Cell index (CI)

HMECs respond to forskolin addition (at t = -0.5 h) with a gradual increase of normalized CI values (**Fig. 26A**). TRAP induced endothelial hyperpermeability,[21] which appears as rapid drop of CI values (**Fig. 26A, B**). Interestingly, the maximum effect caused by TRAP was mitigated by forskolin pretreatment in terms of amplitude and duration (**Fig. 26B**).

A

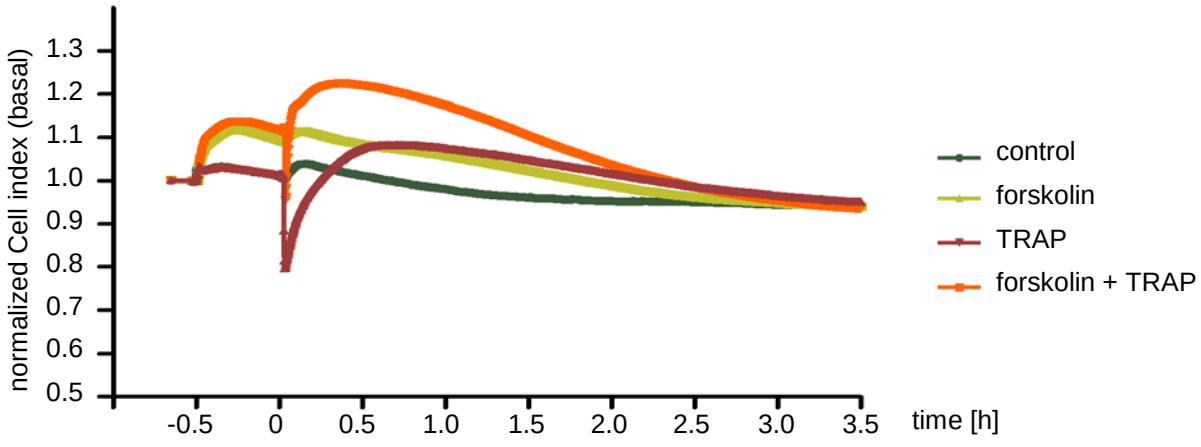

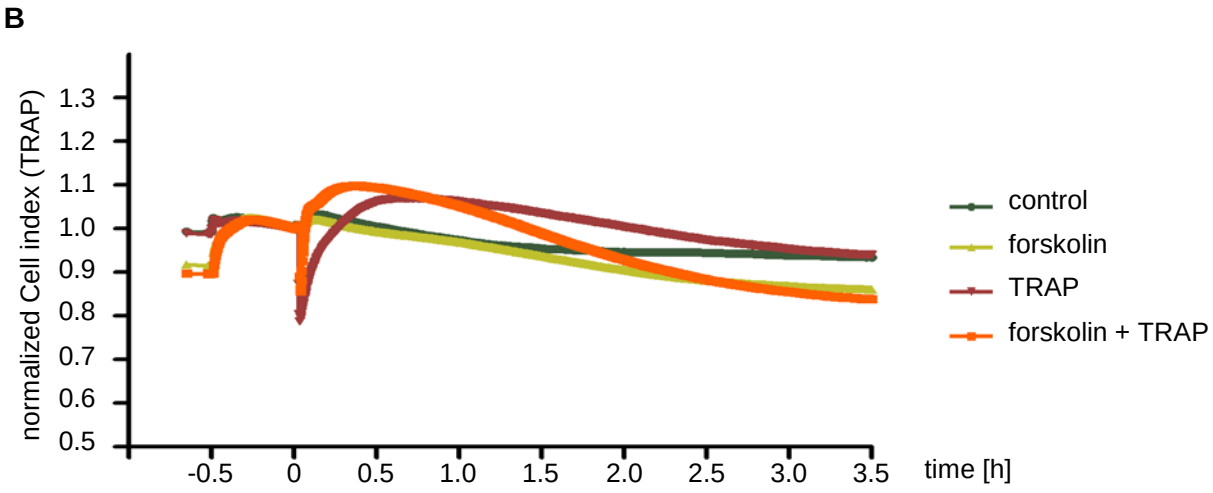

Figure 26. Forskolin elevates the Cell index. HMECs were treated with forskolin (10 µM) for 30 min and subsequently exposed to TRAP (50 µM). The time course of compound-mediated alterations of normalized CI is displayed by a representative experiment. CI is normalized either to (**A**) *basal* levels (before forskolin treatment) or to (**B**) the time point of TRAP addition. The experiment was performed independently three times.

3.2.1.2 Forskolin reduces the TRAP-induced flux of macromolecules

In our second approach, forskolin limited the passage of FITC-dextran (40 kDa) through a HMEC monolayer as assessed with a two-compartment Transwell® assay (pore size 0.4 µm; Corning). Forskolin reduced the *basal* permeability (compared to control), and fully reversed the TRAP-evoked hyperpermeability (**Fig. 27**).

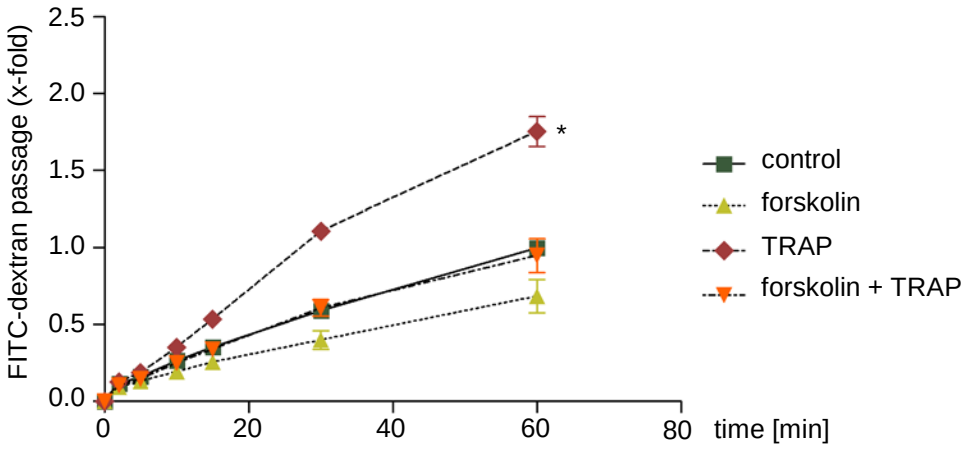

Figure 27. Forskolin reduces the permeability of macromolecules. HMECs were treated with forskolin (10 µM) for 30 min, subsequently FITC-dextran (40 kDa) and TRAP (50 µM) were added. The flux of

FITC-dextran across a HMEC layer was measured with a Transwell® two-compartment system. Samples were taken from the lower compartment at indicated time points. Data are expressed as mean ± S.E.M.. *P < 0.05 in relation to control, one-way ANOVA followed by Newman-Keuls post-hoc test. (n = 3).

3.2.1.3 Forskolin prevents the activation of the contractile cytoskeleton

In order to prove that forskolin positively influences the endothelial barrier function, we analyzed the cytoskeletal rearrangement induced by forskolin with our without TRAP. The phosphorylation of MLC2, indispensable for the actin-myosin interaction, was enhanced 5 min after TRAP addition, but could be reduced by forskolin pre-incubation (**Fig. 28A**). Compared to control cells, treatment with only forskolin induced actin assembly in the periphery. Moreover, forskolin pretreatment also remodeled the typical TRAP-evoked stress fibers into a cortical actin rim (**Fig. 28B**).

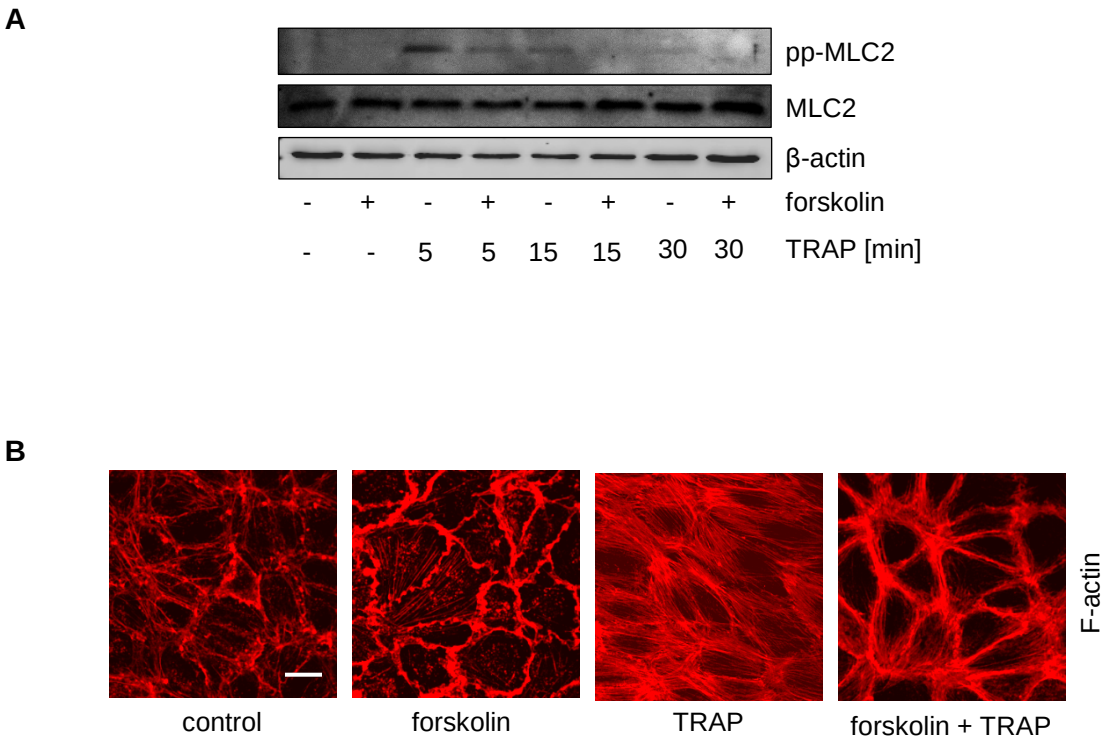

Figure 28. Forskolin prevents the activation of the contractile cytoskeleton. HUVECs were treated with forskolin (10 µM) for 30 min before TRAP (50 µM) was added. (**A**) The di-phosphorylation (T^{18}, S^{19}) of MLC2 was analyzed through Western blotting. (**B**) F-actin distribution was determined by confocal laser scanning microscopy. TRAP (50 µM) was added for 10 min. The bar indicates 20 µm. One representative blot/image out of three independently performed experiments is shown.

Altogether, this accounted for the congruent results of permeability measurement – a decreased flux of macromolecules and elevated impedance values caused by forskolin treatment.

3.2.2 The transient histamine-induced hyperpermeability is hardly detectable by macromolecular permeability measurement but with impedance sensing

The inflammatory mediator histamine causes an immediate activation of the actin cytoskeleton thus increasing endothelial permeability.[43] We aimed for an analysis of the transient cell response to different histamine concentrations.

3.2.2.1 Real-time impedance measurement of the histamine response

Impedance-based analysis detects a rapid decline (max. at 1 min) of normalized CI values upon histamine addition, which is immediately reversed. The detected drop followed a concentration series from 1 µM up to 100 µM (**Fig. 29**).

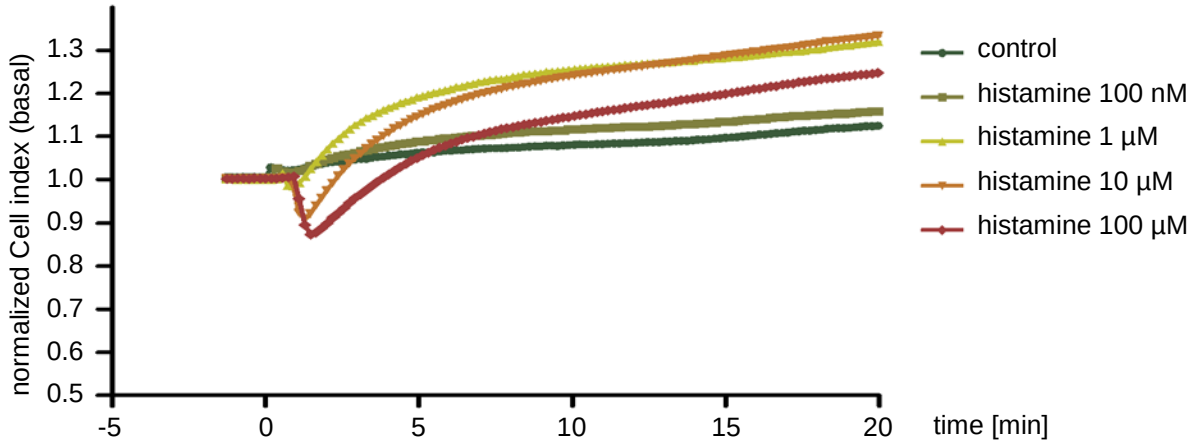

Figure 29. Impedance measurement of the histamine response. HMECs were treated with histamine at indicated concentrations. One representative graph out of three independently performed experiments indicates the changes of the normalized CI. Normalization to CI values just before histamine treatment.

3.2.2.2 Measurement of macromolecular permeability lacks sensitivity for histamine-induced hyperpermeability

Although histamine increased the permeability of macromolecules at any observed time point, the assays reliability is very limited. No precise concentration dependence was detectable, since the mean of 1 µM histamine was higher than for 10 µM. Moreover, the data revealed no statistical difference (at t = 30 min) due to the huge occurring standard errors (**Fig. 30**).

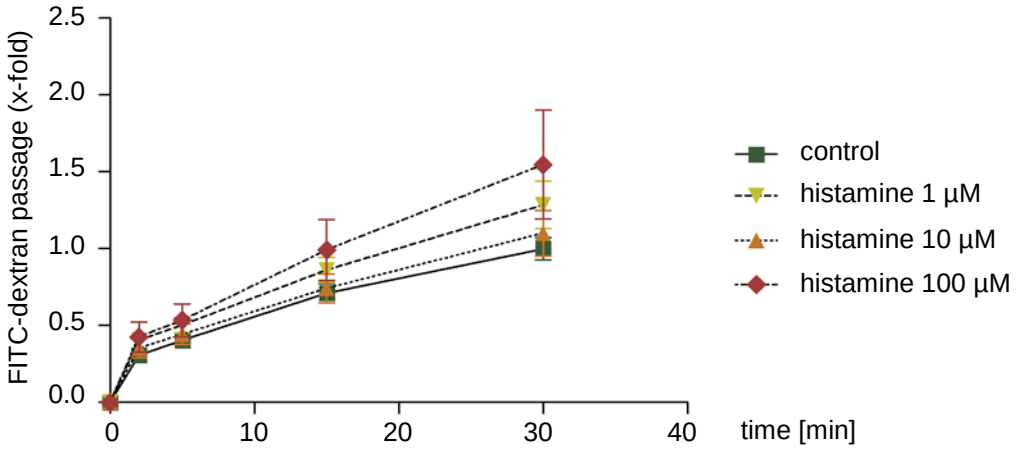

Figure 30. MP measurement after histamine treatment. HMECs were treated with histamine at indicated concentrations. Macromolecular permeability of FITC-dextran (40 kDa) was measured with a Transwell® two-compartment system, where samples were taken from the basolateral side at indicated time points. Data are expressed as mean ± S.E.M.. *P < 0.05 in relation to control, one-way ANOVA followed by Newman-Keuls post-hoc test. (n = 5).

We demonstrated that the rapid and very transient effect of histamine could reliably be detected in a concentration-dependent manner by real-time impedance sensing. In contrast, the MP approach was lacking sensitivity, which caused huge standard errors and no clear relation between the applied concentrations and the measured response.

3.2.3 Inhibition of RhoA kinase (ROCK) increases *basal* permeability, but prevents TRAP-triggered barrier disruption

ROCK, a downstream target of active RhoA, induces phosphorylation of MYPT1, and therefore alters the endothelial barrier function (see **1.2.3.4**). We analyzed the endothelial response to the blocking of ROCK by the pharmacological inhibitor Y-27632 in the two permeability detection systems.

3.2.3.1 Y-27632 itself decreases CI values, but also limits the TRAP response

Treatment of HMECs with Y-27632 induced a sustained and strong reduction (30 %) of the normalized *basal* CI values within 30 min. In contrast, TRAP addition caused a transient, less pronounced drop (15%) of normalized CI levels (**Fig. 31A**). Interestingly, pretreatment with Y-27632 weakened the TRAP response in terms of amplitude and duration (**Fig. 31B**).

A

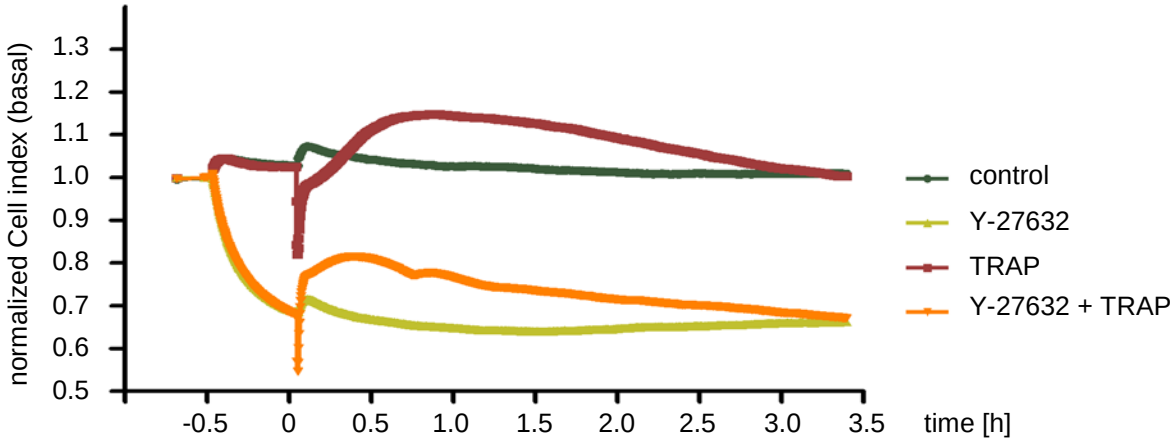

B

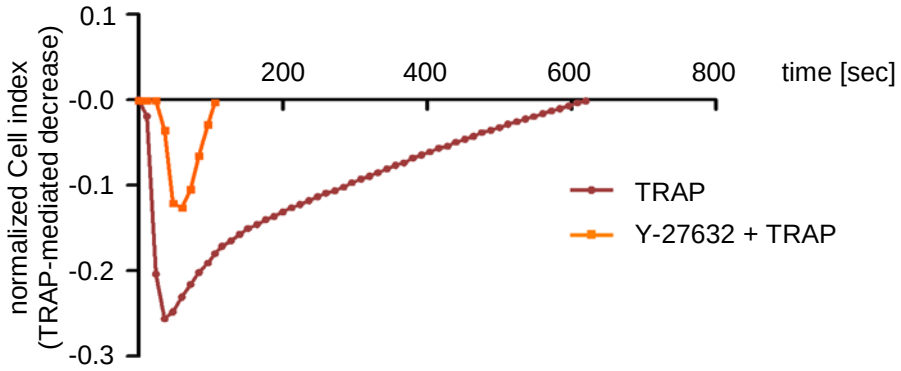

Figure 31. Y-27632 itself decreases CI values, but limits the TRAP response. HMECs were treated with Y-27632 (10 µM) for 30 min before TRAP (50 µM) was added. (**A**) CI is normalized to *basal* levels (before Y-27632 treatment). (**B**) The TRAP-induced drop of CI values below the control levels is displayed. One representative graph out of three independently performed experiments is shown.

3.2.3.2 Y-27632 itself elevates macromolecular permeability, but also abolishes the TRAP-evoked increase of permeability

ROCK inhibition with Y-27632 (10 µM) significantly elevated the flux of macromolecules across a HMEC monolayer by about 30 % within 30 min (**Fig. 32A**). Of note, TRAP treatment doubled the passage of FITC-dextran after 60 min. However, the TRAP-initiated increase in MP could be fully prevented by Y-27632 pre-incubation (**Fig. 32B**).

A

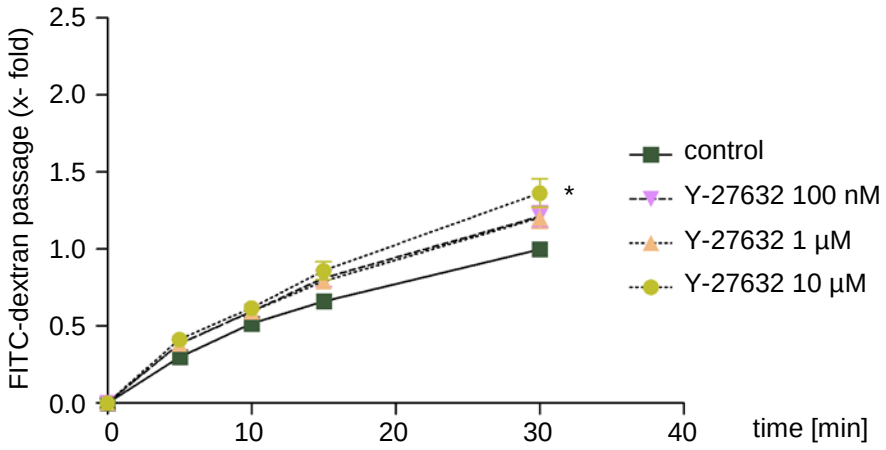

B

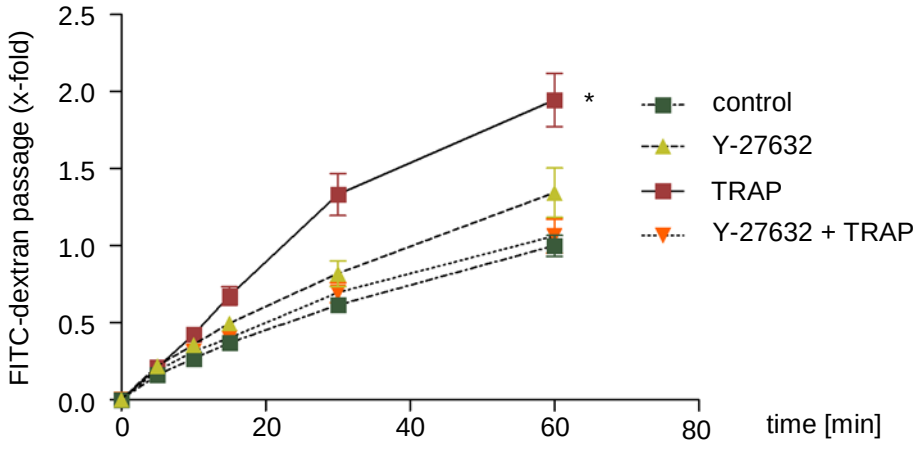

Figure 32. Y-27632 itself elevates MP, but protects against TRAP effects. (**A**) HMECs were treated with Y-27632 at indicated concentrations immediately before FITC-dextran (40 kDa) was added. (**B**) HMECs were pre-incubated with Y-27632 (10 µM) 30 min, then FITC-dextran (40 kDa) and successively TRAP (50 µM) were added. The passage of FITC-dextran across the cell layer was measured with a Transwell® two-compartment system. Samples were taken from the lower compartment at indicated time points. Data are expressed as mean ± S.E.M.. *P < 0.05 in relation to control, one-way ANOVA followed by Newman-Keuls post-hoc test. (n = 3).

3.2.3.3 Y-27632 inhibits the activation of MLC2 and stress fiber formation

Y-27632 completely abolished *basal* and TRAP-evoked phosphorylation of MLC2 (**Fig 33A, B**). Also the TRAP-induced actin remodeling into stress fibers was prevented by Y-27632 pretreatment (**Fig. 33B**).

A

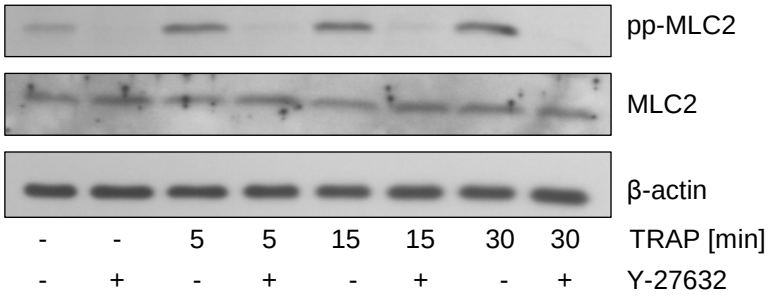

B

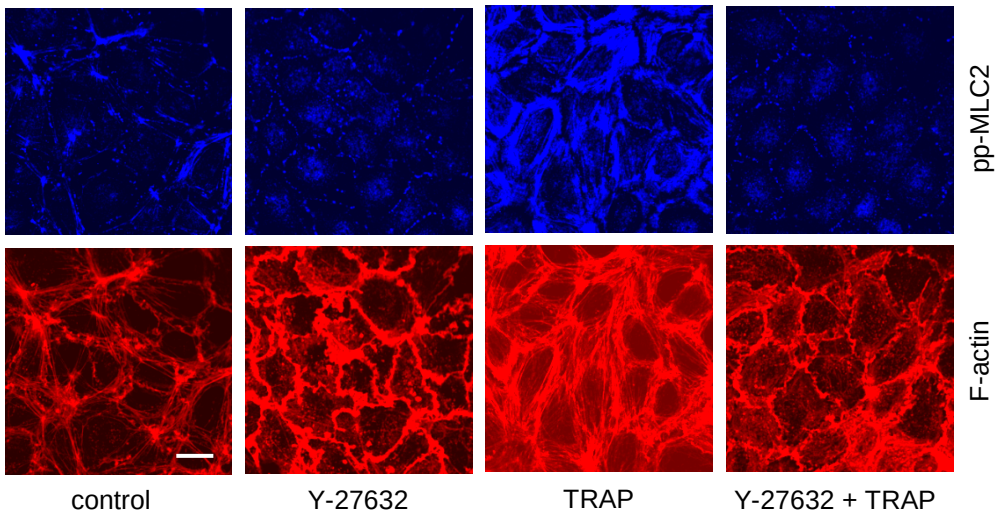

Figure 33. Y-27632 prevents the activation of the contractile cytoskeleton. HUVECs were treated with Y-27632 (10 µM) for 30 min before TRAP (50 µM) was added. (**A**) The di-phosphorylation (T^{18}, S^{19}) of MLC2 was analyzed through Western blotting. (**B**) F-actin distribution and di-phosphorylation of MLC2 were determined by confocal laser scanning microscopy. TRAP (50 µM) was added for 10 min. The bar indicates 20 µm. One representative blot/image out of three independently performed experiments is shown.

We revealed that ROCK inhibition with Y-27632 initially increased the permeability of endothelial cells. Surprisingly, we detected a massive drop of impedance values (about 200 % of the TRAP effect), but only a slight increase in FITC-dextran flux (only about 30 % of the TRAP effect). Nevertheless, Y-27632 diminished the TRAP-mediated endothelial hyperpermeability in terms of impedance sensing, MP measurement and stress fiber formation.

3.2.4 Controversial results upon inhibition of myosin

As actomyosin interaction is indispensable for the regulation of the endothelial barrier, we further characterized the influence of blebbistatin – a selective myosin II inhibitor – known to detach myosin II from actin, in the two permeability detection systems.[122]

3.2.4.1 Blebbistatin alone decreases CI values and abrogates the TRAP effect

Blebbistatin immediately induced a decrease of normalized CI values – about 20 % within 30 min and 40 % after 3 h. Furthermore, blebbistatin fully prevented the typical TRAP-triggered drop of CI values (**Fig. 34**).

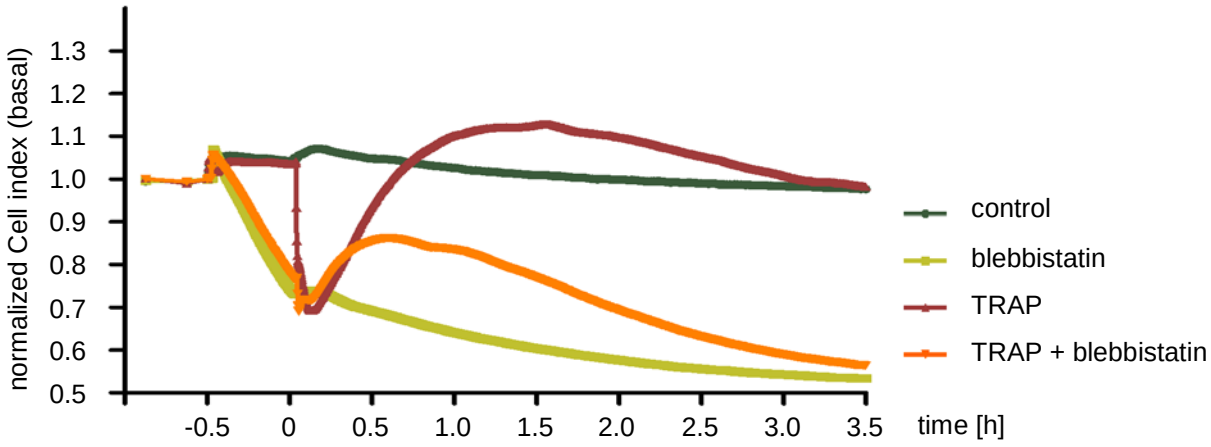

Figure 34 Blebbistatin alone decreases the CI and abrogates the TRAP effect. HMECs were treated with blebbistatin (10 µM) for 30 min and subsequently exposed to TRAP (50 µM). The time course of compound-mediated alterations of normalized CI is displayed by a representative experiment. CI is normalized to *basal* levels (before blebbistatin treatment). Three independent experiments were performed.

3.2.4.2 Blebbistatin does not affect macromolecular permeability

Blebbistatin did not influence the endothelial permeability of FITC-dextran compared to untreated cells over a time period of 90 min (**Fig. 35A**). Moreover, also the TRAP-induced increase of MP is not altered by blebbistatin pretreatment (**Fig. 35B**).

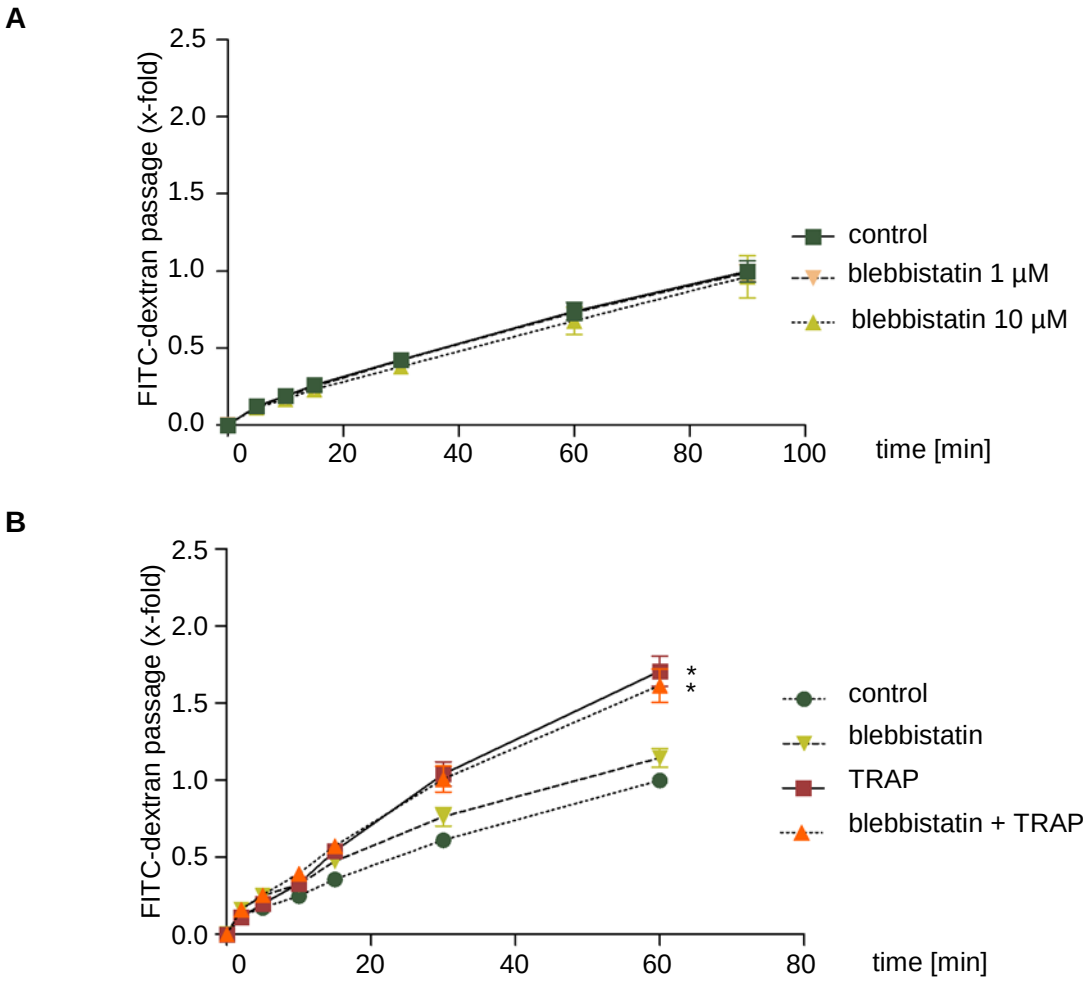

Figure 35 **Blebbistatin does not affect MP.** (**A**) HMECs were treated with blebbistatin at indicated concentrations immediately before FITC-dextran (40 kDa) was added. (**B**) HMECs were exposed to blebbistatin (10 µM) for 30 min, then FITC-dextran (40 kDa) and successively TRAP (50 µM) were added. (**A, B**)The passage of FITC-dextran across the cell layer was measured with a Transwell® two-compartment system. Samples were taken from the lower compartment at indicated time points. Data are expressed as mean ± S.E.M.. *P < 0.05 in relation to control, one-way ANOVA followed by Newman-Keuls post-hoc test. (n = 3).

3.2.4.3 Blebbistatin does not influence the contractile cytoskeleton

Immunofluorescence staining of F-actin and phosphorylated MLC2 revealed no major alterations of blebbistatin treated cells – neither under control conditions nor after TRAP activation (**Fig. 27**).

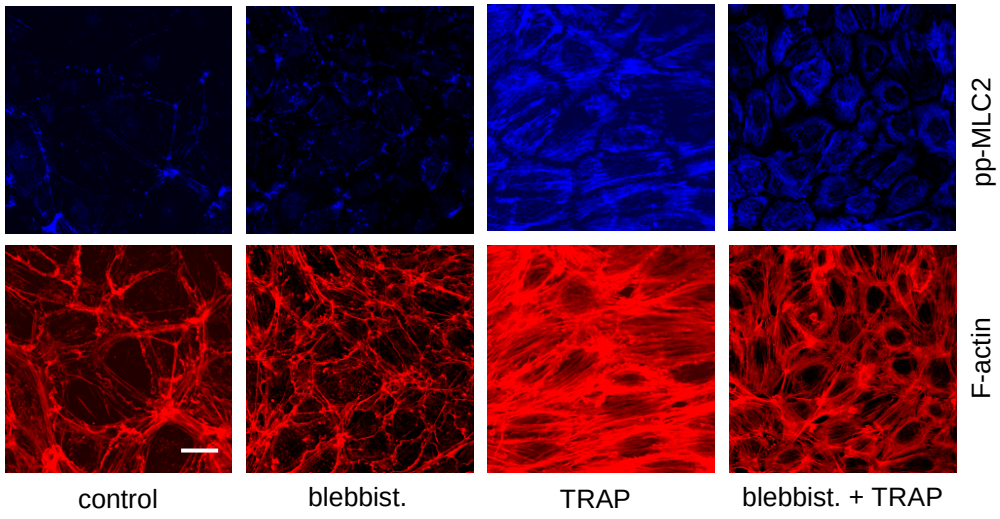

Figure 36 Blebbistatin does not influence the contractile cytoskelton. HUVECs were treated with blebbistatin (10 µM) for 30 min before TRAP (50 µM) was added for 10 min. F-actin distribution and di-phosphorylation of MLC2 (T^{18},S^{19}) were determined by confocal laser scanning microscopy. The bar indicates 20 µm. One representative image out of three independently performed experiments is shown.

We found discrepancies in MP and impedance measurement when endothelial cells were challenged with the myosin II inhibitor blebbistatin. Although blebbistatin itself decreased the impedance signal, it still fully abrogated the TRAP-induced drop of impedance values. In contrast to these observations, blebbistatin exerted no effect on the passage of macromolecules and did not affect the contractile cytoskeleton.

4 DISCUSSION

4.1 Targeting endothelial hyperpermeability as promising anti-inflammatory strategy

Inflammation is a protective attempt to resolve infections or tissue injury. Circulating leukocytes run through the adhesion cascade – including the steps of capturing, rolling, activation, firm adhesion and transmigration – to overcome the endothelial barrier in order to counteract invading pathogens at the site of inflammation.[105] Nevertheless, an exceeding or permanent inflammatory activation is harmful to the host and results in inflammation-related disease progression. The release of inflammatory mediators, reactive oxygen species (ROS) and cytotoxic enzymes from leukocytes as well as the subsequently induced edema formation causes serious tissue damages and organ dysfunction. For decades, the interaction between leukocytes and microvessel walls has been considered as critical step for tissue injury.[123] Consequently, research efforts majorly focused on the inhibition of specific adhesive ligands mediating leukocyte–endothelium interaction.[123-126] However, this anti-adhesive strategy has not shown benefits in clinical trials.[127] This might be explained by recent studies, which suggested that the process of leukocyte adhesion and migration is not directly responsible for vascular leakage, but might be induced by the release of inflammatory mediators and ROS.[123, 128, 129]

These findings suggest the direct targeting of endothelial hyperpermeability as promising approach to prevent vascular damage during inflammation. Thus, not only the direct effects of inflammatory mediators on endothelial cells, but also the leukocyte-associated increase of permeability should be attenuated.[123]

Therefore, we characterized novel targets in the regulation of endothelial permeability and evaluated the most appropriate methods for the analysis of barrier function:

(1) We disclosed IAPs as novel regulators of endothelial hyperpermeability and RhoA activation in response to thrombin. In consequence, IAP antagonism was proven to successfully protect the endothelial barrier against thrombin-mediated stress fiber formation, cell contraction and destabilization of AJs.

(2) Moreover, we for the first time compared the advantages and limitations of classic macromolecular permeability measurement and sophisticated impedance sensing as methods for the analysis of endothelial barrier function *in vitro*.

4.2 The role of IAPs in inflammation

Beyond their prominent role in cancer cell biology, IAPs emerged as regulators of signal transduction events that promote inflammation. Numerous studies highlighted the importance of IAPs as modulators of NFκB and MAPK activation in TNF-receptor (TNFR) signaling.[130-132] For example, in the TNFα-induced canonical NFκB pathway, cIAPs are required for non-degradative ubiquitination of the receptor interacting protein 1 (RIP1), which induces NFκB activation. In contrast, cIAPs impede the non-canonical NFκB activation through the constitutive degradation of the NFκB-inducing kinase (NIK).[133] Furthermore, IAPs were described as signal transducers in the innate immune response after activation of pattern recognition receptors (PPRs). Recognition of pathogen-associated molecular patterns (PAMPs), like *e.g.* bacterial lipopolysaccharides (LPS), or endogenous danger-associated molecular patterns (DAMPs) by PPRs induces an inflammatory cell response.[134] Analogously to TNFR signaling, IAPs regulate ubiquitin-dependent signaling processes downstream of the activation of important PPRs (such as toll-like receptor 4, NOD-like receptor (NLR) 1/2 or RIG-1), which again culminate in the activation of NFκB and MAPKs.[91] Interestingly, a subset of intracellular PPRs, the NLRs, can activate the inflammasome in macrophages and neutrophils upon PAMP or DAMP exposition.[135] The inflammasome, a multimeric protein complex, leads to the activation of the pro-inflammatory caspase-1, which converts pro-IL-1β into mature IL-1β, a potent inflammatory cytokine.[136] Although the process of caspase-1 activation is not understood in detail, IAPs seem to be critical modulators of the inflammasome assembly. It was recently demonstrated that cIAP1 and cIAP2 are effectors of the inflammasome and, thus, required for an efficient caspase-1 activation.[137] Moreover, the study underlines the anti-inflammatory potential of IAP antagonists, as the inflammasome response in an experimental model of peritonitis was suppressed. In contrast to the observation that IAPs promote the inflammatory response, Vince *et al*. reported that IAPs limit the IL-1β activation. Inhibition or depletion of IAPs triggered the inflammasome-dependent cleavage of IL-1β. In conclusion, the role of IAPs in leukocyte activation needs further examinations.

Even though the endothelium functions as multifaceted regulator of the inflammatory response, the knowledge about the function of IAPs in endothelial cells is still very limited. So far it is known that IAPs positively regulate the production of TNFα-induced cytokines and chemokines (*e.g.* IL-6, -8, GM-CSF, MCP-1, CXCL-1), thus triggering the inflammatory response. Indeed, IAP antagonists diminished the TNFα-induced expression of these inflammatory mediators in HUVECs.[138] Moreover, the inhibition of IAPs was reported to block TNFα-evoked vascular inflammation by suppressing the activation of

endothelial cells, without sensitizing them to apoptosis.[139] Our group revealed that treatment with an IAP antagonist prevents leukocyte recruitment to the site of inflammation *in vivo*.[4] Further *in vitro* experiments showed a decreased expression of the intercellular adhesion molecule (ICAM)-1 through impaired TNFR signaling and a reduced MAPK activation upon loss of IAPs.

4.2.1 A novel role for IAPs as regulators of the thrombin-induced endothelial hyperpermeability

Besides TNFα, the serine protease thrombin is also a pivotal mediator of the inflammatory response. In addition to its central role in the coagulation cascade, thrombin triggers distinct signaling pathways in vascular cells: in the endothelium, thrombin induces characteristic phenotypic changes, including increased permeability, morphological alterations and elevated leukocyte trafficking.[140] Thrombin is endogenously produced on the surface of injured endothelial cells,[114] and, for instance, found at elevated levels in severe lung disorders (ALI, ARDS) or atherosclerosis.[141-143] In endothelial cells, activation of the predominantly expressed thrombin receptor PAR-1 induces a massive dysfunction of the endothelial barrier.[144, 145] This activation is mediated either through cleavage of the receptor's extracellular N-terminus and consequent exposure of a new N-terminal motif (by thrombin) or simply by mimicking this unmasked tethered ligand with a small peptide (by TRAP).[21, 140]

In the present study, we for the first time elucidate the role of IAPs in the context of pro-inflammatory thrombin signaling. Herein, we show that inhibition of IAPs prevents the typical thrombin-caused endothelial barrier disruption.

4.2.1.1 IAP antagonists prevent endothelial barrier dysfunction in functional assays and the underlying molecular events

We could demonstrate that two structurally different IAP antagonists (ABT, Smac085) significantly reduce TRAP-mediated endothelial hyperpermeability, as assessed with two commonly accepted functional permeability assays (measurement of macromolecular permeability and TEER). The TRAP-induced flux of the labeled tracer molecule (FITC-dextran, 40 kDa) was decreased by both IAP antagonists at any observed time point, but most explicit at the latest time point due to the cumulative nature of this method. Complementary, the real-time measurement of TEER revealed that IAP antagonism protected against the initial and maximal effect of TRAP and, moreover, promoted the subsequent recovery of the endothelial barrier.

We aimed at explaining the observed barrier protective effects of IAP inhibition on a molecular level through analysis of key parameters of endothelial barrier function: activation of the contractile machinery (phosphorylation of MLC2), actin remodeling (stress fiber formation) and disassembly of AJs (phosphorylation of VE-cadherin). Well matching to the observation in the functional assays, ABT positively affected all three molecular determinants. The rapid thrombin-evoked stress fiber formation (analyzed after 5 min), as well as the phosphorylation events of MLC2 (after 5 and 15 min), were suppressed by IAP inhibition. Additionally, ABT stabilizes AJs *via* the decreased phosphorylation of VE-cadherin (after 15 and 30 min). Noteworthy, disruption of AJs might not only occur after phosphorylation of junctional proteins, but also directly *via* acto-myosin driven cellular retraction.[18] This explains why we found early barrier stabilizing effects of ABT in functional assays, but detected a decrease of VE-cadherin phosphorylation only after 15 min. Interestingly, the phosphorylation of VE-cadherin is required for successful leukocyte diapedesis.[146] Hence, our data confirms previous *in vivo* experiments from Mayer *et al*., which demonstrated that ABT inhibits leukocyte transmigration.[4]

4.2.1.2 Unraveling the underlying signaling events

The role of IAPs in TNFR-signaling is well understood, but their contribution in PAR-signaling is completely unknown. Both signaling pathways are able to induce the cellular stress response in form of enhanced MAPK activity. Our previous study showed that ABT suppressed the TNFα-mediated activation of p38 and JNK.[4] In contrast, ABT does not affect the thrombin-caused activation of the permeability-regulating MAPKs (p38, ERK, JNK). ABT neither influenced the typical thrombin-caused rise in $[Ca^{2+}]_i$, nor the activation of distinct PKCs.

Knowing that RhoA is a major regulator of stress fiber formation,[147] and due to the fact that ABT circumvented the thrombin-induced cytoskeletal remodeling, we hypothesized that IAPs might be crucially involved in RhoA signaling.

4.2.2 IAPs as regulators of RhoA signaling

In our study, we demonstrate for the first time that IAPs are indispensable for the full RhoA activation in response to thrombin. Both, the genetic depletion and the pharmacological inhibition of IAPs abrogated the induced activation of the barrier disruption-mediating small GTPase RhoA as well as the subsequent stress fiber formation. However, the activity of the counter-regulating GTPase Rac1 was not altered upon IAP inhibition. Beyond that, we identified IAPs as unknown binding partners of RhoA.

4.2.2.1 The role of individual IAPs

The initial characterization of IAP expression in HUVECs revealed that thrombin does not alter the respective protein amount. Surprisingly, cIAP2 was not present in our setting and, therefore, excluded from further considerations. This can be explained by the structural properties of cIAP2: Recently, cIAP2 was found as stable dimer with a high intrinsic activity of the E3 ligase domain, thus triggering its permanent auto-ubiquitination and subsequent degradation.[86]

In order to further elucidate the role of individual IAP family members, we performed affinity precipitation experiments and immunocytological stainings of the contractile machinery after depletion of either XIAP or cIAP1. Most importantly, we revealed that the TRAP-caused RhoA activation and the subsequent cytoskeletal activation depend rather on XIAP than cIAP1. Only gene silencing of XIAP is able to induce the same phenotypic changes as treatment with an IAP antagonist. At first sight, this is astonishing, since IAP antagonists induce the rapid degradation of cIAP1, whereas the levels of XIAP remain unaltered.[76, 148] IAP antagonists activate the E3 ligase activity of cIAP1 by promoting RING dimerization, which, in turn, induces its proteasomal degradation.[86] In contrast to this observation, the RING activity of XIAP is *per se* not altered by IAP inhibitors.[149] Nevertheless, the Smac mimetic ABT was designed and evaluated as potent inhibitor of XIAP by binding its BIR3 domain in a nanomolar range.[88] Altogether, this suggests that either the complete loss of XIAP or at least blocking its BIR3 domain is required for the prevention of RhoA activation, whereas the loss of cIAP1 seems to be irrelevant.

Interestingly, we recently could demonstrate that rather cIAP1 than XIAP is predominantly responsible for the TNFα-induced ICAM-1 expression.[4] This provides evidence that IAP family members exert different functions in the endothelium and, therefore, are not compensable.

4.2.2.2 Interaction of IAPs and small GTPases

Furthermore, we found a direct interaction of XIAP and RhoA, which appeared to be independent of the RhoA nucleotide loading, *e.g.* the activation state. Until now, an association of IAPs with Rho GTPases has only been described for Rac1.[74] For example, in fruit flies, the IAP homologue *Drosophila* IAP1 (DIAP1) was shown to affect cell migration through an interaction with Rac1, notably also independent of its activity.[150] An exciting study from the Rajalingam group reported for MEFs and HeLa cells that IAPs directly bind GTP- and GDP-loaded Rac1 before initiating its proteasomal degradation.[103] Therefore, one might hypothesize a conserved mechanism behind the binding of IAPs to small GTPases, independently of their activation status. As cIAP1, XIAP and DIAP1 share the appearance of BIR and RING domains, further investigations are needed to characterize the molecular interaction with members of the small GTPases family.

Moreover, the Rajalingam study highlighted that cIAP1 and XIAP not only bind to Rac1, but additionally act as direct E3 ligases for Rac1 poly-ubiquitination and degradation.[103] In consequence, IAP inhibition led to an increased Rac1 activity and an enhanced cell migration. They also showed that RhoA is regulated by IAPs, since the *basal* activity of RhoA was suppressed by an IAP antagonist, although this effect was not subject of further investigations. In accordance to that study, our data demonstrate that in the human endothelium RhoA activity (induced by thrombin or RhoA overexpression) is controlled by IAPs, especially XIAP. In contrast, however, Rac1 is not regulated by IAPs in endothelial cells.

4.2.2.3 IAPs as possible upstream regulators of RhoA activity

Further studies are needed to identify possible upstream targets of RhoA signaling after IAP inhibition and the exact mechanism behind the involvement of XIAP. We might speculate that XIAP could directly target RhoA like Smurf1, an E3 ligase known to be an upstream mediator of RhoA-ROCK-MLC2 signaling.[151] Notably, gene silencing of Smurf1 in HEK 293T cells induced a cortical actin arrangement, a phenotype similar to our observations after XIAP silencing.[152]

Moreover, IAP inhibition could also modulate typical upstream regulators of RhoA activity, such as GEFs, GAPs or GDIs. Although the knowledge in this field is very limited, a study in cancer cells revealed that XIAP binds to RhoGDI, thus decreasing RhoGDI activity, which in turn enhances actin polymerization and cell motility.[153] One might speculate that XIAP inhibition could enforce RhoGDI activity and thereby limit RhoA activity in our system. IAPs could also possibly enhance the binding of GEFs to RhoA or alter the

interaction with GAPs. Although a role for IAPs in the regulation of GEFs and GAPs is currently not described, other E3 ligases are known to affect GEF and GAP activity.[154] For example, Smurf1, in addition to RhoA, was found to ubiquitinate hPEM-2, a Cdc42 GEF, thus affecting cellular migration.[155] Furthermore, the activation of RhoA is modulated by ubiquitination events of LARG, which represents an important RhoA GEF.[156]

4.2.3 Conclusion

We provided evidence that IAPs, especially XIAP, are important (patho-)physiological modulators of endothelial permeability by interfering with RhoA activation. In addition to the existing literature on XIAP in the immune regulation, this represents a novel role for XIAP as positive regulator of the inflammatory response. Moreover, we introduced IAP antagonism as promising pharmacological approach for the prevention of endothelial hyperpermeability.

As small molecule IAP inhibitors are not detrimental to normal tissue and proven to be well tolerated in the human organism,[157] it would be interesting to pursue our scientific findings in preclinical and clinical studies.

4.3 Analysis of the endothelial barrier function *in vitro*

As we have seen in the first part, *in vitro* assays for the measurement of the endothelial barrier function are indispensable for the identification and characterization of new pharmacological targets. Even though *in vitro* models do not reflect the complexe structure of the microvasculature (including pericytes, smooth muscle cells, ECM) and, therefore, overestimate the permeability compared to the situation *in vivo*,[158, 159] the use of these simplified models enables a precise control of experimental conditions for the detailed analysis of potential targets and the underlying signaling events.

In this work, we for the first time investigated the individual advantages and limitations of two widely used *in vitro* methods for the analysis of the endothelial barrier function: the well-established measurement of macromolecular permeability with a Transwell® two-compartment system and a modern impedance sensing device (xCELLigence™).

Therefore, we tested different established barrier-modulating compounds in both permeability assays and compared the results to alterations of the F-actin cytoskeleton and the activation of the contractile machinery as universal indicators of endothelial integrity.

4.3.1 Comparing the results from macromolecular permeability measurement and impedance sensing

Given that two different types of analysis parameters, flux of macromolecules and cellular impedance, are utilized for the characterization of barrier properties, it is not surprising that not always congruent observations were made.

The biophysical dimension impedance provides information about morphological properties of cells.[54] Altered cell-cell contacts and cell-substratum interactions influence the ion conducting properties of a cell layer. This presents a rather artificial readout parameter as mainly the permeability of small ions is evaluated. In contrast, the real flux of macromolecules across the cellular barrier mimics the physiological function of the endothelium *in vivo*.[13] Nevertheless, the defined pore size of the filter as well as the homogenous weight of the added tracer molecule differs from the physiological situation.

4.3.1.1 Congruent results in both permeability assays after forskolin treatment

Our results for the treatment of HMECs with the barrier enhancer forskolin prior to TRAP addition confirm the applicability of MP and as well as impedance measurement as general indicators for endothelial permeability. As proof of concept, we showed that forskolin abrogates the activation of MLC2 and inhibited stress fiber formation. In accordance to our observations in the endothelium, Wegener *et al.* demonstrated barrier protective properties of forskolin in porcine brain epithelial cells in all major *in vitro* permeability assays (MP, TEER and impedance).[160] Interestingly, a theoretical model of the performed impedance analysis revealed that the barrier protective effects of forskolin were partially caused by cell-substratum reinforcement and not only from strengthening of IEJs. As this discrimination is not feasible with MP or TEER measurement, the possibility to mathematically re-evaluate impedance data represents an advantage for the advanced user of impedance-based assays.

4.3.1.2 The use of histamine reveals the limitations of macromolecular permeability measurement

The rapid and transient histamine-induced permeability response can be monitored in real-time by impedance sensing, whereas the cumulative MP method is lacking sensitivity, which caused huge standard errors and no clear correlation between the applied concentrations and the measured effects. Our impedance data are perfectly matching to the time points of MLC2 activation found in the literature. The maximum phosphorylation of MLC2 occurs after 30 s, persists for 90 s and then returns to base level after 5 min.[43] Impedance values immediately drop upon histamine exposure, reach the maximum decline after about 1 min and are drawn back to *basal* conditions after 5 min latest. Surprisingly, histamine does not only decrease endothelial barrier function by a transient disruption of cell-cell contacts, but subsequently enhances barrier properties, partly through the restoration of intercellular adhesions, and mainly through an increasing cell-matrix interaction.[161] These effects are displayed by impedance sensing, as we detect a drop of impedance values within minutes and a subsequent increase above control levels. This dual nature of the histamine effect is masked in MP measurement, as only an increase of FITC-dextran passage is detectable.

4.3.1.3 ROCK inhibition increases *basal* permeability, but clearly prevents TRAP-induced barrier disruption

The results from both permeability assays indicated that inhibition of ROCK with Y-27632 elevates endothelial permeability under *basal* conditions, but protects against TRAP-induced barrier dysfunction. Obviously, ROCK has opposing activities in the regulation of the endothelial barrier function: it shows intrinsic barrier protective properties at cell margins and an inducible barrier-disruptive activity at F-actin stress fibers.[162] Treatment of HMECs with Y-27632 alone moderately elevates the flux of macromolecules, whereas a massive drop of impedance values is detected. Even though the phosphorylation of MLC2 is completely suppressed by Y-27632, ROCK inhibition considerably alters the F-actin morphology, which might be the cause for the elevated macromolecular permeability and the dramatic impedance decline. Our results and findings from others indicate that the interpretation Western blot results might be misleading without further permeability assays, as Y-27632 increases *basal* permeability despite a decreased activation of MLC2.[163] In contrast, ROCK inhibition clearly prevented the TRAP-induced flux of macromolecules across the cell layer and, furthermore, reduced the TRAP-evoked impedance drop. Here, both observations correlate with the suppression of MLC2 activity and the suppression of stress fiber assembly.

4.3.1.4 Blebbistatin evokes controversial responses in both permeability assays

Treatment with blebbistatin shows contradictory results in both permeability assays as it dramatically affects impedance sensing, whereas macromolecular permeability is not altered at all. Blebbistatin is known to abolish the cellular tension as it inhibits the myosin II binding to actin.[122] Cellular morphology is mainly controlled by two opposing systems: intercellular adhesion and cellular tension.[164] Obviously, blebbistatin treatment alters the cell shape only *via* the decrease of intracellular tension, as it does not affect the composition of adherens junctions.[165] Notably, the thrombin-induced phosphorylation of MLC2 and the F-actin polymerization is not influenced by blebbistatin.[122] We, therefore, conclude that impedance sensing displays mainly blebbistatin-mediated cell morphology changes caused by a decreased cellular tension, whereas the permeability of macromolecules is not affected as intercellular adhesions are not influenced by blebbistatin.

4.3.2 Conclusion

Real-time impedance measurement is a highly sensitive and label-free method to monitor cell morphology changes. Alterations of the endothelial barrier function are associated with such morphological changes. This is reflected by different ion fluxes in impedance measurement and by macromolecular fluxes in the Transwell® assay.

However, morphological changes are not exclusively related to the endothelial barrier. We found that impedance data only partially correlated with permeability and, moreover, was not always easy to interpret. Therefore, we suggest utilizing it as complementary tool to acquire further information about the barrier characteristics. For example, real-time monitoring of impedance allows the determination of the ideal time point for the examination of the cytoskeleton or to perform macromolecular permeability measurement.

5 SUMMARY

The vascular endothelium represents an attractive drug target system for the development of new anti-inflammatory strategies, as it regulates the extravasation of leukocytes, solutes and plasma proteins due to its barrier function. Dysfunction of the endothelial barrier is a key feature of many severe diseases with an inflammatory component, such as sepsis, ALI or atherosclerosis. As drugs that specifically target endothelial barrier-regulating systems are widely lacking, there is a strong demand for the identification of pharmacological targets. Therefore, sensitive and reliable methods for the analysis of the endothelial barrier function are indispensable.

First, we could identify IAPs as crucial regulators of the thrombin-induced inflammatory response by mediating RhoA activation, which evokes endothelial hyperpermeability. We furthermore revealed that IAP antagonists prevent endothelial barrier dysfunction, stabilize AJs, suppress cellular contraction and inhibit stress fiber formation independently of Ca^{2+}, PKC or MAPK signaling pathways. Interestingly, RhoA activation and the subsequent downstream events (stress fiber assembly, activation of the contractile machinery) were blocked by IAP inhibition or specific gene knockdown of XIAP. Additionally, a direct interaction of XIAP and RhoA was reported, which occurred irrespective of the RhoA activation status.

In conclusion, we found a new function for IAPs (especially XIAP) as positive regulators of inflammatory processes (*i.e.* the regulation of the endothelial barrier function) extending the existing knowledge on IAPs in the immune regulation. In consequence, IAP antagonism represents a promising approach for the treatment of hyperpermeability-associated disorders.

Secondly, we for the first time compared the conventional macromolecular permeability measurement (with a Transwell® two-compartment system) with the modern impedance sensing (with a xCELLigence™ RTCA analyzer) as methods for the analysis of the endothelial barrier function. Therefore, we studied the effects of different well established barrier-modulating compounds in both permeability assays and compared the results to alterations of the F-actin cytoskeleton and the activation of motor proteins (MLC2). Altogether, impedance sensing is a highly sensitive method with an extraordinary time resolution for the detection cell morphology changes, which, however, do not necessarily correlate with permeability changes. In contrast, the Transwell® system, which depicts the real flux of macromolecules across a cell layer, has limitations in terms of sensitivity and time resolution. Consequently, we recommend the complementary use of both methods and to reconsider their individual limitations, since each technique alone can not fully determine all consequences of barrier-modulating compounds.

6 REFERENCES

1. Yuan, S.Y. & Rigor, R.R. in Regulation of Endothelial Barrier Function (San Rafael (CA), 2010).
2. Fulda, S. & Vucic, D. Targeting IAP proteins for therapeutic intervention in cancer. *Nat Rev Drug Discov* **11**, 109-24 (2012).
3. Gyrd-Hansen, M. & Meier, P. IAPs: from caspase inhibitors to modulators of NF-kappaB, inflammation and cancer. *Nat Rev Cancer* **10**, 561-74 (2010).
4. Mayer, B.A. et al. Inhibitor of apoptosis proteins as novel targets in inflammatory processes. *Arterioscler Thromb Vasc Biol* **31**, 2240-50 (2011).
5. Aird, W.C. Spatial and temporal dynamics of the endothelium. *J Thromb Haemost* **3**, 1392-406 (2005).
6. Cooke, J.P. The endothelium: a new target for therapy. *Vasc Med* **5**, 49-53 (2000).
7. Feletou, M. in The Endothelium: Part 1: Multiple Functions of the Endothelial Cells-Focus on Endothelium-Derived Vasoactive Mediators (San Rafael (CA), 2011).
8. Scallan, J., Huxley, V.H. & Korthuis, R.J. in Capillary Fluid Exchange: Regulation, Functions, and Pathology (San Rafael (CA), 2010).
9. Peterson, K. et al. in Drug Class Review: Nonsteroidal Antiinflammatory Drugs (NSAIDs): Final Update 4 Report (Portland (OR), 2010).
10. Rhen, T. & Cidlowski, J.A. Antiinflammatory action of glucocorticoids--new mechanisms for old drugs. *N Engl J Med* **353**, 1711-23 (2005).
11. Foley, J.F. Focus issue: understanding mechanisms of inflammation. *Sci Signal* **6**, eg2 (2013).
12. van Nieuw Amerongen, G.P. & van Hinsbergh, V.W. Targets for pharmacological intervention of endothelial hyperpermeability and barrier function. *Vascul Pharmacol* **39**, 257-72 (2002).
13. Komarova, Y. & Malik, A.B. Regulation of endothelial permeability via paracellular and transcellular transport pathways. *Annu Rev Physiol* **72**, 463-93 (2010).
14. Minshall, R.D., Sessa, W.C., Stan, R.V., Anderson, R.G. & Malik, A.B. Caveolin regulation of endothelial function. *Am J Physiol Lung Cell Mol Physiol* **285**, L1179-83 (2003).
15. Vandenbroucke, E., Mehta, D., Minshall, R. & Malik, A.B. Regulation of endothelial junctional permeability. *Ann N Y Acad Sci* **1123**, 134-45 (2008).
16. Mehta, D. & Malik, A.B. Signaling mechanisms regulating endothelial permeability. *Physiol Rev* **86**, 279-367 (2006).
17. Goldblum, S.E., Ding, X. & Campbell-Washington, J. TNF-alpha induces endothelial cell F-actin depolymerization, new actin synthesis, and barrier dysfunction. *Am J Physiol* **264**, C894-905 (1993).
18. Dejana, E., Orsenigo, F. & Lampugnani, M.G. The role of adherens junctions and VE-cadherin in the control of vascular permeability. *J Cell Sci* **121**, 2115-22 (2008).
19. Shen, Q., Wu, M.H. & Yuan, S.Y. Endothelial contractile cytoskeleton and microvascular permeability. *Cell Health Cytoskelet* **2009**, 43-50 (2009).
20. van Hinsbergh, V.W. & van Nieuw Amerongen, G.P. Intracellular signalling involved in modulating human endothelial barrier function. *J Anat* **200**, 549-60 (2002).
21. Cirino, G. et al. Thrombin functions as an inflammatory mediator through activation of its receptor. *J Exp Med* **183**, 821-7 (1996).
22. Gerszten, R.E. et al. Specificity of the thrombin receptor for agonist peptide is defined by its extracellular surface. *Nature* **368**, 648-51 (1994).
23. Kumar, P. et al. Molecular mechanisms of endothelial hyperpermeability: implications in inflammation. *Expert Rev Mol Med* **11**, e19 (2009).
24. Ahmmed, G.U. & Malik, A.B. Functional role of TRPC channels in the regulation of endothelial permeability. *Pflugers Arch* **451**, 131-42 (2005).
25. Smyth, J.T. et al. Activation and regulation of store-operated calcium entry. *J Cell Mol Med* **14**, 2337-49 (2010).

26. Dudek, S.M. & Garcia, J.G. Cytoskeletal regulation of pulmonary vascular permeability. *J Appl Physiol* **91**, 1487-500 (2001).
27. Shen, Q., Rigor, R.R., Pivetti, C.D., Wu, M.H. & Yuan, S.Y. Myosin light chain kinase in microvascular endothelial barrier function. *Cardiovasc Res* **87**, 272-80 (2010).
28. Lum, H. & Malik, A.B. Mechanisms of increased endothelial permeability. *Can J Physiol Pharmacol* **74**, 787-800 (1996).
29. Rigor, R.R., Shen, Q., Pivetti, C.D., Wu, M.H. & Yuan, S.Y. Myosin light chain kinase signaling in endothelial barrier dysfunction. *Med Res Rev* **33**, 911-33 (2013).
30. Garcia, J.G., Davis, H.W. & Patterson, C.E. Regulation of endothelial cell gap formation and barrier dysfunction: role of myosin light chain phosphorylation. *J Cell Physiol* **163**, 510-22 (1995).
31. Sandoval, R. et al. Ca(2+) signalling and PKCalpha activate increased endothelial permeability by disassembly of VE-cadherin junctions. *J Physiol* **533**, 433-45 (2001).
32. Borbiev, T. et al. Role of CaM kinase II and ERK activation in thrombin-induced endothelial cell barrier dysfunction. *Am J Physiol Lung Cell Mol Physiol* **285**, L43-54 (2003).
33. Borbiev, T. et al. p38 MAP kinase-dependent regulation of endothelial cell permeability. *Am J Physiol Lung Cell Mol Physiol* **287**, L911-8 (2004).
34. Kiemer, A.K. et al. Inhibition of p38 MAPK activation via induction of MKP-1: atrial natriuretic peptide reduces TNF-alpha-induced actin polymerization and endothelial permeability. *Circ Res* **90**, 874-81 (2002).
35. Arndt, P.G. et al. Inhibition of c-Jun N-terminal kinase limits lipopolysaccharide-induced pulmonary neutrophil influx. *Am J Respir Crit Care Med* **171**, 978-86 (2005).
36. Yuan, S.Y. Protein kinase signaling in the modulation of microvascular permeability. *Vascul Pharmacol* **39**, 213-23 (2002).
37. Etienne-Manneville, S. & Hall, A. Rho GTPases in cell biology. *Nature* **420**, 629-35 (2002).
38. Hall, A. & Nobes, C.D. Rho GTPases: molecular switches that control the organization and dynamics of the actin cytoskeleton. *Philos Trans R Soc Lond B Biol Sci* **355**, 965-70 (2000).
39. Spindler, V., Schlegel, N. & Waschke, J. Role of GTPases in control of microvascular permeability. *Cardiovasc Res* **87**, 243-53 (2010).
40. van Nieuw Amerongen, G.P., van Delft, S., Vermeer, M.A., Collard, J.G. & van Hinsbergh, V.W. Activation of RhoA by thrombin in endothelial hyperpermeability: role of Rho kinase and protein tyrosine kinases. *Circ Res* **87**, 335-40 (2000).
41. Gainor, J.P., Morton, C.A., Bell, D.R., Vincent, P.A. & Minnear, F.L. Platelet phospholipids decrease vascular endothelial permeability via a novel signaling pathway independent of cAMP/protein kinase A. *Ann N Y Acad Sci* **905**, 315-8 (2000).
42. Perez-Moreno, M., Jamora, C. & Fuchs, E. Sticky business: orchestrating cellular signals at adherens junctions. *Cell* **112**, 535-48 (2003).
43. Moy, A.B., Shasby, S.S., Scott, B.D. & Shasby, D.M. The effect of histamine and cyclic adenosine monophosphate on myosin light chain phosphorylation in human umbilical vein endothelial cells. *J Clin Invest* **92**, 1198-206 (1993).
44. Langeler, E.G. & van Hinsbergh, V.W. Norepinephrine and iloprost improve barrier function of human endothelial cell monolayers: role of cAMP. *Am J Physiol* **260**, C1052-9 (1991).
45. Kooistra, M.R., Corada, M., Dejana, E. & Bos, J.L. Epac1 regulates integrity of endothelial cell junctions through VE-cadherin. *FEBS Lett* **579**, 4966-72 (2005).

46. Birukova, A.A. et al. Rac GTPase is a hub for protein kinase A and Epac signaling in endothelial barrier protection by cAMP. *Microvasc Res* **79**, 128-38 (2010).
47. Wojciak-Stothard, B. & Ridley, A.J. Rho GTPases and the regulation of endothelial permeability. *Vascul Pharmacol* **39**, 187-99 (2002).
48. Miles, A.A. & Miles, E.M. Vascular reactions to histamine, histamine-liberator and leukotaxine in the skin of guinea-pigs. *J Physiol* **118**, 228-57 (1952).
49. Ley, K. & Arfors, K.E. Segmental differences of microvascular permeability for FITC-dextrans measured in the hamster cheek pouch. *Microvasc Res* **31**, 84-99 (1986).
50. Giaever, I. & Keese, C.R. A morphological biosensor for mammalian cells. *Nature* **366**, 591-2 (1993).
51. Siflinger-Birnboim, A. et al. Molecular sieving characteristics of the cultured endothelial monolayer. *J Cell Physiol* **132**, 111-7 (1987).
52. Ehringer, W.D., Wang, O.L., Haq, A. & Miller, F.N. Bradykinin and alpha-thrombin increase human umbilical vein endothelial macromolecular permeability by different mechanisms. *Inflammation* **24**, 175-93 (2000).
53. Giaever, I. & Keese, C.R. Micromotion of mammalian cells measured electrically. *Proc Natl Acad Sci U S A* **88**, 7896-900 (1991).
54. Yu, N. et al. Real-time monitoring of morphological changes in living cells by electronic cell sensor arrays: an approach to study G protein-coupled receptors. *Anal Chem* **78**, 35-43 (2006).
55. Xiao, C. & Luong, J.H. On-line monitoring of cell growth and cytotoxicity using electric cell-substrate impedance sensing (ECIS). *Biotechnol Prog* **19**, 1000-5 (2003).
56. Xiao, C., Lachance, B., Sunahara, G. & Luong, J.H. An in-depth analysis of electric cell-substrate impedance sensing to study the attachment and spreading of mammalian cells. *Anal Chem* **74**, 1333-9 (2002).
57. Lo, C.M., Keese, C.R. & Giaever, I. Monitoring motion of confluent cells in tissue culture. *Exp Cell Res* **204**, 102-9 (1993).
58. Stolwijk, J.A. et al. Impedance analysis of adherent cells after in situ electroporation: non-invasive monitoring during intracellular manipulations. *Biosens Bioelectron* **26**, 4720-7 (2011).
59. Opp, D. et al. Use of electric cell-substrate impedance sensing to assess in vitro cytotoxicity. *Biosens Bioelectron* **24**, 2625-9 (2009).
60. Bagnaninchi, P.O. & Drummond, N. Real-time label-free monitoring of adipose-derived stem cell differentiation with electric cell-substrate impedance sensing. *Proc Natl Acad Sci U S A* **108**, 6462-7 (2011).
61. Hsu, C.C., Tsai, W.C., Chen, C.P., Lu, Y.M. & Wang, J.S. Effects of negative pressures on epithelial tight junctions and migration in wound healing. *Am J Physiol Cell Physiol* **299**, C528-34 (2010).
62. Wang, H.S., Keese, C.R., Giaever, I. & Smith, T.J. Prostaglandin E2 alters human orbital fibroblast shape through a mechanism involving the generation of cyclic adenosine monophosphate. *J Clin Endocrinol Metab* **80**, 3553-60 (1995).
63. Tiruppathi, C., Malik, A.B., Del Vecchio, P.J., Keese, C.R. & Giaever, I. Electrical method for detection of endothelial cell shape change in real time: assessment of endothelial barrier function. *Proc Natl Acad Sci U S A* **89**, 7919-23 (1992).
64. Dubrez-Daloz, L., Dupoux, A. & Cartier, J. IAPs: more than just inhibitors of apoptosis proteins. *Cell Cycle* **7**, 1036-46 (2008).
65. Srinivasula, S.M. & Ashwell, J.D. IAPs: what's in a name? *Mol Cell* **30**, 123-35 (2008).
66. Crook, N.E., Clem, R.J. & Miller, L.K. An apoptosis-inhibiting baculovirus gene with a zinc finger-like motif. *J Virol* **67**, 2168-74 (1993).

67. Uren, A.G., Coulson, E.J. & Vaux, D.L. Conservation of baculovirus inhibitor of apoptosis repeat proteins (BIRPs) in viruses, nematodes, vertebrates and yeasts. *Trends Biochem Sci* **23**, 159-62 (1998).
68. Eckelman, B.P., Salvesen, G.S. & Scott, F.L. Human inhibitor of apoptosis proteins: why XIAP is the black sheep of the family. *EMBO Rep* **7**, 988-94 (2006).
69. Mace, P.D., Shirley, S. & Day, C.L. Assembling the building blocks: structure and function of inhibitor of apoptosis proteins. *Cell Death Differ* **17**, 46-53 (2010).
70. Eckelman, B.P. & Salvesen, G.S. The human anti-apoptotic proteins cIAP1 and cIAP2 bind but do not inhibit caspases. *J Biol Chem* **281**, 3254-60 (2006).
71. Bertrand, M.J. & Vandenabeele, P. The Ripoptosome: death decision in the cytosol. *Mol Cell* **43**, 323-5 (2011).
72. Varfolomeev, E., Wayson, S.M., Dixit, V.M., Fairbrother, W.J. & Vucic, D. The inhibitor of apoptosis protein fusion c-IAP2.MALT1 stimulates NF-kappaB activation independently of TRAF1 AND TRAF2. *J Biol Chem* **281**, 29022-9 (2006).
73. Fulda, S., Rajalingam, K. & Dikic, I. Ubiquitylation in immune disorders and cancer: from molecular mechanisms to therapeutic implications. *EMBO Mol Med* **4**, 545-56 (2012).
74. Oberoi-Khanuja, T.K. & Rajalingam, K. IAPs as E3 ligases of Rac1: shaping the move. *Small GTPases* **3**, 131-6 (2012).
75. MacFarlane, M., Merrison, W., Bratton, S.B. & Cohen, G.M. Proteasome-mediated degradation of Smac during apoptosis: XIAP promotes Smac ubiquitination in vitro. *J Biol Chem* **277**, 36611-6 (2002).
76. Varfolomeev, E. et al. IAP antagonists induce autoubiquitination of c-IAPs, NF-kappaB activation, and TNFalpha-dependent apoptosis. *Cell* **131**, 669-81 (2007).
77. Xu, P. et al. Quantitative proteomics reveals the function of unconventional ubiquitin chains in proteasomal degradation. *Cell* **137**, 133-45 (2009).
78. Lopez, J. & Meier, P. To fight or die - inhibitor of apoptosis proteins at the crossroad of innate immunity and death. *Curr Opin Cell Biol* **22**, 872-81 (2010).
79. Gyrd-Hansen, M. et al. IAPs contain an evolutionarily conserved ubiquitin-binding domain that regulates NF-kappaB as well as cell survival and oncogenesis. *Nat Cell Biol* **10**, 1309-17 (2008).
80. Lopez, J. et al. CARD-mediated autoinhibition of cIAP1's E3 ligase activity suppresses cell proliferation and migration. *Mol Cell* **42**, 569-83 (2011).
81. Fulda, S. Exploiting inhibitor of apoptosis proteins as therapeutic targets in hematological malignancies. *Leukemia* **26**, 1155-65 (2012).
82. Du, C., Fang, M., Li, Y., Li, L. & Wang, X. Smac, a mitochondrial protein that promotes cytochrome c-dependent caspase activation by eliminating IAP inhibition. *Cell* **102**, 33-42 (2000).
83. Chai, J. et al. Structural and biochemical basis of apoptotic activation by Smac/DIABLO. *Nature* **406**, 855-62 (2000).
84. Vucic, D. & Fairbrother, W.J. The inhibitor of apoptosis proteins as therapeutic targets in cancer. *Clin Cancer Res* **13**, 5995-6000 (2007).
85. Vince, J.E. et al. IAP antagonists target cIAP1 to induce TNFalpha-dependent apoptosis. *Cell* **131**, 682-93 (2007).
86. Feltham, R. et al. Smac mimetics activate the E3 ligase activity of cIAP1 protein by promoting RING domain dimerization. *J Biol Chem* **286**, 17015-28 (2011).
87. Liu, Z. et al. Structural basis for binding of Smac/DIABLO to the XIAP BIR3 domain. *Nature* **408**, 1004-8 (2000).
88. Oost, T.K. et al. Discovery of potent antagonists of the antiapoptotic protein XIAP for the treatment of cancer. *J Med Chem* **47**, 4417-26 (2004).
89. de Almagro, M.C. & Vucic, D. The inhibitor of apoptosis (IAP) proteins are critical regulators of signaling pathways and targets for anti-cancer therapy. *Exp Oncol* **34**, 200-11 (2012).

90. Flygare, J.A. et al. Discovery of a potent small-molecule antagonist of inhibitor of apoptosis (IAP) proteins and clinical candidate for the treatment of cancer (GDC-0152). *J Med Chem* **55**, 4101-13 (2012).
91. Damgaard, R.B. & Gyrd-Hansen, M. Inhibitor of apoptosis (IAP) proteins in regulation of inflammation and innate immunity. *Discov Med* **11**, 221-31 (2011).
92. Ades, E.W. et al. HMEC-1: establishment of an immortalized human microvascular endothelial cell line. *J Invest Dermatol* **99**, 683-90 (1992).
93. Bouis, D., Hospers, G.A., Meijer, C., Molema, G. & Mulder, N.H. Endothelium in vitro: a review of human vascular endothelial cell lines for blood vessel-related research. *Angiogenesis* **4**, 91-102 (2001).
94. Bradford, M.M. A rapid and sensitive method for the quantitation of microgram quantities of protein utilizing the principle of protein-dye binding. *Anal Biochem* **72**, 248-54 (1976).
95. Smith, P.K. et al. Measurement of protein using bicinchoninic acid. *Anal Biochem* **150**, 76-85 (1985).
96. Laemmli, U.K. Cleavage of structural proteins during the assembly of the head of bacteriophage T4. *Nature* **227**, 680-5 (1970).
97. Kurien, B.T. & Scofield, R.H. Protein blotting: a review. *J Immunol Methods* **274**, 1-15 (2003).
98. Furst, R. et al. Atrial natriuretic peptide protects against histamine-induced endothelial barrier dysfunction in vivo. *Mol Pharmacol* **74**, 1-8 (2008).
99. Nagel, W., Somieski, P. & Katz, U. Selective inhibition of Cl(-) conductance in toad skin by blockers of Cl(-) channels and transporters. *Am J Physiol Cell Physiol* **281**, C1223-32 (2001).
100. Zamore, P.D. RNA interference: big applause for silencing in Stockholm. *Cell* **127**, 1083-6 (2006).
101. Benard, V. & Bokoch, G.M. Assay of Cdc42, Rac, and Rho GTPase activation by affinity methods. *Methods Enzymol* **345**, 349-59 (2002).
102. Ren, X.D. & Schwartz, M.A. Determination of GTP loading on Rho. *Methods Enzymol* **325**, 264-72 (2000).
103. Oberoi, T.K. et al. IAPs regulate the plasticity of cell migration by directly targeting Rac1 for degradation. *EMBO J* **31**, 14-28 (2012).
104. Grynkiewicz, G., Poenie, M. & Tsien, R.Y. A new generation of Ca2+ indicators with greatly improved fluorescence properties. *J Biol Chem* **260**, 3440-50 (1985).
105. Ley, K., Laudanna, C., Cybulsky, M.I. & Nourshargh, S. Getting to the site of inflammation: the leukocyte adhesion cascade updated. *Nat Rev Immunol* **7**, 678-89 (2007).
106. Fernandez-Borja, M., van Buul, J.D. & Hordijk, P.L. The regulation of leucocyte transendothelial migration by endothelial signalling events. *Cardiovasc Res* **86**, 202-10 (2010).
107. Schulte, D. et al. Stabilizing the VE-cadherin-catenin complex blocks leukocyte extravasation and vascular permeability. *EMBO J* **30**, 4157-70 (2011).
108. Lampugnani, M.G. & Dejana, E. Adherens junctions in endothelial cells regulate vessel maintenance and angiogenesis. *Thromb Res* **120 Suppl 2**, S1-6 (2007).
109. Kluger, M.S., Clark, P.R., Tellides, G., Gerke, V. & Pober, J.S. Claudin-5 controls intercellular barriers of human dermal microvascular but not human umbilical vein endothelial cells. *Arterioscler Thromb Vasc Biol* **33**, 489-500 (2013).
110. Potter, M.D., Barbero, S. & Cheresh, D.A. Tyrosine phosphorylation of VE-cadherin prevents binding of p120- and beta-catenin and maintains the cellular mesenchymal state. *J Biol Chem* **280**, 31906-12 (2005).
111. Bogatcheva, N.V. & Verin, A.D. The role of cytoskeleton in the regulation of vascular endothelial barrier function. *Microvasc Res* **76**, 202-7 (2008).
112. Kim, K.M. et al. Molecular characterization of myosin phosphatase in endothelium. *J Cell Physiol* **227**, 1701-8 (2012).

113. Ito, M., Nakano, T., Erdodi, F. & Hartshorne, D.J. Myosin phosphatase: structure, regulation and function. *Mol Cell Biochem* **259**, 197-209 (2004).
114. Bogatcheva, N.V., Garcia, J.G. & Verin, A.D. Molecular mechanisms of thrombin-induced endothelial cell permeability. *Biochemistry (Mosc)* **67**, 75-84 (2002).
115. Putney, J.W. Pharmacology of store-operated calcium channels. *Mol Interv* **10**, 209-18 (2010).
116. Spiering, D. & Hodgson, L. Dynamics of the Rho-family small GTPases in actin regulation and motility. *Cell Adh Migr* **5**, 170-80 (2011).
117. Moorman, J.P., Luu, D., Wickham, J., Bobak, D.A. & Hahn, C.S. A balance of signaling by Rho family small GTPases RhoA, Rac1 and Cdc42 coordinates cytoskeletal morphology but not cell survival. *Oncogene* **18**, 47-57 (1999).
118. Wang, C.Y., Mayo, M.W., Korneluk, R.G., Goeddel, D.V. & Baldwin, A.S., Jr. NF-kappaB antiapoptosis: induction of TRAF1 and TRAF2 and c-IAP1 and c-IAP2 to suppress caspase-8 activation. *Science* **281**, 1680-3 (1998).
119. Bubik, M.F. et al. A novel approach to prevent endothelial hyperpermeability: the Crataegus extract WS(R) 1442 targets the cAMP/Rap1 pathway. *J Mol Cell Cardiol* **52**, 196-205 (2012).
120. Ludwig, A., Sommer, A. & Uhlig, S. Assessment of endothelial permeability and leukocyte transmigration in human endothelial cell monolayers. *Methods Mol Biol* **763**, 319-32 (2011).
121. Waschke, J., Drenckhahn, D., Adamson, R.H., Barth, H. & Curry, F.E. cAMP protects endothelial barrier functions by preventing Rac-1 inhibition. *Am J Physiol Heart Circ Physiol* **287**, H2427-33 (2004).
122. Goeckeler, Z.M., Bridgman, P.C. & Wysolmerski, R.B. Nonmuscle myosin II is responsible for maintaining endothelial cell basal tone and stress fiber integrity. *Am J Physiol Cell Physiol* **295**, C994-1006 (2008).
123. He, P. Leucocyte/endothelium interactions and microvessel permeability: coupled or uncoupled? *Cardiovasc Res* **87**, 281-90 (2010).
124. Kubes, P., Suzuki, M. & Granger, D.N. Modulation of PAF-induced leukocyte adherence and increased microvascular permeability. *Am J Physiol* **259**, G859-64 (1990).
125. Sumagin, R., Lomakina, E. & Sarelius, I.H. Leukocyte-endothelial cell interactions are linked to vascular permeability via ICAM-1-mediated signaling. *Am J Physiol Heart Circ Physiol* **295**, H969-H977 (2008).
126. Simmons, D.L. Anti-adhesion therapies. *Curr Opin Pharmacol* **5**, 398-404 (2005).
127. Becker, K.J. Anti-leukocyte antibodies: LeukArrest (Hu23F2G) and Enlimomab (R6.5) in acute stroke. *Curr Med Res Opin* **18 Suppl 2**, s18-22 (2002).
128. Phillipson, M., Kaur, J., Colarusso, P., Ballantyne, C.M. & Kubes, P. Endothelial domes encapsulate adherent neutrophils and minimize increases in vascular permeability in paracellular and transcellular emigration. *PLoS One* **3**, e1649 (2008).
129. Zeng, M., Zhang, H., Lowell, C. & He, P. Tumor necrosis factor-alpha-induced leukocyte adhesion and microvessel permeability. *Am J Physiol Heart Circ Physiol* **283**, H2420-30 (2002).
130. Varfolomeev, E. et al. Cellular inhibitors of apoptosis are global regulators of NF-kappaB and MAPK activation by members of the TNF family of receptors. *Sci Signal* **5**, ra22 (2012).
131. Shu, H.B., Takeuchi, M. & Goeddel, D.V. The tumor necrosis factor receptor 2 signal transducers TRAF2 and c-IAP1 are components of the tumor necrosis factor receptor 1 signaling complex. *Proc Natl Acad Sci U S A* **93**, 13973-8 (1996).
132. Mahoney, D.J. et al. Both cIAP1 and cIAP2 regulate TNFalpha-mediated NF-kappaB activation. *Proc Natl Acad Sci U S A* **105**, 11778-83 (2008).
133. Vucic, D. TRAF2 and cellular IAPs: a critical link in TNFR family signaling. *Adv Exp Med Biol* **691**, 63-78 (2011).

134. Akira, S., Uematsu, S. & Takeuchi, O. Pathogen recognition and innate immunity. *Cell* **124**, 783-801 (2006).
135. Davis, B.K., Wen, H. & Ting, J.P. The inflammasome NLRs in immunity, inflammation, and associated diseases. *Annu Rev Immunol* **29**, 707-35 (2011).
136. Labbe, K. & Saleh, M. Cell death in the host response to infection. *Cell Death Differ* **15**, 1339-49 (2008).
137. Labbe, K., McIntire, C.R., Doiron, K., Leblanc, P.M. & Saleh, M. Cellular inhibitors of apoptosis proteins cIAP1 and cIAP2 are required for efficient caspase-1 activation by the inflammasome. *Immunity* **35**, 897-907 (2011).
138. Kearney, C.J. et al. Inhibitor of Apoptosis Proteins (IAPs) and Their Antagonists Regulate Spontaneous and Tumor Necrosis Factor (TNF)-induced Proinflammatory Cytokine and Chemokine Production. *J Biol Chem* **288**, 4878-90 (2013).
139. Luong le, A. & Evans, P.C. Targeting inhibitor of apoptosis proteins to block vascular inflammation. *Arterioscler Thromb Vasc Biol* **31**, 2165-6 (2011).
140. Minami, T. et al. Thrombin and phenotypic modulation of the endothelium. *Arterioscler Thromb Vasc Biol* **24**, 41-53 (2004).
141. Kipnis, E. et al. Massive alveolar thrombin activation in Pseudomonas aeruginosa-induced acute lung injury. *Shock* **21**, 444-51 (2004).
142. Welty-Wolf, K.E., Carraway, M.S., Ortel, T.L. & Piantadosi, C.A. Coagulation and inflammation in acute lung injury. *Thromb Haemost* **88**, 17-25 (2002).
143. Wei, H.J. et al. Thrombomodulin domains attenuate atherosclerosis by inhibiting thrombin-induced endothelial cell activation. *Cardiovasc Res* **92**, 317-27 (2011).
144. Lee, H. & Hamilton, J.R. Physiology, pharmacology, and therapeutic potential of protease-activated receptors in vascular disease. *Pharmacol Ther* **134**, 246-59 (2012).
145. van Nieuw Amerongen, G.P., Draijer, R., Vermeer, M.A. & van Hinsbergh, V.W. Transient and prolonged increase in endothelial permeability induced by histamine and thrombin: role of protein kinases, calcium, and RhoA. *Circ Res* **83**, 1115-23 (1998).
146. Turowski, P. et al. Phosphorylation of vascular endothelial cadherin controls lymphocyte emigration. *J Cell Sci* **121**, 29-37 (2008).
147. Pellegrin, S. & Mellor, H. Actin stress fibres. *J Cell Sci* **120**, 3491-9 (2007).
148. Yang, Q.H. & Du, C. Smac/DIABLO selectively reduces the levels of c-IAP1 and c-IAP2 but not that of XIAP and livin in HeLa cells. *J Biol Chem* **279**, 16963-70 (2004).
149. Nakatani, Y. et al. Regulation of ubiquitin transfer by XIAP, a dimeric RING E3 ligase. *Biochem J* **450**, 629-38 (2013).
150. Geisbrecht, E.R. & Montell, D.J. A role for Drosophila IAP1-mediated caspase inhibition in Rac-dependent cell migration. *Cell* **118**, 111-25 (2004).
151. Sahai, E., Garcia-Medina, R., Pouyssegur, J. & Vial, E. Smurf1 regulates tumor cell plasticity and motility through degradation of RhoA leading to localized inhibition of contractility. *J Cell Biol* **176**, 35-42 (2007).
152. Wang, H.R. et al. Regulation of cell polarity and protrusion formation by targeting RhoA for degradation. *Science* **302**, 1775-9 (2003).
153. Liu, J. et al. X-linked inhibitor of apoptosis protein (XIAP) mediates cancer cell motility via Rho GDP dissociation inhibitor (RhoGDI)-dependent regulation of the cytoskeleton. *J Biol Chem* **286**, 15630-40 (2011).
154. Ding, F., Yin, Z. & Wang, H.R. Ubiquitination in Rho signaling. *Curr Top Med Chem* **11**, 2879-87 (2011).
155. Yamaguchi, K., Ohara, O., Ando, A. & Nagase, T. Smurf1 directly targets hPEM-2, a GEF for Cdc42, via a novel combination of protein interaction modules in the ubiquitin-proteasome pathway. *Biol Chem* **389**, 405-13 (2008).

156. Yang, Y. et al. CYLD regulates RhoA activity by modulating LARG ubiquitination. *PLoS One* **8**, e55833 (2013).
157. Wong, H. et al. Dogs are more sensitive to antagonists of inhibitor of apoptosis proteins than rats and humans: a translational toxicokinetic/toxicodynamic analysis. *Toxicol Sci* **130**, 205-13 (2012).
158. Albelda, S.M. et al. Permeability characteristics of cultured endothelial cell monolayers. *J Appl Physiol* **64**, 308-22 (1988).
159. Steinberg, B.E., Goldenberg, N.M. & Lee, W.L. Do viral infections mimic bacterial sepsis? The role of microvascular permeability: A review of mechanisms and methods. *Antiviral Res* **93**, 2-15 (2012).
160. Wegener, J., Hakvoort, A. & Galla, H.J. Barrier function of porcine choroid plexus epithelial cells is modulated by cAMP-dependent pathways in vitro. *Brain Res* **853**, 115-24 (2000).
161. Moy, A.B. et al. Histamine alters endothelial barrier function at cell-cell and cell-matrix sites. *Am J Physiol Lung Cell Mol Physiol* **278**, L888-98 (2000).
162. van Nieuw Amerongen, G.P. et al. Involvement of Rho kinase in endothelial barrier maintenance. *Arterioscler Thromb Vasc Biol* **27**, 2332-9 (2007).
163. Bogatcheva, N.V. et al. The suppression of myosin light chain (MLC) phosphorylation during the response to lipopolysaccharide (LPS): beneficial or detrimental to endothelial barrier? *J Cell Physiol* **226**, 3132-46 (2011).
164. Lecuit, T. & Lenne, P.F. Cell surface mechanics and the control of cell shape, tissue patterns and morphogenesis. *Nat Rev Mol Cell Biol* **8**, 633-44 (2007).
165. Ivanov, A.I., Hunt, D., Utech, M., Nusrat, A. & Parkos, C.A. Differential roles for actin polymerization and a myosin II motor in assembly of the epithelial apical junctional complex. *Mol Biol Cell* **16**, 2636-50 (2005).

7 APPENDIX

7.1 Publications

7.1.1 Original publications

Hornburger M.C., Mayer B.A., Leonhardt S., Willer E.A., Zahler S., Beyerle A., Rajalingam K., Vollmar A.M., Fürst R. A novel role for inhibitor of apoptosis proteins (IAPs) as regulators of endothelial barrier function by mediating RhoA activation. *FASEB J*. In revision.

Hornburger M.C., Mayer B.A., Zahler S., Beyerle A., Wegener J., Vollmar A.M., Fürst R. A comperative study of in vitro methods analyzing endothelial barrier function – conventional macromolecular permeability measurement versus sophisticated impedance sensing. In preparation.

7.1.2 Abstracts

Hornburger M.C., Mayer B.A., Rehberg M., Krombach F., Vollmar A.M., Fürst R. Analysis of endothelial barrier function by macromolecular permeability measurement and impedance sensing – two sides of a story. IBCA 2011, August 10-12, Regensburg, Germany

Hornburger M.C., Mayer B.A., Willer E.A., Leonhardt S., Vollmar A.M., Fürst R. More than just cell death regulators: inhibitor of apoptosis proteins (IAPs) as modulators of endothelial permeability. Interact 2012, March 29-30, Munich, Germany

Hornburger M.C., Mayer B.A., Vollmar A.M., Wegener J., Fürst R. A comparative study of in vitro methods analyzing endothelial barrier function – conventional macromolecular permeability measurement versus sophisticated impedance sensing. DPhG Annual Meeting 2012, October 10-13, Greifswald, Germany

Hornburger M.C., Mayer B.A., Oberoi T., Willer E.A., Leonhardt S., Vollmar A.M., Rajalingam K., Fürst R. Inhibitor of apoptosis proteins (IAPs) antagonists protect against thrombin-induced endothelial hyperpermeability by preventing RhoA activation. DGPT Annual Meeting 2013, March 5-7, Halle, Germany

7.2 Acknowledgements

Diese Arbeit wurde an der Ludwig-Maximilians-Universität München, Department Pharmazie, am Lehrstuhl für Pharmazeutische Biologie von Frau Professor Dr. Angelika Vollmar unter der Betreuung von Herrn Professor Dr. Robert Fürst angefertigt. Herr Professor Dr. Fürst hat zwischenzeitlich eine Berufung der Goethe-Universität Frankfurt angenommen, wo er den Lehrstuhl für Pharmazeutische Biologie übernahm. Ihnen möchte ich an allererster Stelle danken, dass sie mir die Möglichkeit in ihrer Gruppe zu promovieren gegeben haben. Vielen Dank für die hervorragende fachliche und persönliche Betreuung, die hilfreichen Ratschläge und Diskussionen, sowie die Bereitschaft, sich immer die nötige Zeit für die Mitarbeiter zu nehmen. Ganz besonders jedoch möchte ich mich bei beiden für die freie Wahl des Arbeitsplatzes nach dem Umzug der Gruppe von Herrn Professor Dr. Fürst nach Frankfurt bedanken! Das ist keine Selbstverständlichkeit und zeugt von ihrem großen persönlichen Einsatz für das Wohl ihrer Mitarbeiter.

Ein recht herzliches Dankeschön geht an meine wissenschaftliche Mentorin, Frau Dr. Bettina Mayer, für ihre exzellente Vorarbeit auf dem Gebiet der *Inhibitor of apoptosis proteins (IAPs) im Endothel*, sowie die Einführung in den „wissenschaftlichen Alltag“ und ihre ständige Diskussionsbereitschaft zu vielfältigsten Themen. Vielen Dank auch an Frau Dr. Andrea Beyerle für ihre andauernden Anstrengungen bei der Verfassung der Manuskripte für die Original Publikationen, und darüber hinaus viel Erfolg beim weiteren Erforschen der *IAPs*. An dieser Stelle möchte ich auch vielmals Herrn Prof. Dr. Zahler für die zahlreichen Ratschläge und technischen Hilfestellungen danken.

Den Mitgliedern meines Prüfungskomitees gilt mein aufrichtiger Dank für Ihre Zeit und Mühe: Prof. Dr. Christian Wahl-Schott, Prof. Dr. Franz Paintner, Prof. Dr. Franz Bracher und Prof. Dr. Wolfgang Friess.

Des Weiteren möchte ich mich bei unseren Kollaborationspartner bedanken: Dr. Krishna Rajalingam und Tripat Oberoi vom Institute für Biochemie II, Goethe-Universität, Frankfurt für Ihre Experimente und die lebhaften Diskussionen auf dem Gebiet der RhoA-IAP Interaktion. Prof. Dr. Joe Wegener, Institut für Analytische Chemie und Biosensorik, Universität Regenburg, für seine Erläuterungen zur Impedanz-Messung und die Experimente mit dem ECIS® Gerät.

Ein großes Dankeschön an alle aktuellen und ehemaligen Mitglieder des Arbeitskreis Vollmar für das super Arbeitsklima und die gute Zeit im und außerhalb des Labors. Ein besonderer Dank gilt den Kollegen die (beinahe) parallel ihre Arbeit begonnen haben und mit mir gemeinsam gewachsen sind: Verena, Lena, Sandra, Simone, Tini und Flo. Ebenfalls ein großes Danke den „Ehemaligen“ und Post-Docs, die mir immer gute Vorbilder waren: Elisabeth, Sebastian, Sabine, sowie Hanna, Simone und Karin. Für die tatkräftige Hilfe im Labor möchte ich mich bei Jana, Bianca, Kerstin, Rita und Frau Schnegg bedanken.

Ein besonderer Dank geht an Dr. Martin Bubik, der mich mit großem Eifer beim Coverdesign beraten hat.

Ein großes Merci meinem Bruder und den Freunden für die nötige Abwechslung zur Wissenschaft. *<:o)

Ein riesen Dankeschön meiner Verlobten, Anja, dafür, dass sich selbst der Alltag wie Urlaub anfühlt. Ich freue mich sehr auf unsere gemeinsame Zukunft!

Tiefste Dankbarkeit gilt meinen Eltern, die mir alles ermöglicht haben und mich seit dem allerersten Tage unterstützen. Ihr hättet es nicht besser machen können!